Fracture Design, Placement, and Sequencing in Horizontal Wells

Mukul M. Sharma

Hisanao Ouchi, Amit Katiyar, John Foster

University of Texas at Austin

DE-FE0010808

Outline

- Problem statement: The need for a new model
- Peridynamics Based Hydraulic Fracturing Model
- Model Verification
- Effect of Reservoir Heterogeneity
- Interaction between Hydraulic Fractures and Natural Fractures
- Propagation of multiple fractures in horizontal wells
- Conclusion

Hydraulic Fractures are Complex

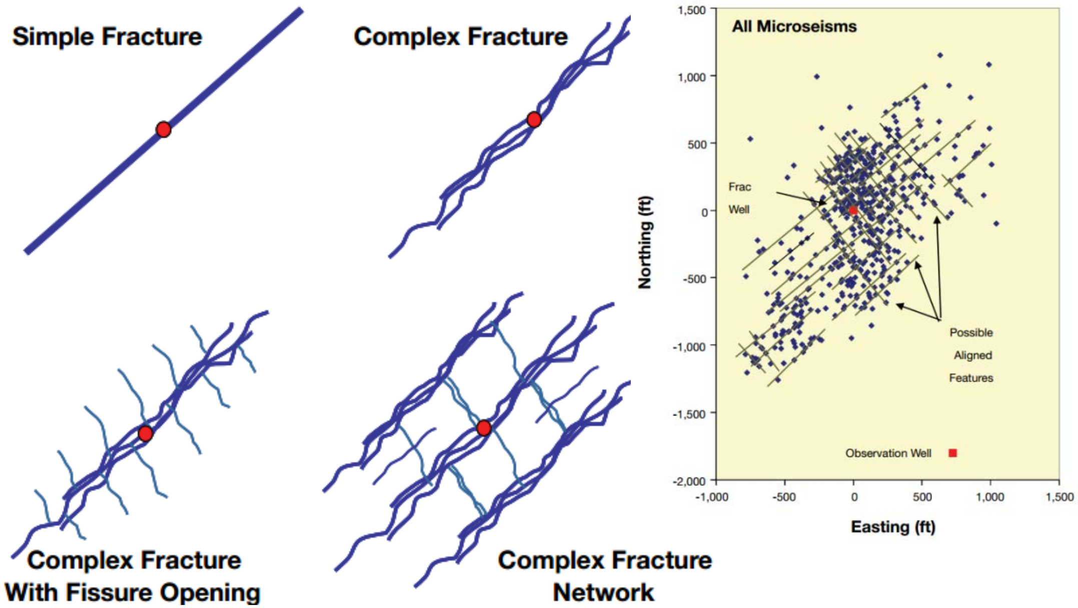

Ref: Warpinski, N.R. et al, SPE 114173, 2008

To optimize stimulation design and completion strategy, we must consider

- Complex **fracture geometry** **(multiple, non-planar)**
- **Fracture networks (interaction with natural fractures)**

Impact of **natural fractures**, **heterogeneities,** poroelasticity, layering, variation in the *in situ* confining stresses etc.

Peridynamics

Unifies the mechanics of <u>continuous</u> and <u>discontinuous media</u>

Silling S. A., *J. Mech. Phys. Solids*, 48, 175-209, 2000

Material points (particle-based discretization)

<u>Non-local interaction</u> (bonds) inside <u>horizon</u>

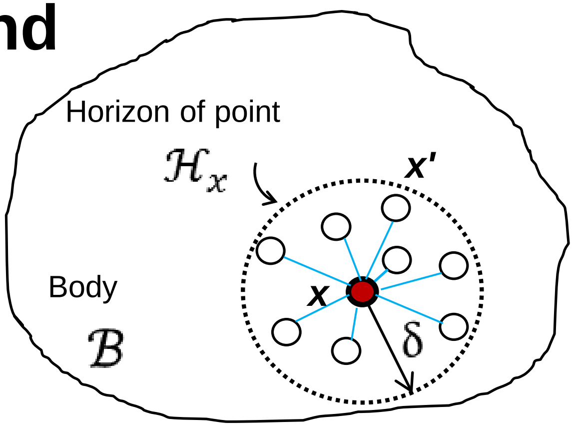

- **Integral Form**

Classical model $\rho[\boldsymbol{x}]\ddot{\boldsymbol{u}}[\boldsymbol{x},t] = \nabla \cdot \boldsymbol{\sigma}[\boldsymbol{x},t] + b[\boldsymbol{x},t]$

Peridynamics $\rho[\boldsymbol{x}]\ddot{\boldsymbol{u}}[\boldsymbol{x},t] = \int_{\mathcal{H}_x} \left(\underline{T}[\boldsymbol{x},t]\langle\boldsymbol{\xi}\rangle - \underline{T}[\boldsymbol{x}',t]\langle-\boldsymbol{\xi}\rangle\right) dV_{x'} + b[\boldsymbol{x},t]$

- **Any Known Constitutive Model in Classical Theory**

Linear elastic body: $\underline{T}[\boldsymbol{x},t]\langle\boldsymbol{\xi}\rangle = \left(\frac{3K\theta}{m}\underline{\omega \boldsymbol{x}} - \frac{15G}{m}\underline{\omega} e^d\right)\frac{\xi}{||\xi||}$

Peridynamics Based Hydraulic Fracturing Model

Peridynamics Based Poroelastic Model

Porous Flow

$$\frac{\partial}{\partial t}(\rho_0[\boldsymbol{x}]\emptyset[\boldsymbol{x}]) = \int_{\mathcal{H}_x} \left(\underline{Q}[\boldsymbol{x}]\langle\boldsymbol{\xi}\rangle - \underline{Q}[\boldsymbol{x}']\langle-\boldsymbol{\xi}\rangle\right) dV_{x'} + R[\boldsymbol{x}] + I[\boldsymbol{x}]$$

$$\underline{Q}[\boldsymbol{x}]\langle\boldsymbol{\xi}\rangle = \frac{\rho_0}{\mu}\frac{4}{\pi\delta^2}\frac{\boldsymbol{\xi}\left(\boldsymbol{K}[\boldsymbol{x}]-\frac{1}{4}tr(\boldsymbol{K}[\boldsymbol{x}])\boldsymbol{I}\right)\boldsymbol{\xi}}{\|\boldsymbol{\xi}\|^4}(\mathrm{P}[\boldsymbol{x}'] - \mathrm{P}[\boldsymbol{x}])$$ (for 2D flow)

Ref: Katiyar A., Foster J. T., Ouchi H., and Sharma M. M., J. Comp. Phys., 261, 209-229, 2014.

P θ

Solid Mechanics

$$\rho_m[\boldsymbol{x}]\ddot{\boldsymbol{u}}[\boldsymbol{x}] = \int_{\mathcal{H}_x}\left(\underline{T}[\boldsymbol{x}]\langle\boldsymbol{\xi}\rangle - \underline{T}[\boldsymbol{x}']\langle-\boldsymbol{\xi}\rangle\right)dV_{x'} + b[\boldsymbol{x}]$$

$$\underline{T}[\mathbf{x}]\langle\xi\rangle = \left[\chi_1\left\{\frac{3\left(K - G/3\right) - 3\alpha P}{m}\right\}\underline{\omega}\langle\mathbf{x}\rangle\|\xi\| + \frac{\chi_2 15G}{m}\left(\|\boldsymbol{\eta}+\xi\| - \|\xi\|\right)\right]\frac{\boldsymbol{\eta}+\xi}{\|\boldsymbol{\eta}+\xi\|}$$

Ref: Turner D.Z., arXiv:1206.5901, LE Q.V. et al, Int. J. Numer. Meth. Engng, 2014

$\emptyset$f Pf, I

Coupling

Fracture Flow

$$\frac{\partial}{\partial t}(\rho_f[\boldsymbol{x}]\emptyset_f[\boldsymbol{x}]) = \int_{\mathcal{H}_x} \left(\underline{Q}_f[\boldsymbol{x}]\langle\boldsymbol{\xi}\rangle - \underline{Q}_f[\boldsymbol{x}']\langle-\boldsymbol{\xi}\rangle\right) dV_{x'} + R_f[\boldsymbol{x}] - I[\boldsymbol{x}]$$

Ref: Ouchi, H., Katiyar A., York, J., Foster, John T., Sharma, Mukul M., J. Comp. Mech., 2015.

Dual Permeability Concept

Before fracture propagation

4 Primary Unknowns : position of element (x,y,z) and matrix pressure

After fracture propagation

5 Primary Unknowns : position of element (x,y,z), matrix pressure, and fracture pressure

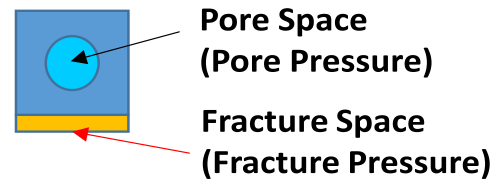

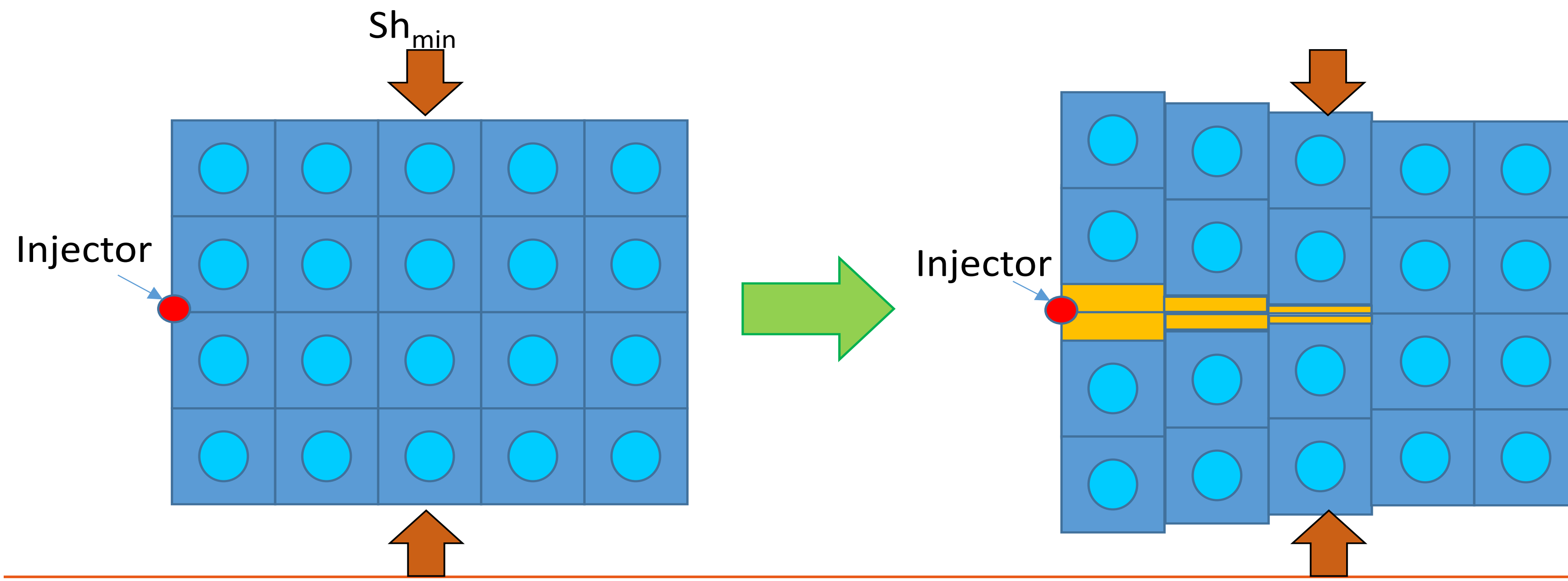

Model Verification

Biot Consolidation Problem (Verification of Poroelastic Model)

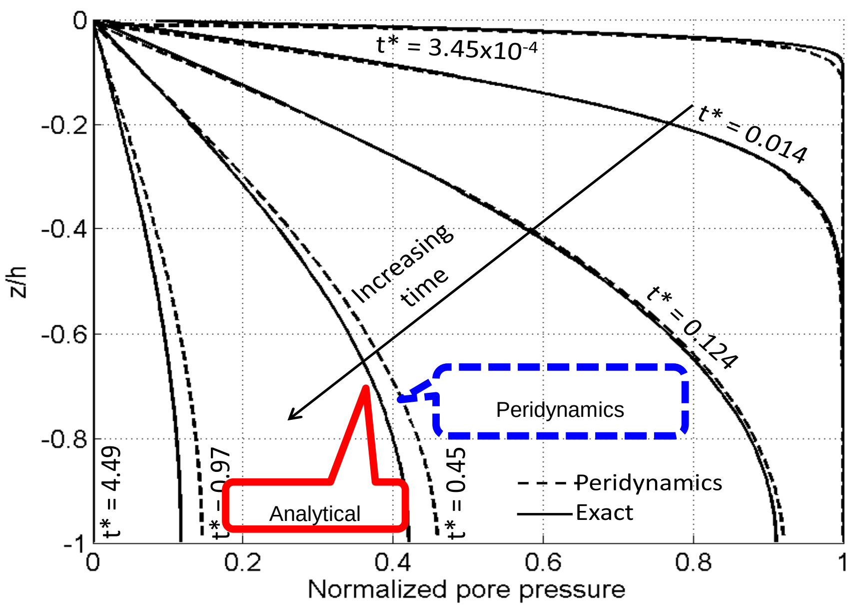

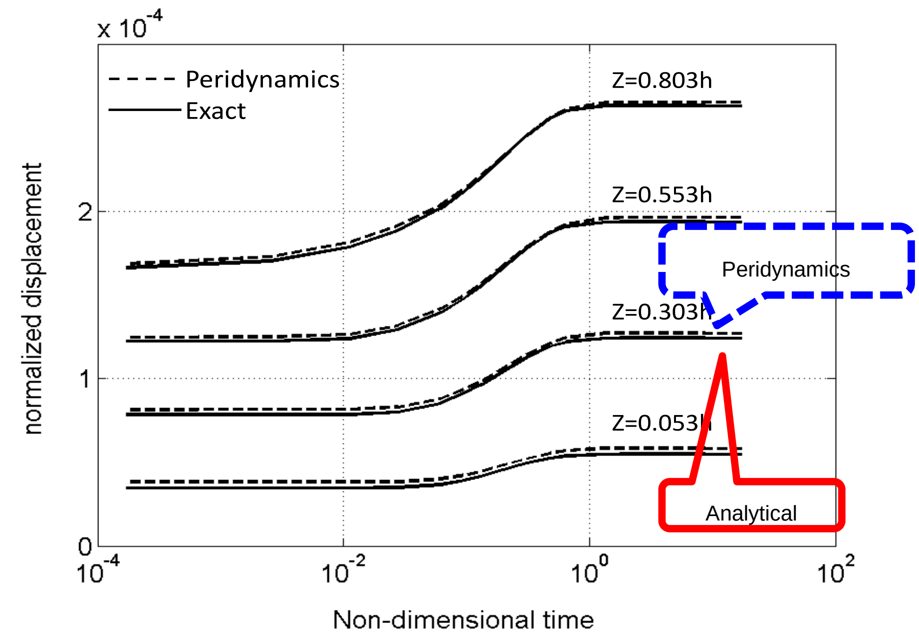

Jaeger J.C et al, Fundamentals of Rock Mechanics, forth edition, 189-P194

2-D Single Fracture Propagation (Comparison with KGD Model)

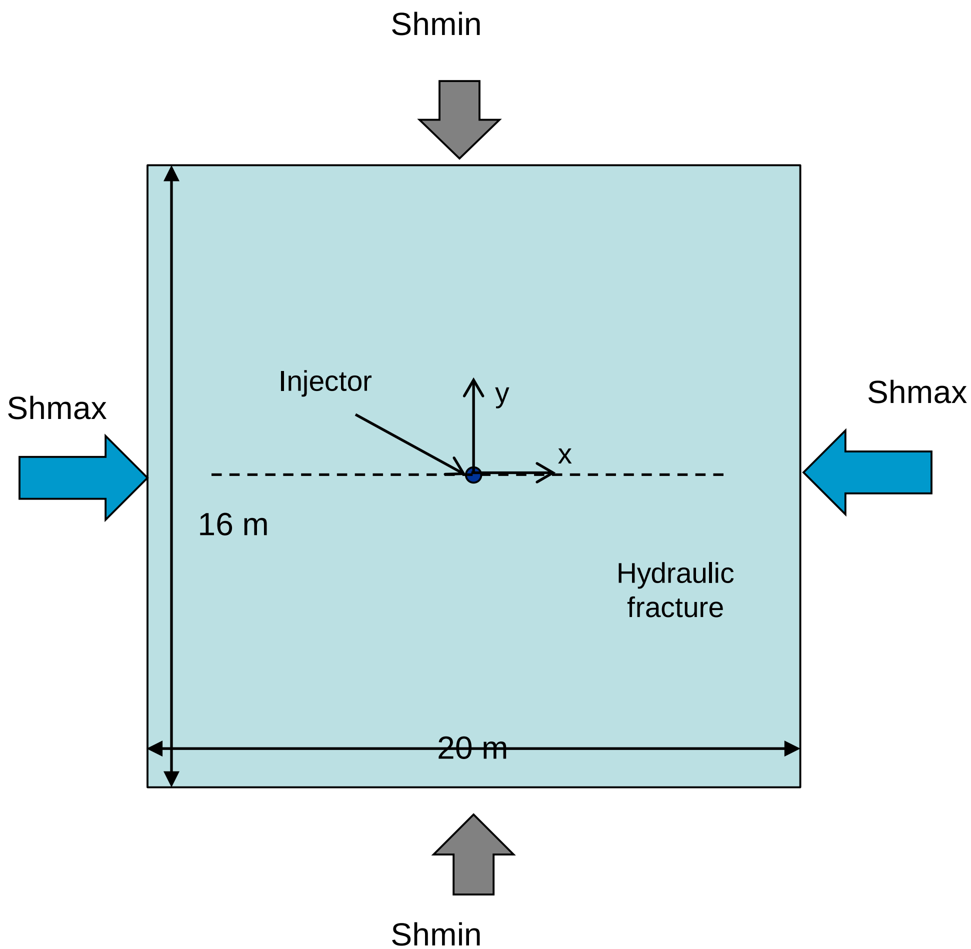

- Young's modulus (GPa) = 60
- Poisson's ratio = 0.25
- Shmax (MPa) = 12
- Shmin (MPa) = 8
- Permeability (nD) = 10
- Porosity = 0.3
- Initial pore pressure (MPa) = 3.2
- Fluid: Water
- Injection rate (m^3/min/m)= 0.12
- Number of elements 200*160

Results: Fracture Half Length and Wellbore Pressure

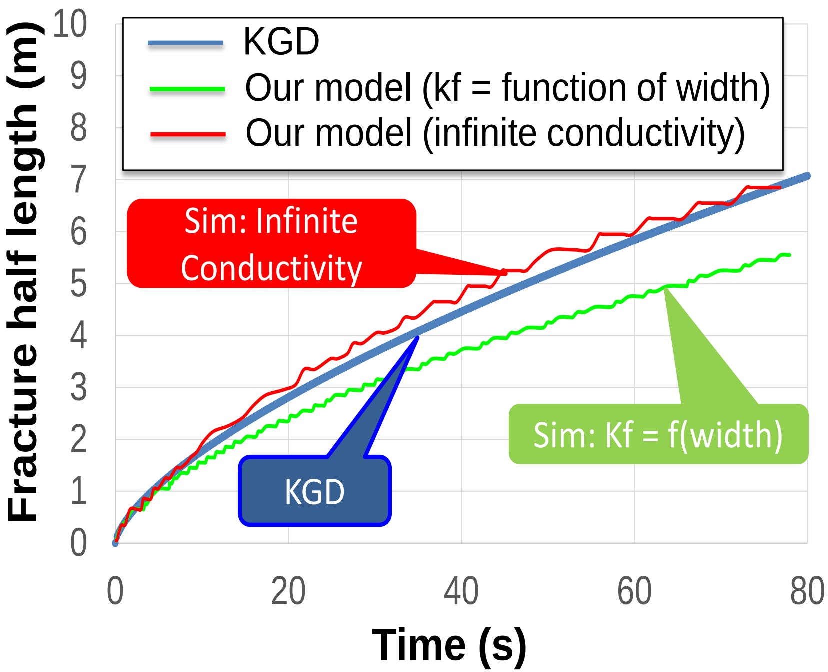

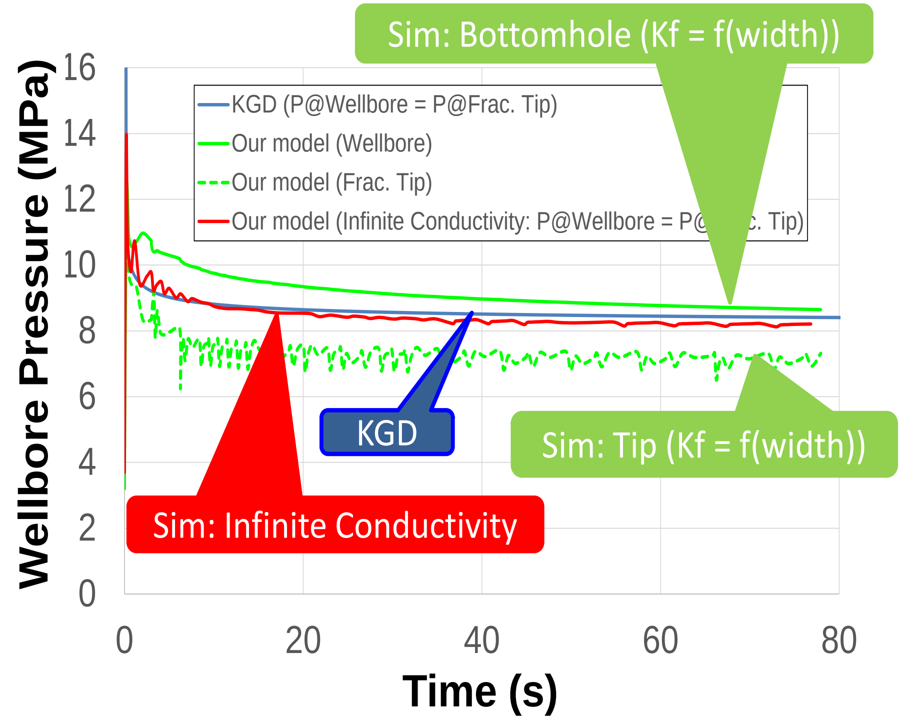

KGD assumes **constant pressure distribution** along a fracture. → **Infinite conductivity** model shows good agreement with KGD.

Results: Stress Distribution around Fracture (Infinite Conductivity Case)

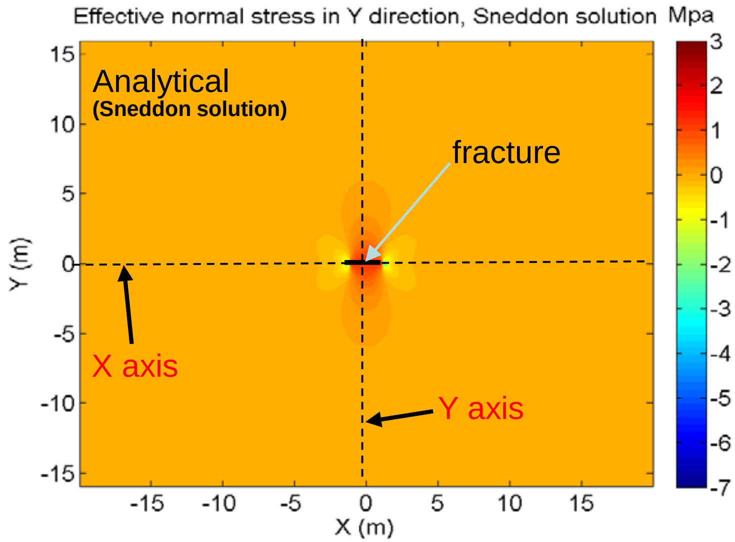

(a)

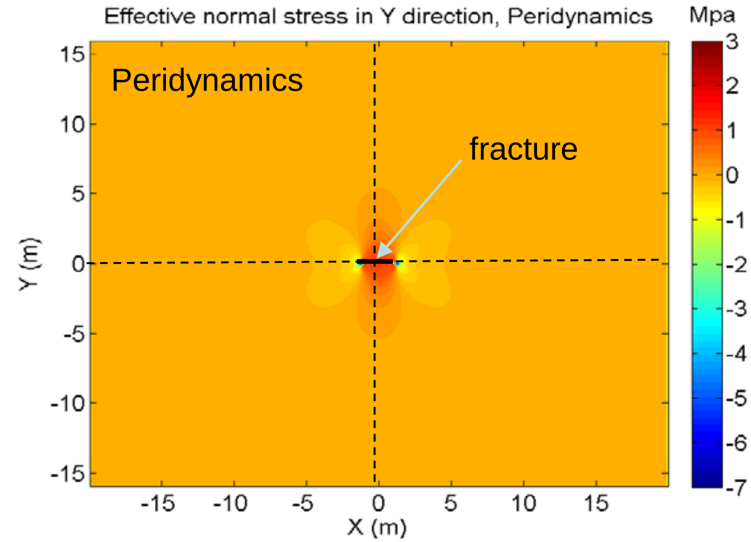

(b)

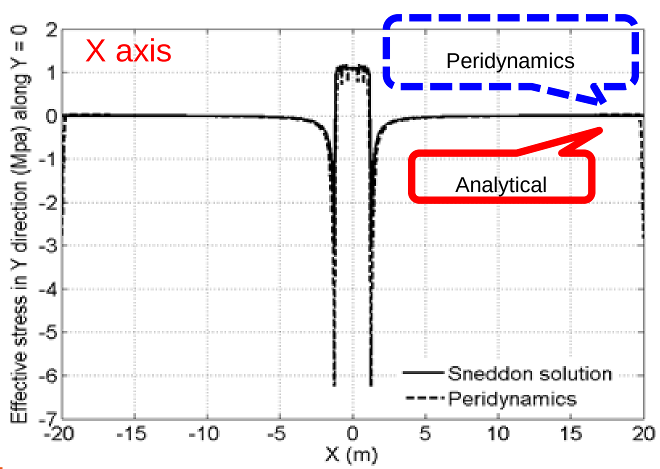

(c)

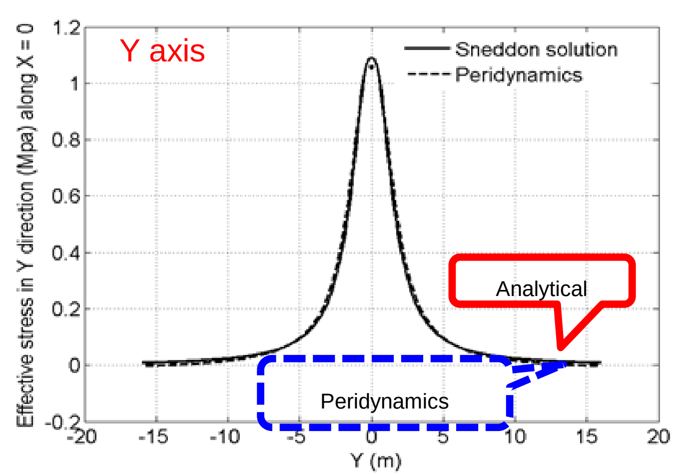

(d)

3-D Single Fracture Propagation (Comparison with PKN Model)

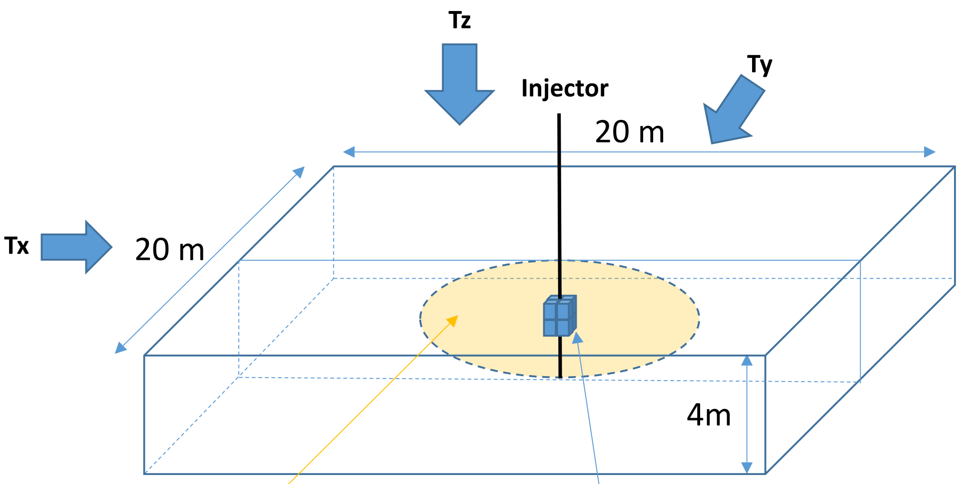

fracture

The eight elements at the center of the simulation domain are representing injection from the injector (dual injection points)

- Young's modulus (GPa) = 60
- Poisson's ratio = 0.25
- Svmax (MPa) = 60
- Shmin (MPa) = 40
- Permeability (nD) = 10
- Fluid: Water
- Injection rate (m^3/min/m)= 0.12
- Number of elements 100*100*20

Results: Fracture Half Length, Fracture Width, and Wellbore Pressure

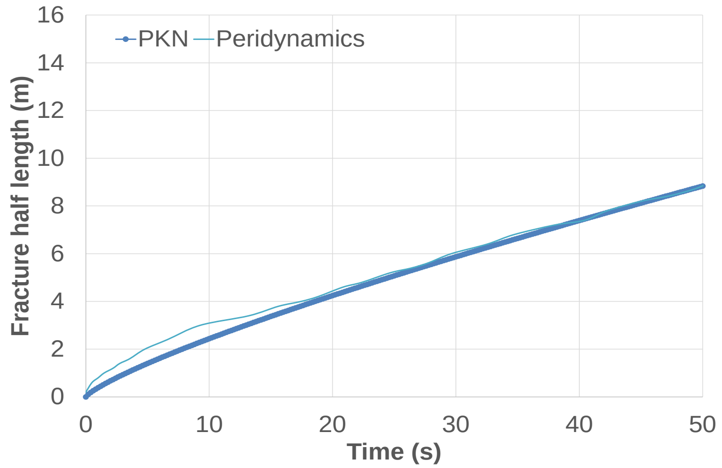

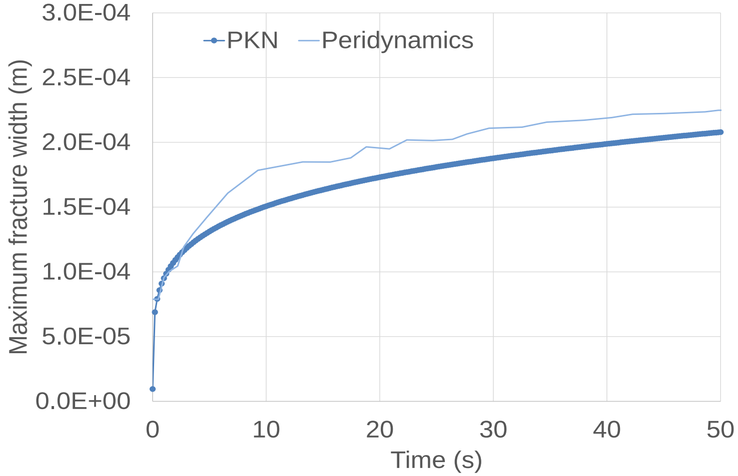

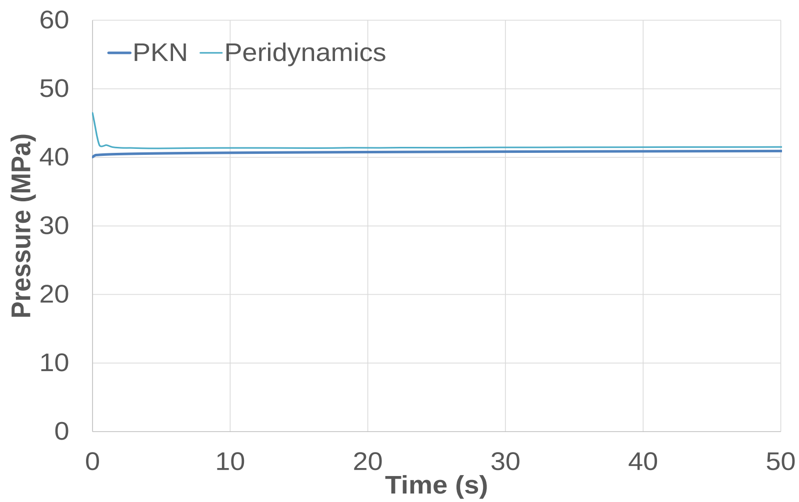

Effect of Reservoir Heterogeneities

Effect of Multi-Scale Heterogeneities

Different scale heterogeneities in the reservoir

layer scale (m order) heterogeneity

http://www.agilegeoscience.com/journal/2011/8/18/niobrara-shale-field-trip.html

How does this multi-scale heterogeneity affect fracture propagation?

sub-layer scale (cm order) heterogeneity

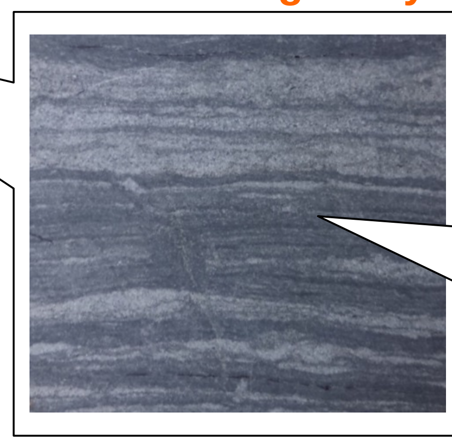

small scale heterogeneity (mm order)

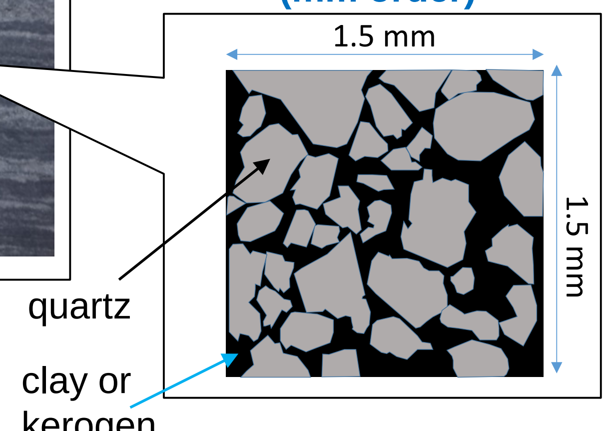

Effect of Layer Boundary

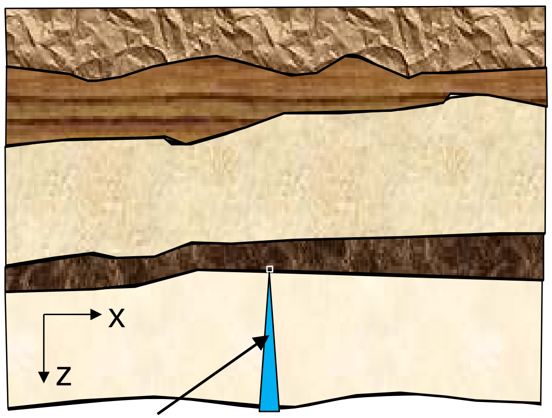

hydraulic fracture

In most of the hydraulic fracturing simulators, only **“crossing”** or **“stopping”** are simulated due to planar propagation assumption.

However, in many cases, fractures can show the following **characteristic propagation behaviors** near the layer interface other than “crossing” or “stopping”.

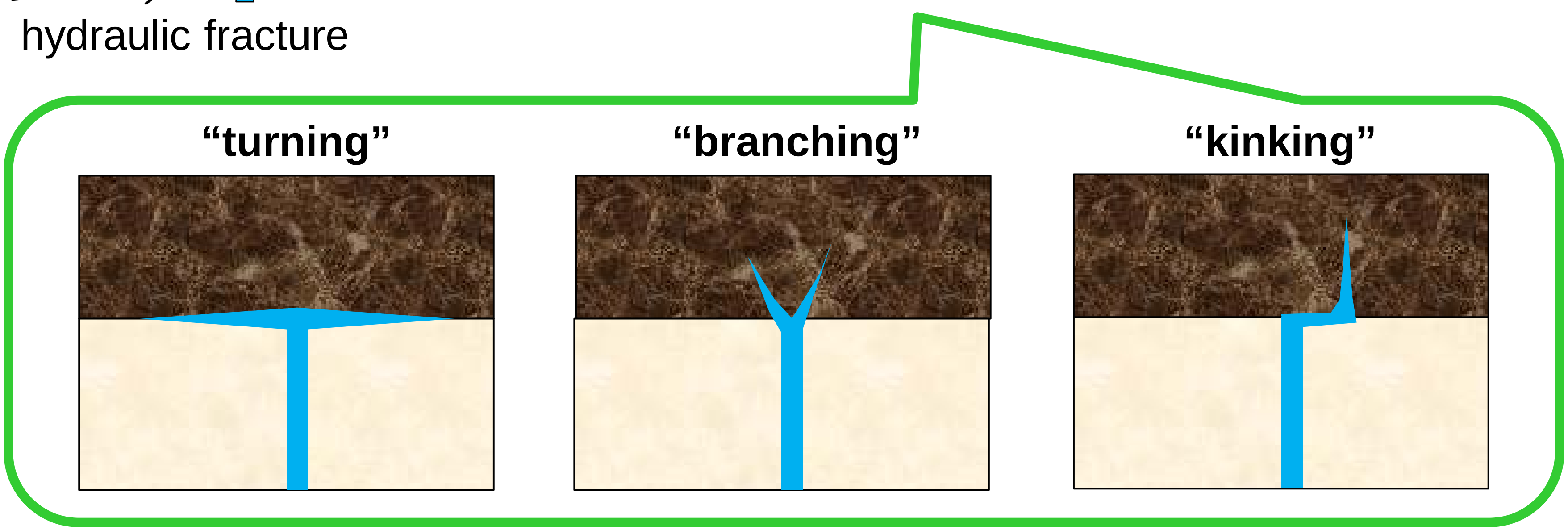

Fracture Propagation in Layered Rocks

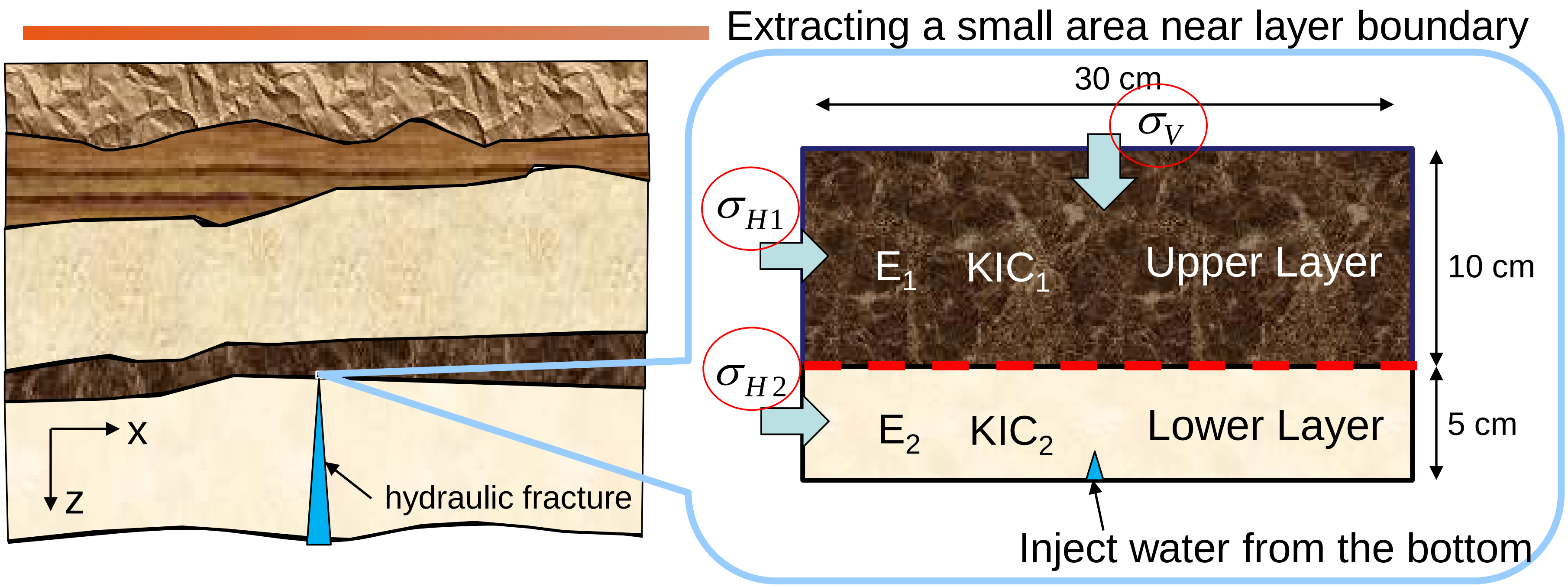

✓ Important parameters:

- **Horizontal-vertical stress contrast**
- **Young's modulus contrast**
- **Weak connection between layers**
- **Layer Dip**
- **Horizontal stress contrast**
- **Toughness contrast**

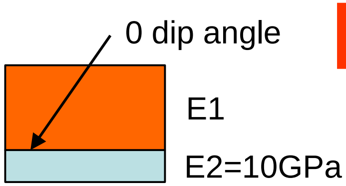

Effect of Layer Stresses
(0 degrees, E2 = 10 GPa)

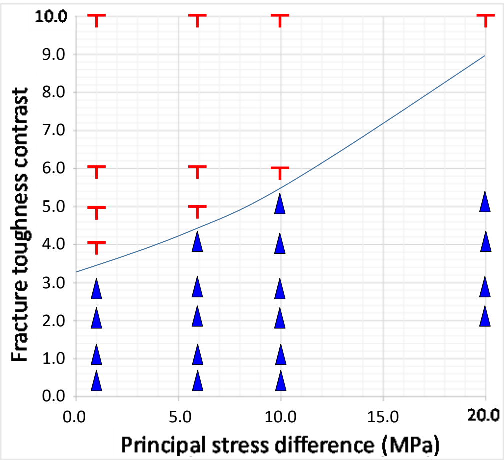

(a) E1 = 10 GPa

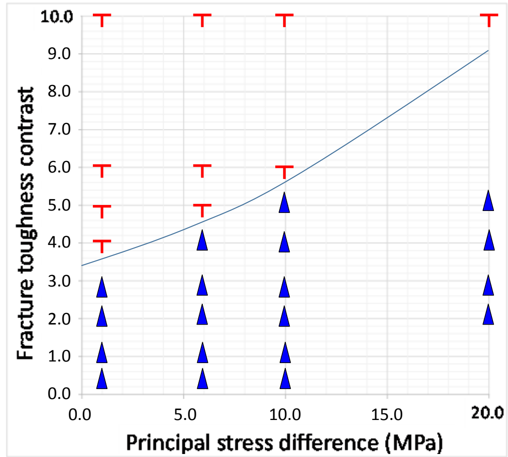

(b) E1 = 20 GPa

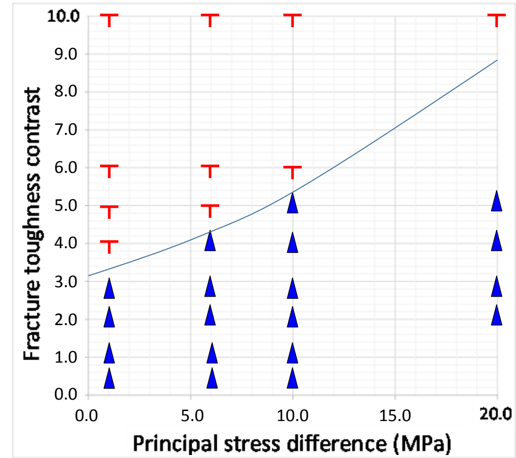

(c) E1 = 40 GPa

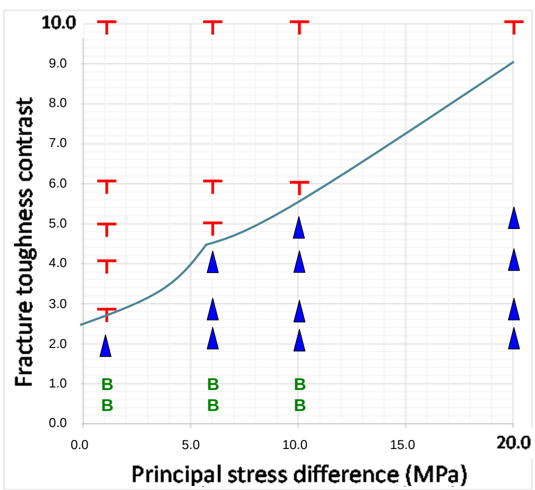

(d) E1 = 80 GPa

T : Turning
▲ : Crossing
B : Branching

Published shale data
Rijken and Cooke (2001)
E: 4.5 - 61.0 GPa
KIC: 0.7 - 2.16 MPa m$^{0.5}$

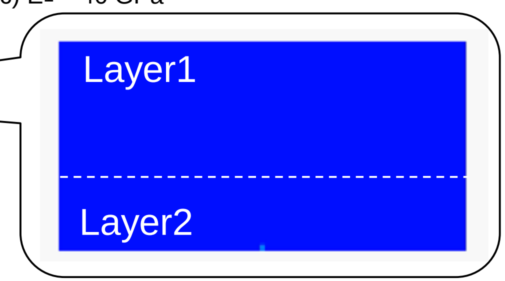

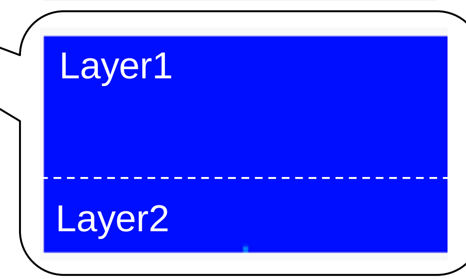

Turning and Branching

- "Turning" is strongly affected by **principal stress difference** and **fracture toughness contrast**.
  - A higher fracture toughness contrast
  - A smaller principal stress difference

  → More fracture turning

- Young's modulus contrast does not have a large influence on fracture turning along the layer interface.

- "Branching" occurs under the following conditions.
  - Very high Young's modulus contrast (> 8.0)
  - Low fracture toughness contrast (< 1.0)

  → e.g. upper layer = calcite vein
  (E = 83.8 GPa, KIC = 0.19 MPa $m^{0.5}$)

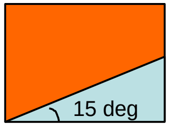

Effect of Dip Angle (15 degrees, E2 = 10 GPa)

But, “Kinking” is observed in most of the cases below the turning criteria.

ping angle cases.

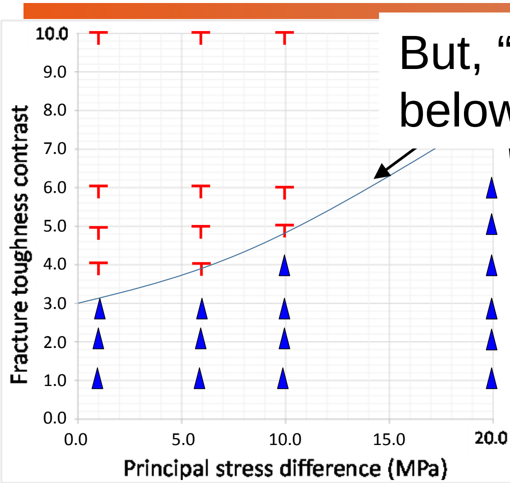

(a) E1 = 10 GPa

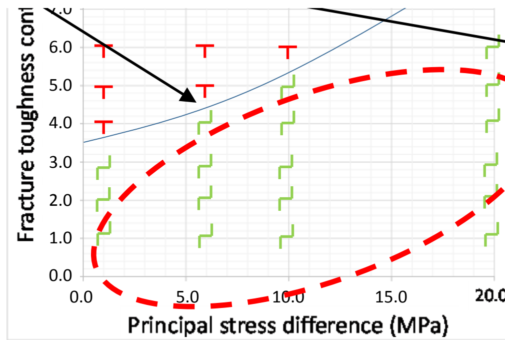

(b) E1 = 20 GPa

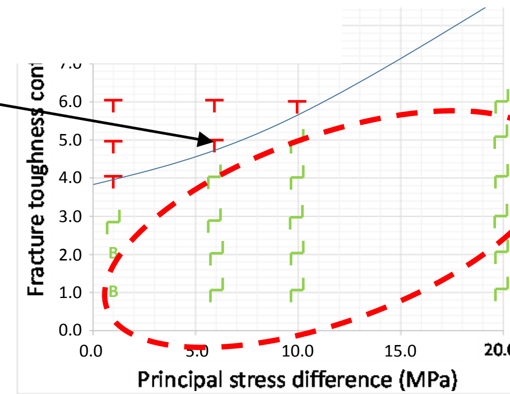

(c) E1 = 40 GPa

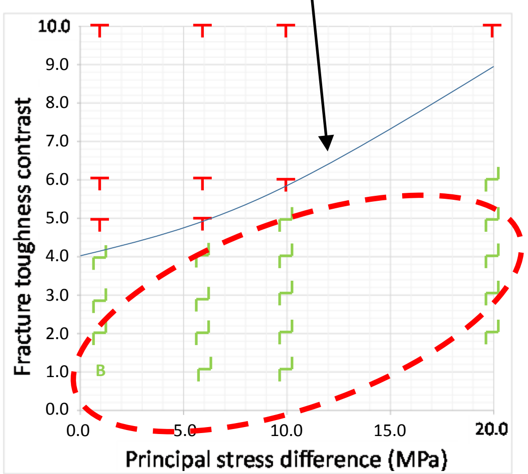

(d) E1 = 80 GPa

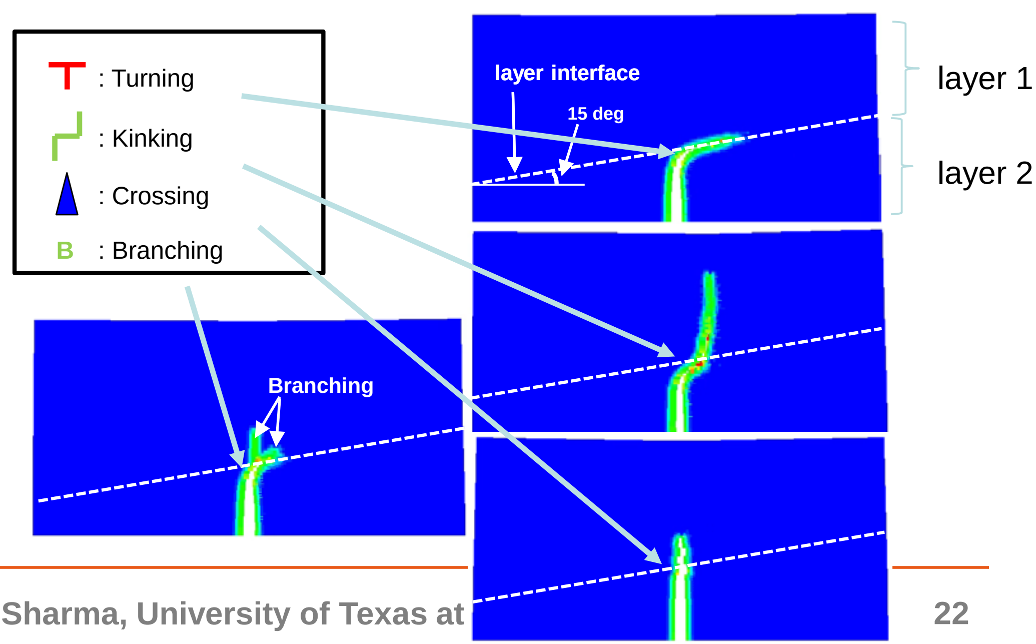

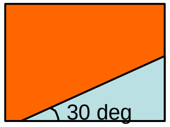

E1

E2=10GPa

Effect of Dip Angle (30 degrees, E2 = 10 GPa)

"Kinking" is observed in every case below the turning criteria.

"Turning" criteria in the high dipping angle cases becomes lower than the lower dipping angle cases.

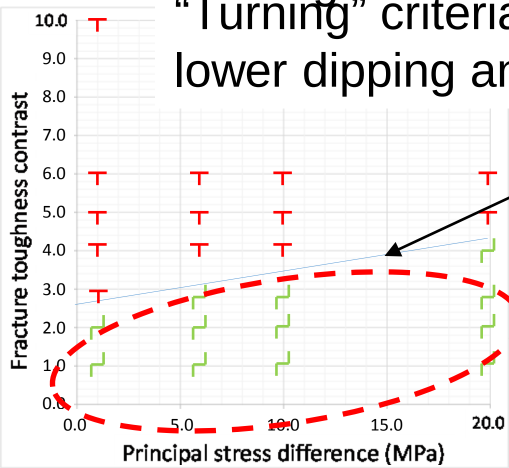

(a) E1 = 10 GPa

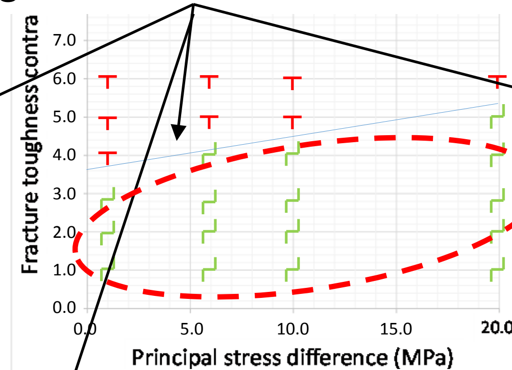

(b) E1 = 20 GPa

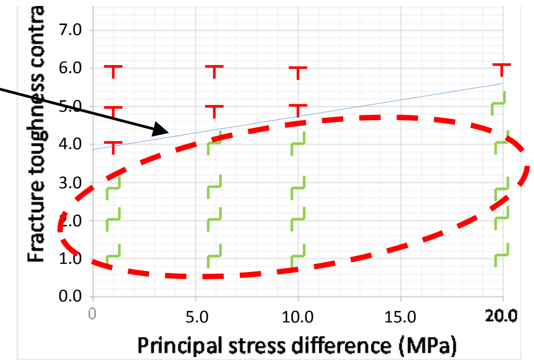

(c) E1 = 40 GPa

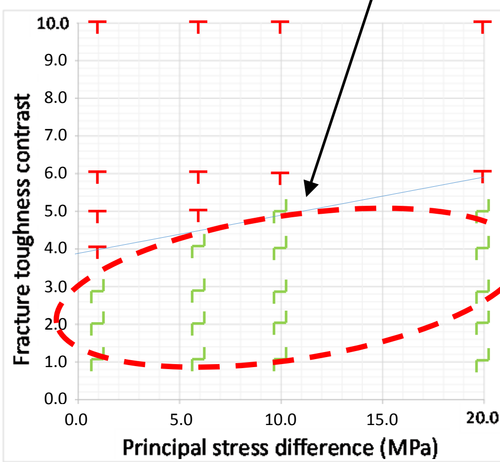

(d) E1 = 80 GPa

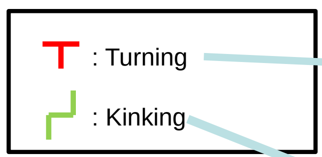

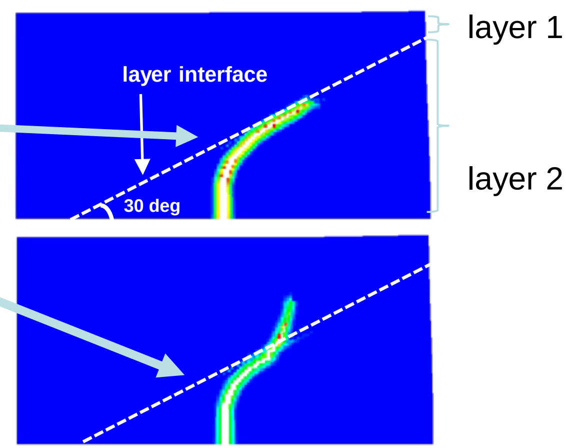

Mechanism of Kinking

The left side stress becomes higher due to smaller strain of upper layer. → The fracture turns to the right side.

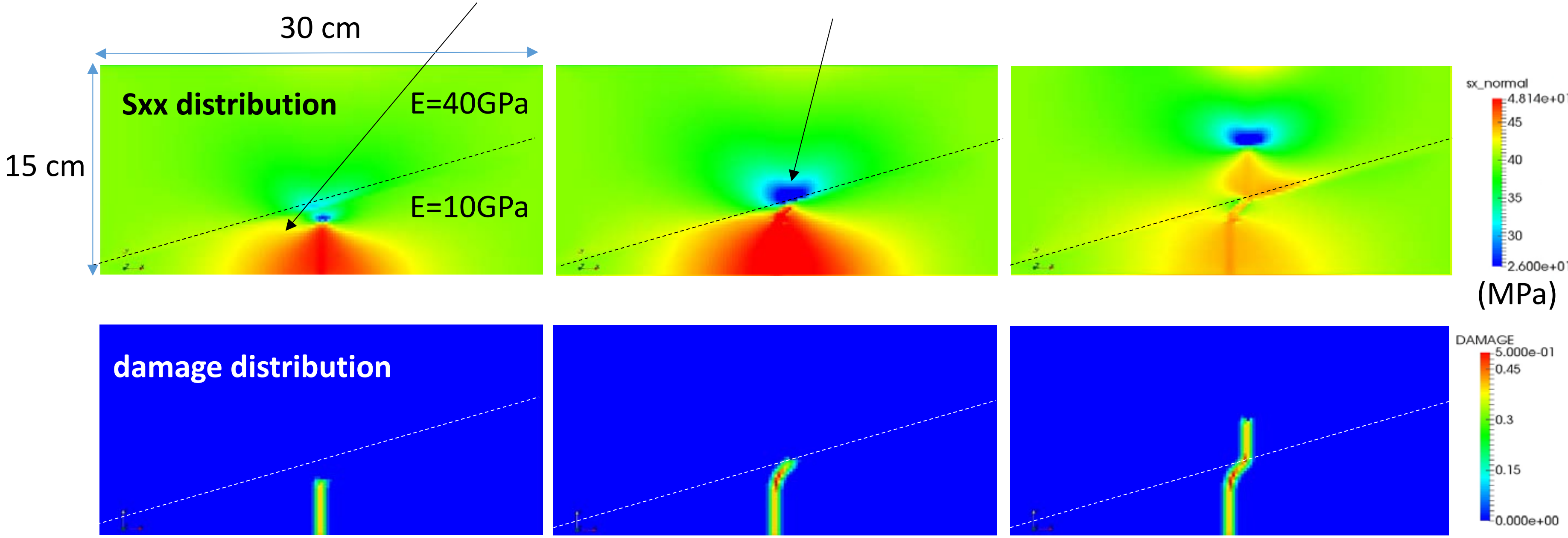

(a) after 0.27 sec (b) after 0.47 sec (c) after 0.5 sec (fraction)

The left side of the fracture is difficult to deform due to the high Young's modulus.

↓

The fracture turns as if avoiding the layer interface.

Effect of Young's modulus contrast on "kinking"

Kinking angle increases with the Young's modulus contrast.

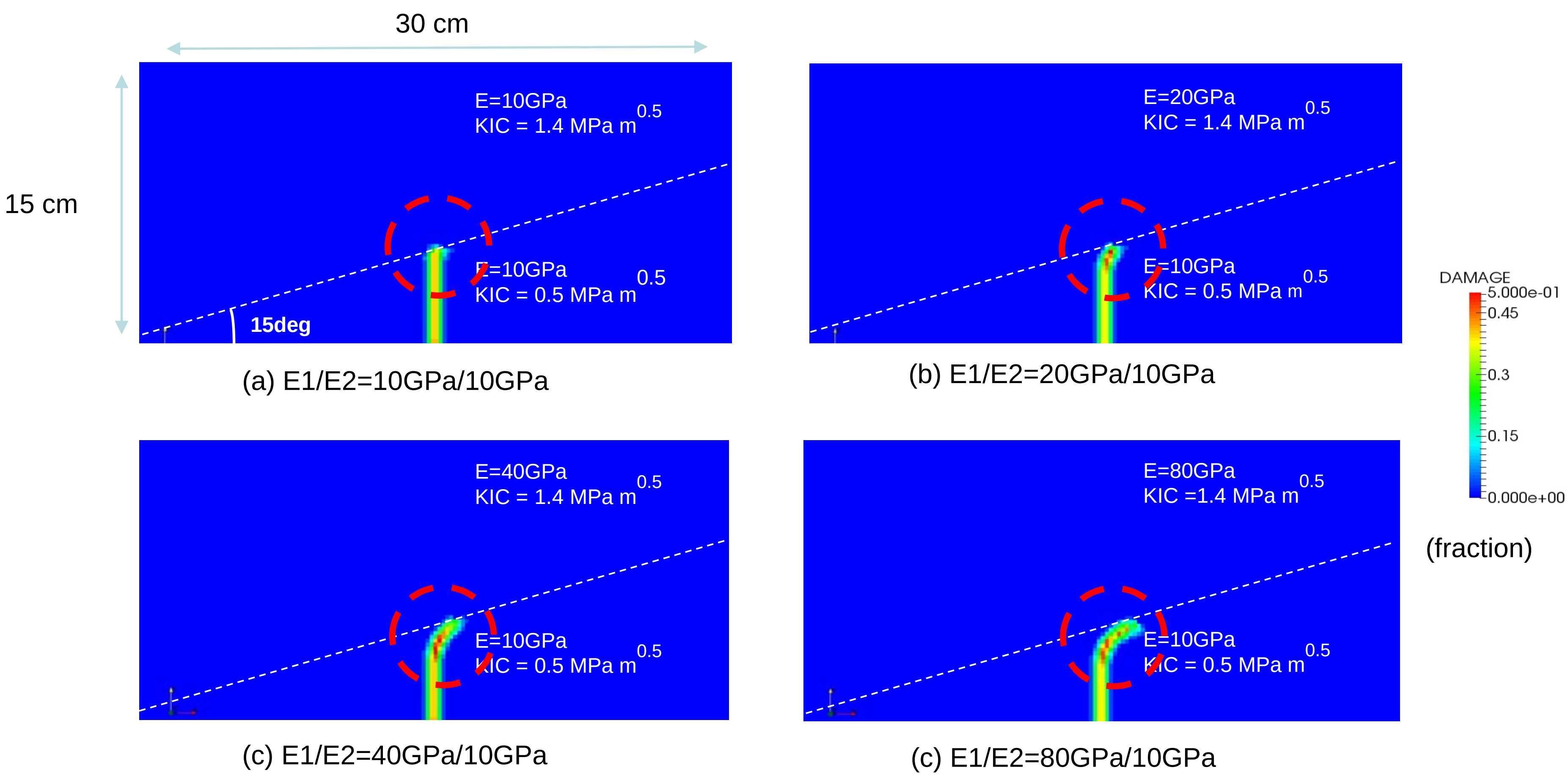

(a) E1/E2=10GPa/10GPa

(b) E1/E2=20GPa/10GPa

(c) E1/E2=40GPa/10GPa

(c) E1/E2=80GPa/10GPa

Effect of fracture toughness contrast on “kinking”

Kinking angle does not depend on the fracture toughness contrast.

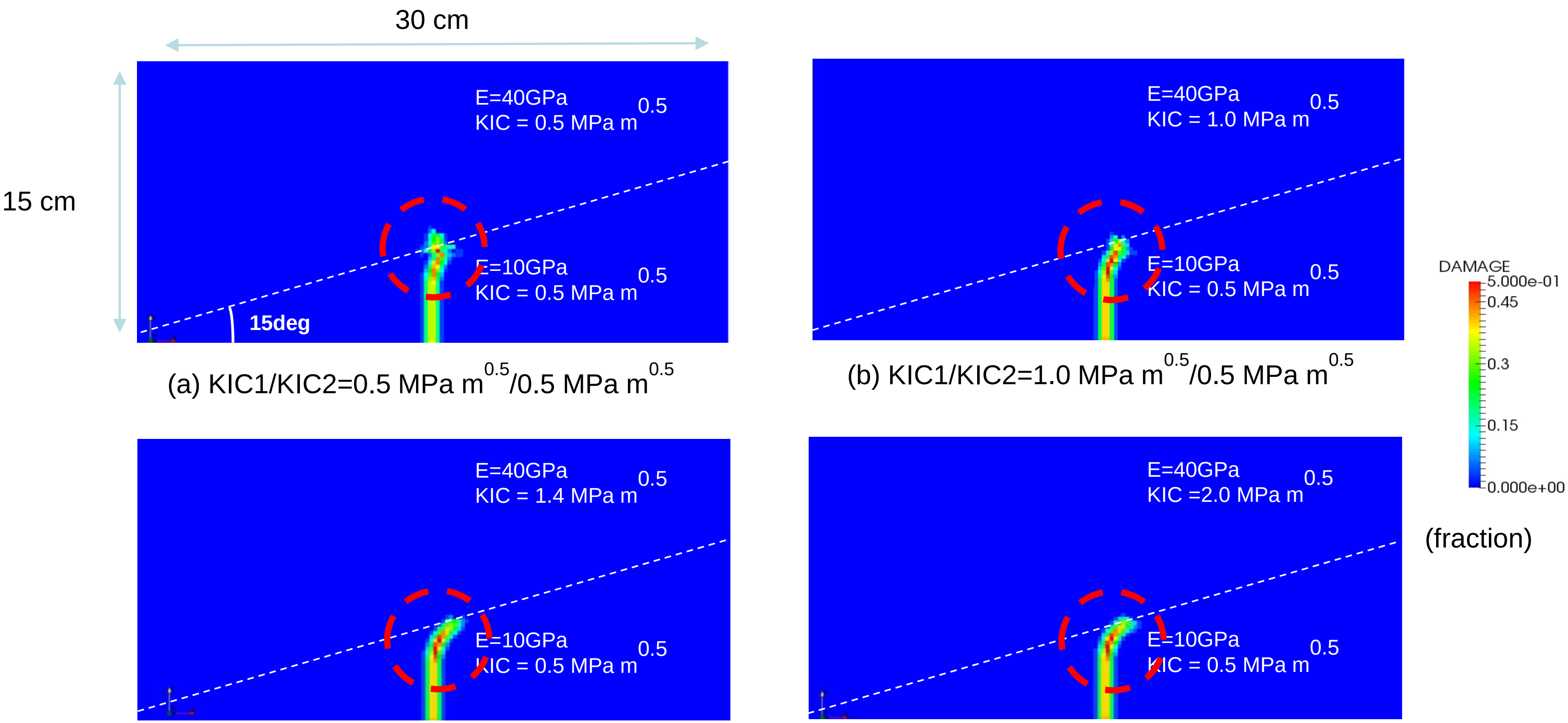

(a) KIC1/KIC2=0.5 MPa $m^{0.5}$/0.5 MPa $m^{0.5}$

(b) KIC1/KIC2=1.0 MPa $m^{0.5}$/0.5 MPa $m^{0.5}$

(c) KIC1/KIC2=1.4 MPa $m^{0.5}$/0.5 MPa $m^{0.5}$

(d) KIC1/KIC2=2.0 MPa $m^{0.5}$/0.5 MPa $m^{0.5}$

Effect of principal stress difference on “kinking”

Kinking angle decreases with increase in stress contrast.

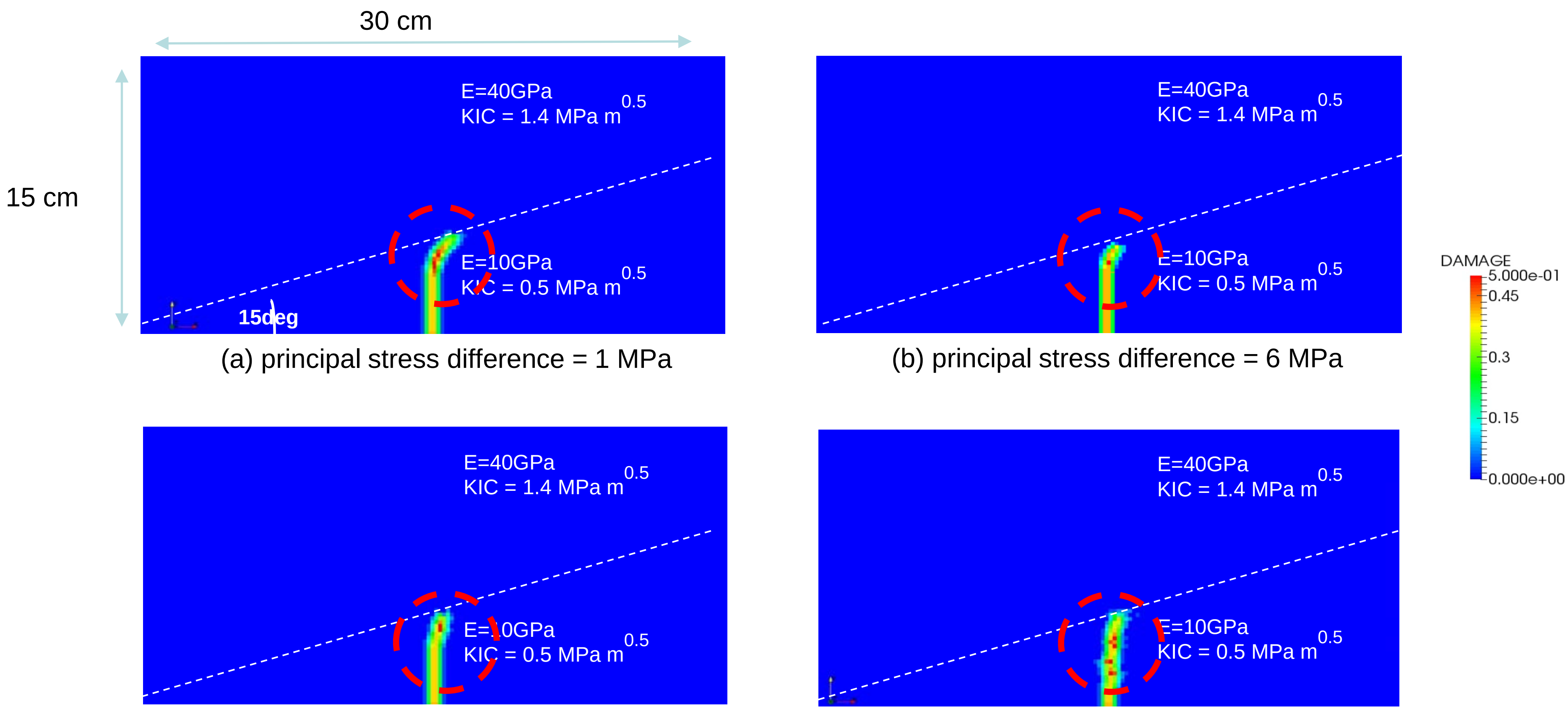

(a) principal stress difference = 1 MPa

(b) principal stress difference = 6 MPa

(c) principal stress difference = 10 MPa

(d) principal stress difference = 20 MPa

Effect of layer dip angle on “kinking”

Higher layer dip angle leads to more kinking.

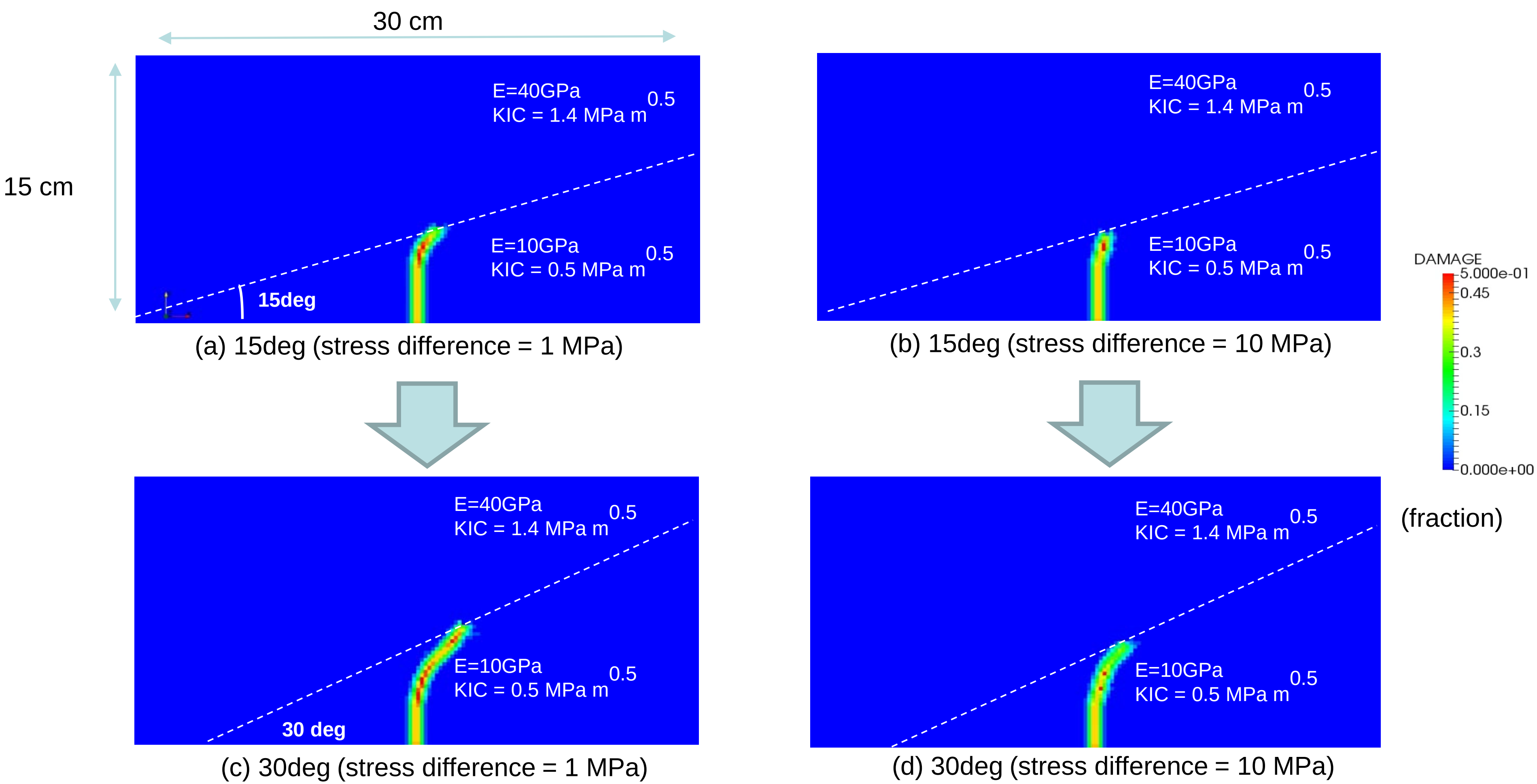

Effect of Bed Dip

If the upper layer is thinner?

3 different layer thickness models

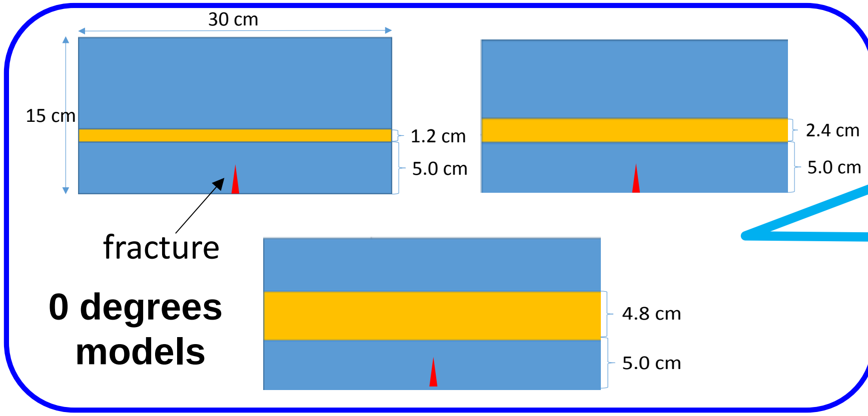

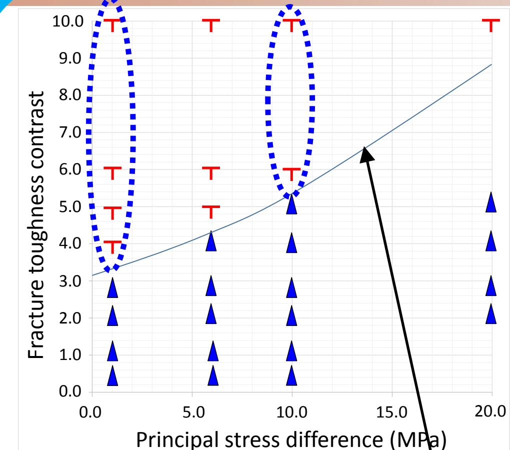

0degree: E1/E2 = 40 GPa / 10 GPa

How the criteria changes with bed dip?

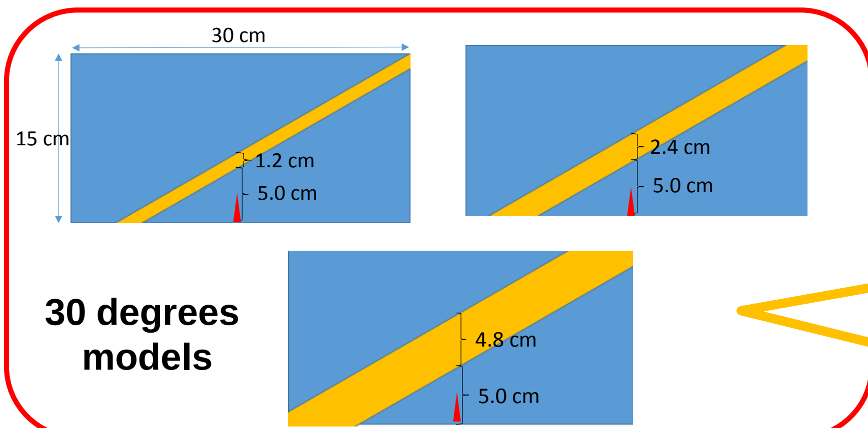

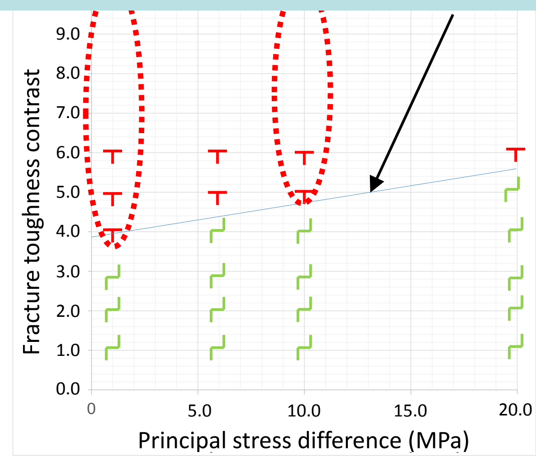

30degree: E1/E2 = 40 GPa / 10 GPa

Effect of Layer Thickness (0 degrees cases)

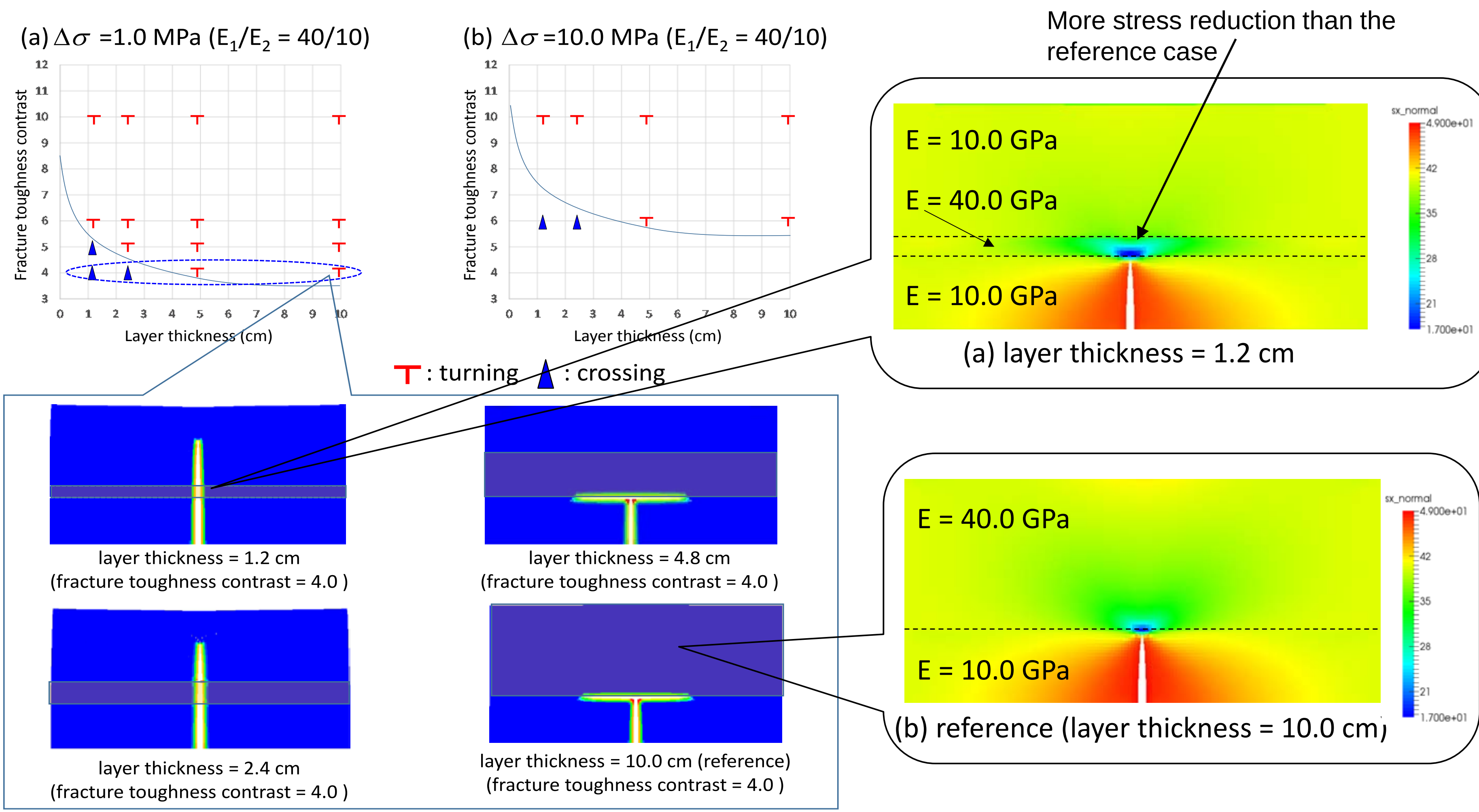

Effect of Layer Thickness (30 degrees cases)

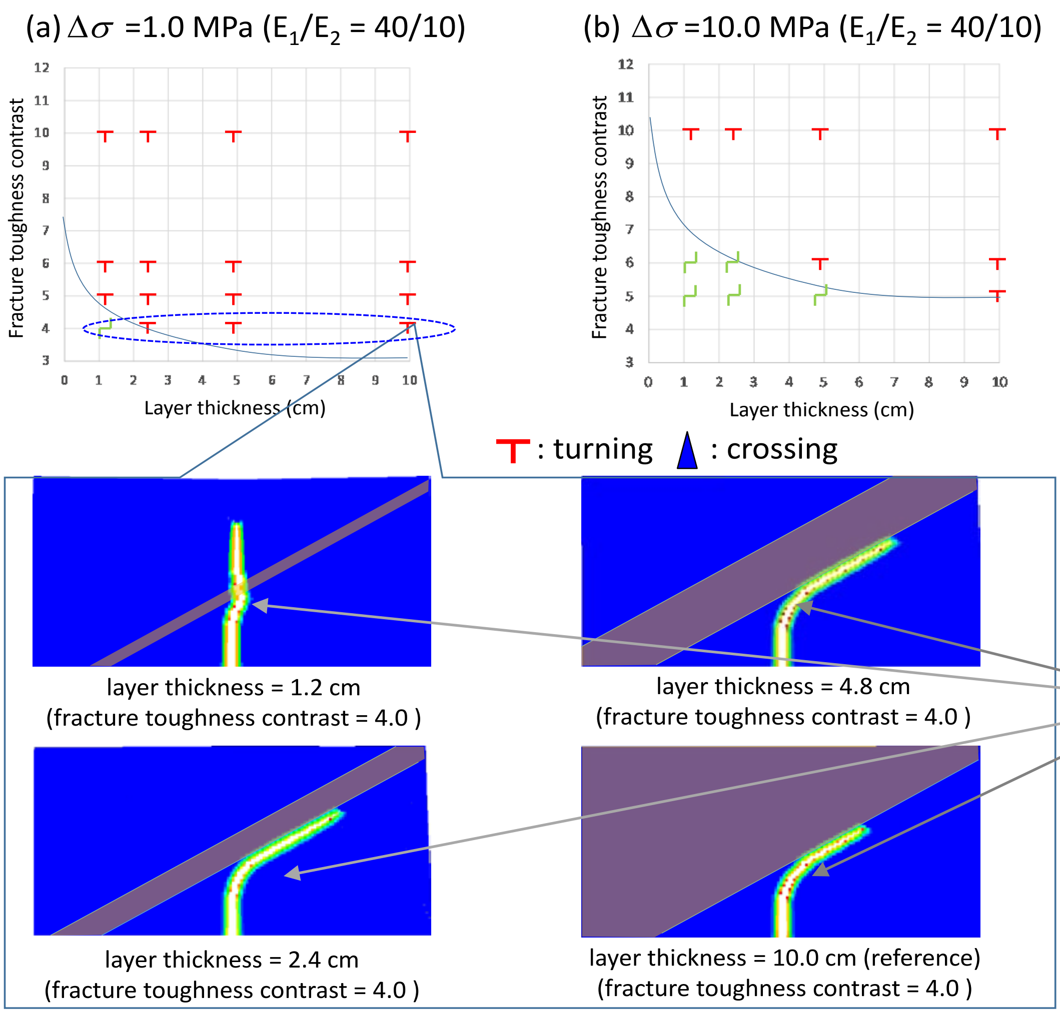

- Turning criteria is strongly affected by the upper layer thickness.
- However, the magnitude of kinking is not affected by the upper layer thickness.

The kinking angles are almost same regardless of the upper layer thickness.

Effect of Weak Surface

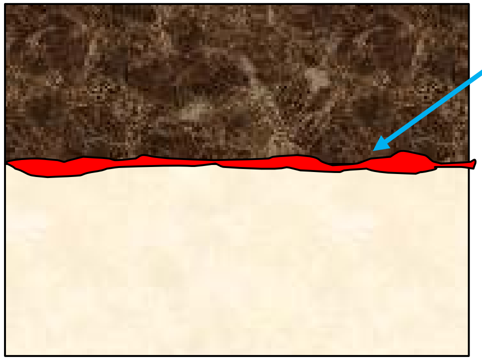

If the layer interface is damaged for some reason, how do the turning criteria change?

Investigating the same cases as the previous fully-bonded cases by setting the following shear failure criteria

- Shear coefficient = 0.6
- Cohesion = 0.0 MPa

Effect of Weak Surface (0 degrees cases)

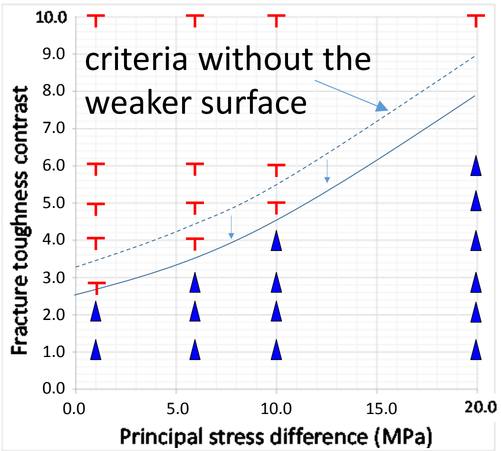

(a) E_1/E_2 = 10 GPa/10 GPa

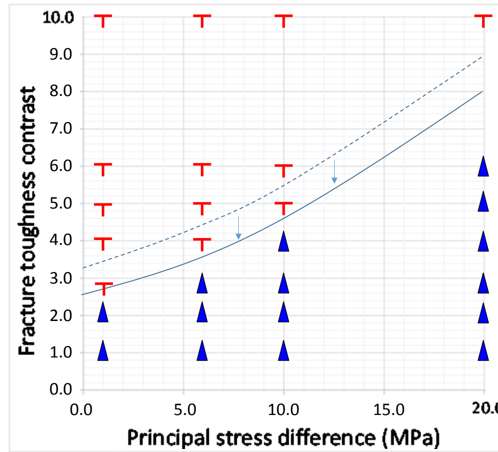

(b) E_1/E_2 = 20 GPa/10 GPa

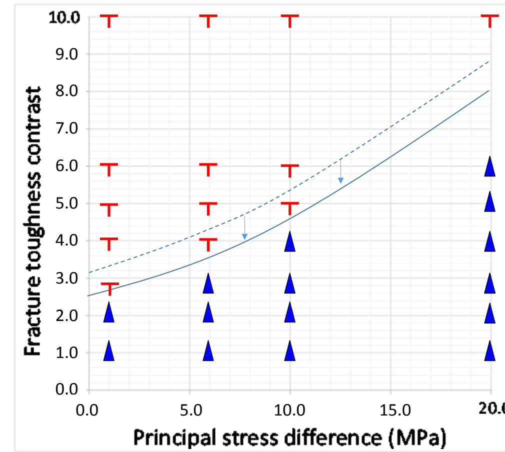

(c) E_1/E_2 = 40 GPa/10 GPa

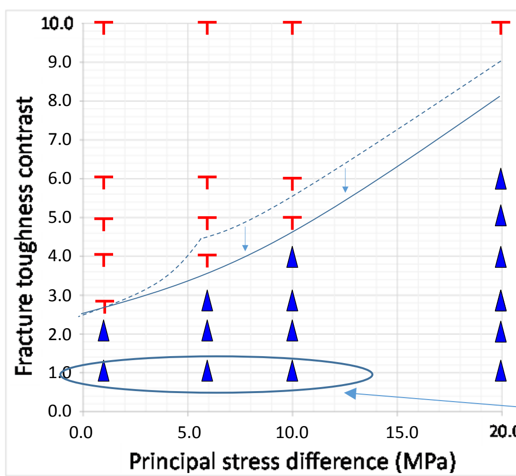

(d) E_1/E_2 = 80 GPa/10 GPa

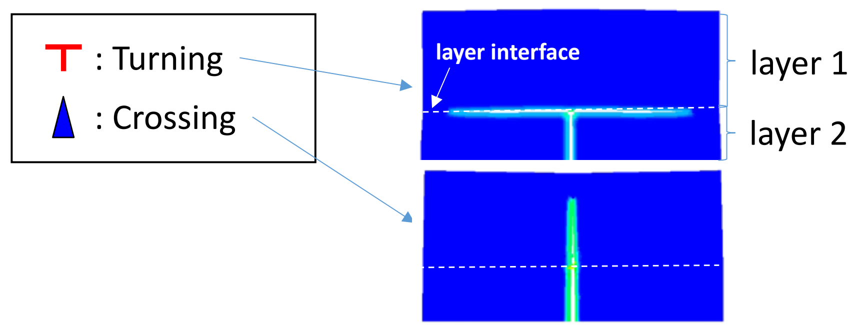

Branching region disappear

Effect of Weak Surface (30 degrees cases)

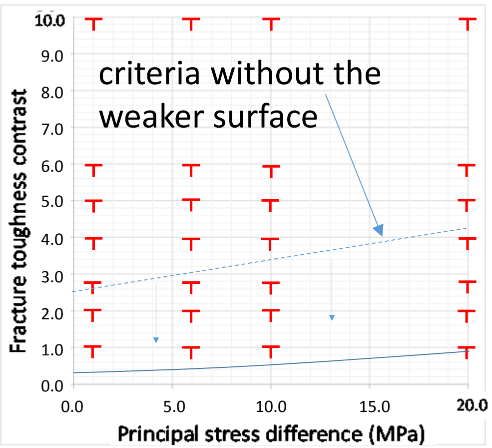

(a) E_1/E_2 = 10 GPa/10 GPa

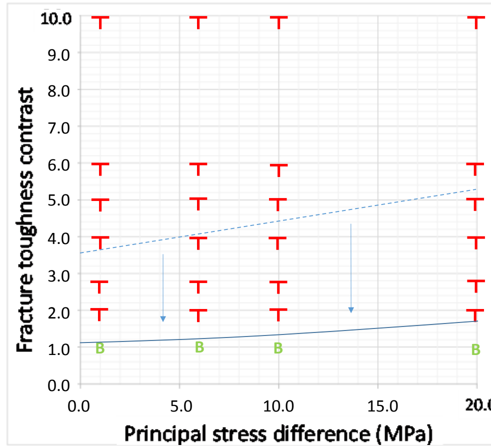

(b) E_1/E_2 = 20 GPa/10 GPa

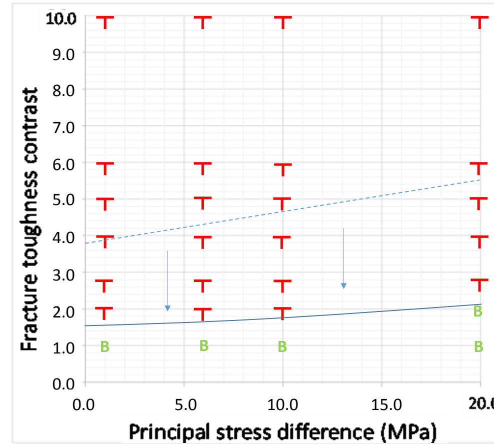

(c) E_1/E_2 = 40 GPa/10 GPa

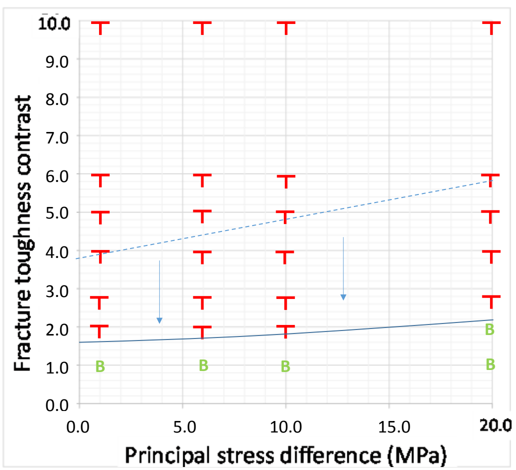

(d) E_1/E_2 = 80 GPa/10 GPa

T : Turning

B : Branching

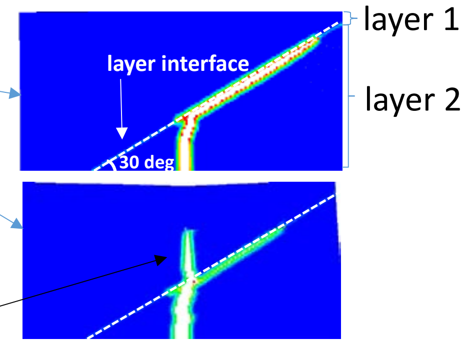

Different type of branching appears in these case.

Effect of cm Scale Sub-Layers

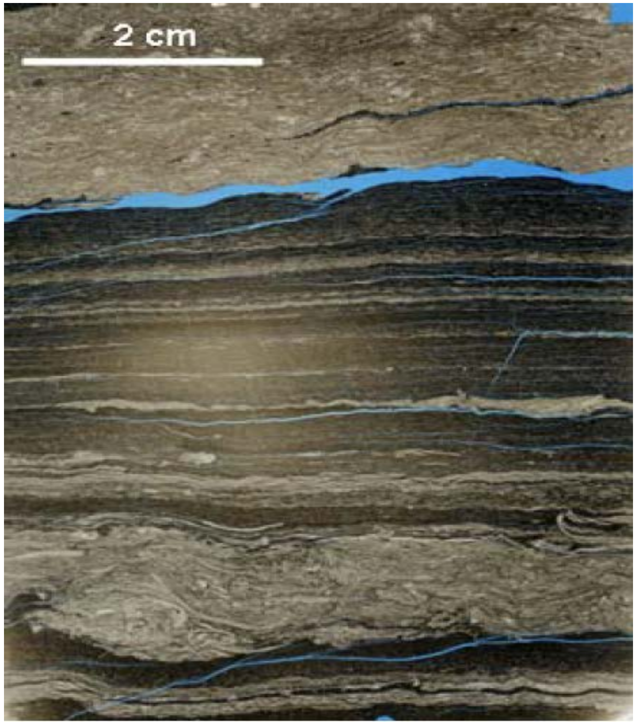

Passey, Q.R., et al. (2010)

Represented by two different models with changing layer dip angle

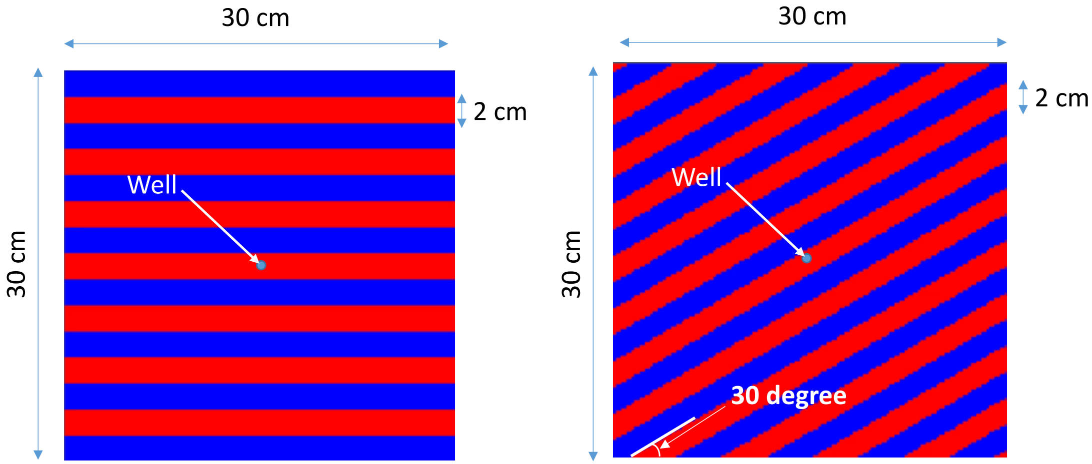

(a) 0 degrees model **(b) 30 degrees model**

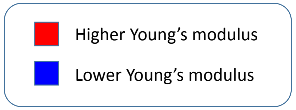

Shale reservoirs are filled with cm scale heterogeneities (sub-layers)

Investigating how multiple layers affect fracture propagation

Effect of cm Scale Sub-Layers (Case Settings)

Principal Stress Difference = 20 MPa (Shmin = 40 MPa, Svmax = 60 Mpa)

Case	Young's modulus 1 (GPa)	Young's modulus 2 (GPa)	Fracture toughness 1 (MPa $m^{0.5}$)	Fracture toughness 2 (MPa $m^{0.5}$)	Energy release rate contrast between layers (hard layer/soft layer)	Layer dip angle
low_contrast	10	20	0.5	0.707	1.00	0
middle_contrast	10	40	0.5	1.000	1.00	0
high_contrast	10	80	0.5	1.414	1.00	0
high_contrast_2	10	80	0.5	0.707	0.25	0
low_contrast_dipping	10	20	0.5	0.707	1.00	30
middle_contrast_dipping	10	40	0.5	1.000	1.00	30
high_contrast_dipping	10	80	0.5	1.414	1.00	30
high_contrast_2_dipping	10	80	0.5	0.707	0.25	30

The relationship among energy release rate, fracture toughness, Poisson's ratio, and Young's modulus in 2-D plane strain condition.

$$G_c = \frac{K_{IC}{}^2\left(1-\nu^2\right)}{E}$$

Effect of cm Scale Sub-Layers (0 degrees: Low and Middle E Contrast)

E1/E2 = 20/10; KIC1/KIC2 = 0.7/0.5; Dip angle = 0

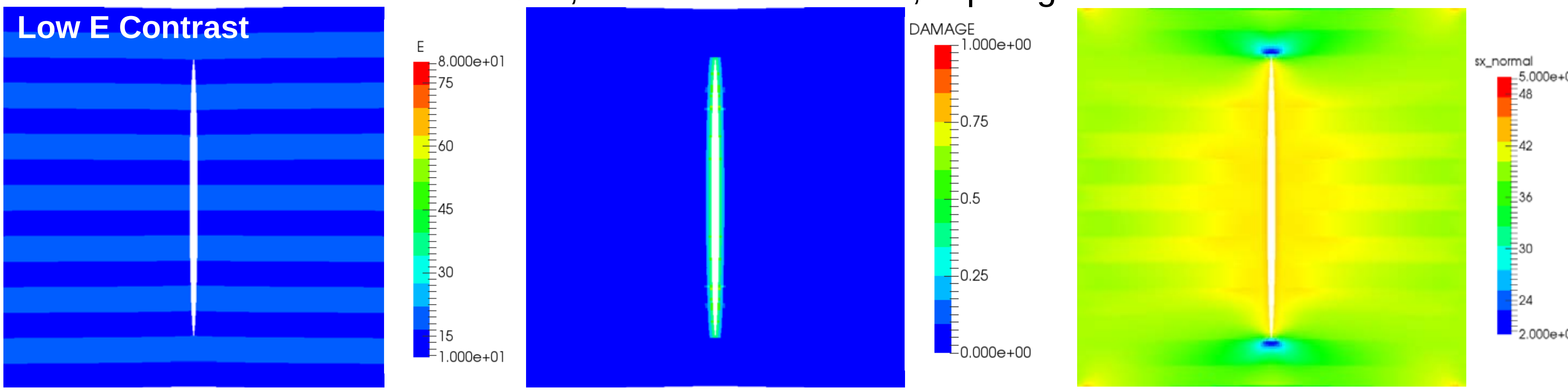

Young's modulus **Damage** **Sxx (MPa)**

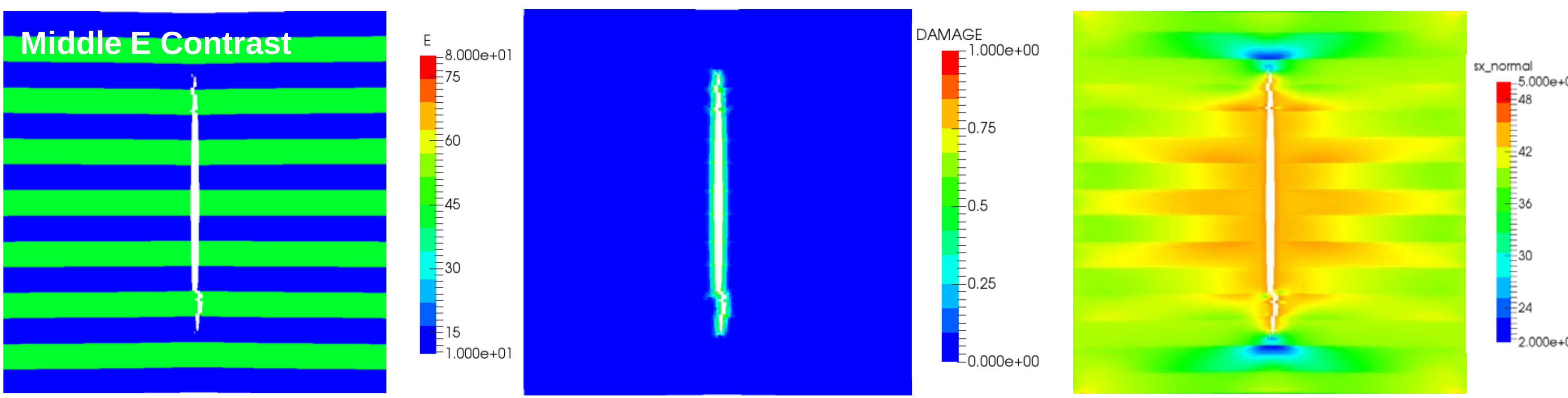

E1/E2 = 40/10; KIC1/KIC2 = 1.0/0.5; Dip angle = 0

Effect of cm Scale Sub-Layers (0 degrees: High E Contrast)

E1/E2 = 80/10; KIC1/KIC2 = 1.4/0.5; Dip angle = 0

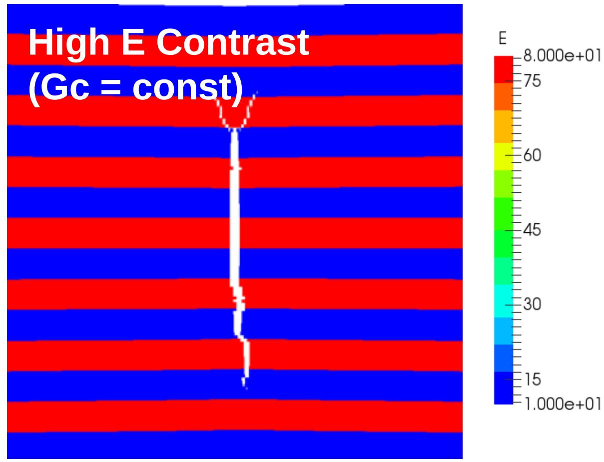

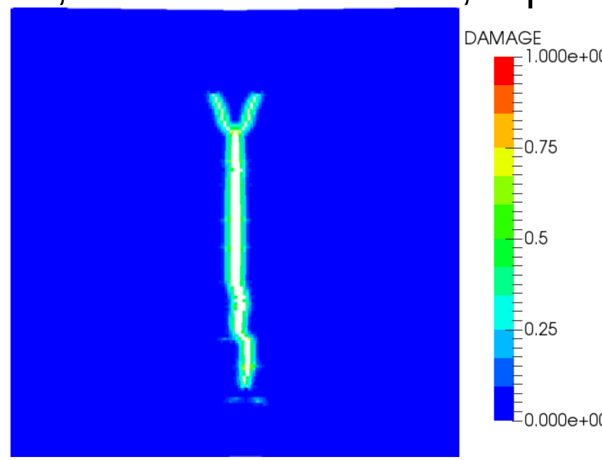

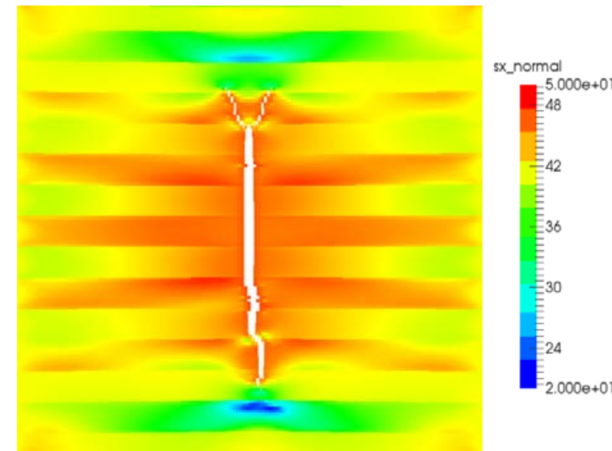

Young's modulus **Damage** **Sxx (MPa)**

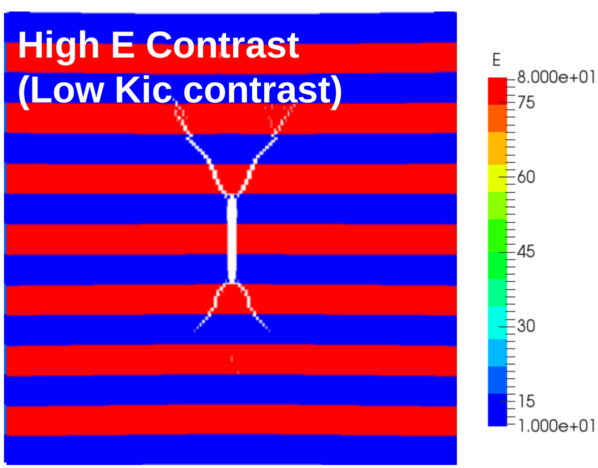

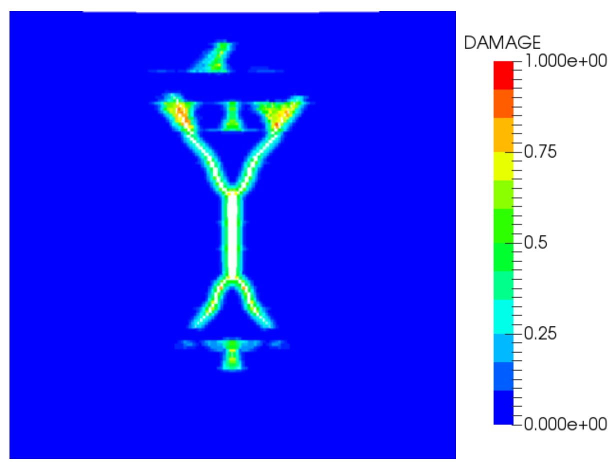

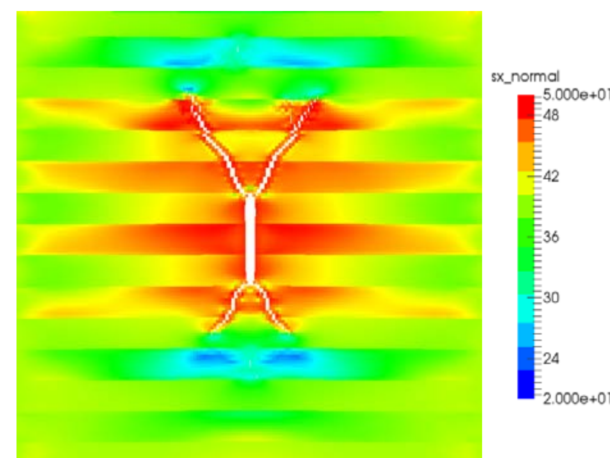

E1/E2 = 80/10; KIC1/KIC2 = 0.7/0.5; Dip angle = 0

Effect of cm scale sub-layers (30 degrees: Low and Middle E Contrast)

E1/E2 = 20/10; KIC1/KIC2 = 0.7/0.5; Dip angle = 30

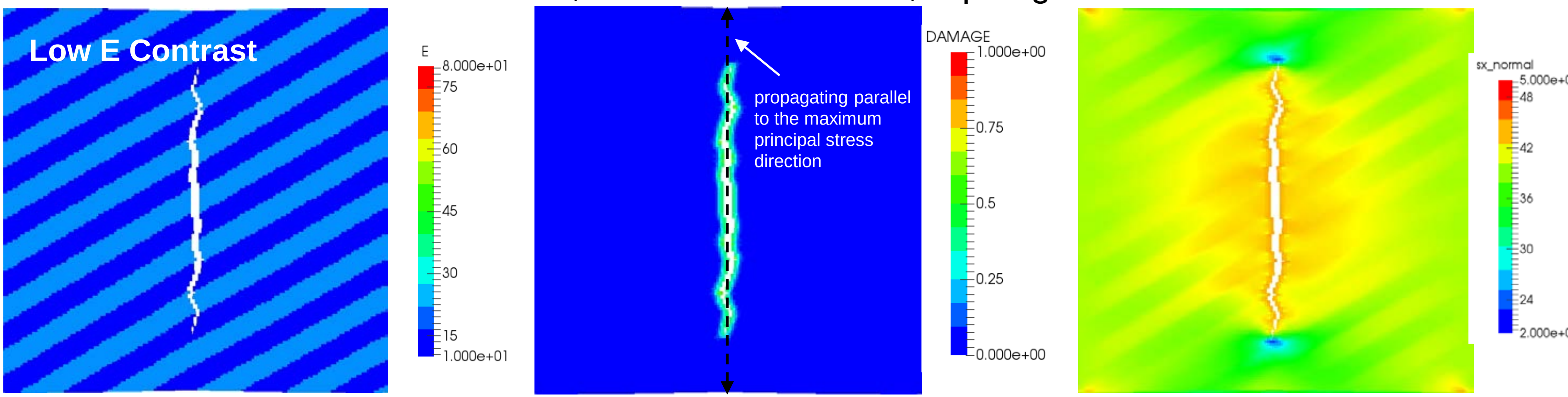

Young's modulus | Damage | Sxx (MPa)

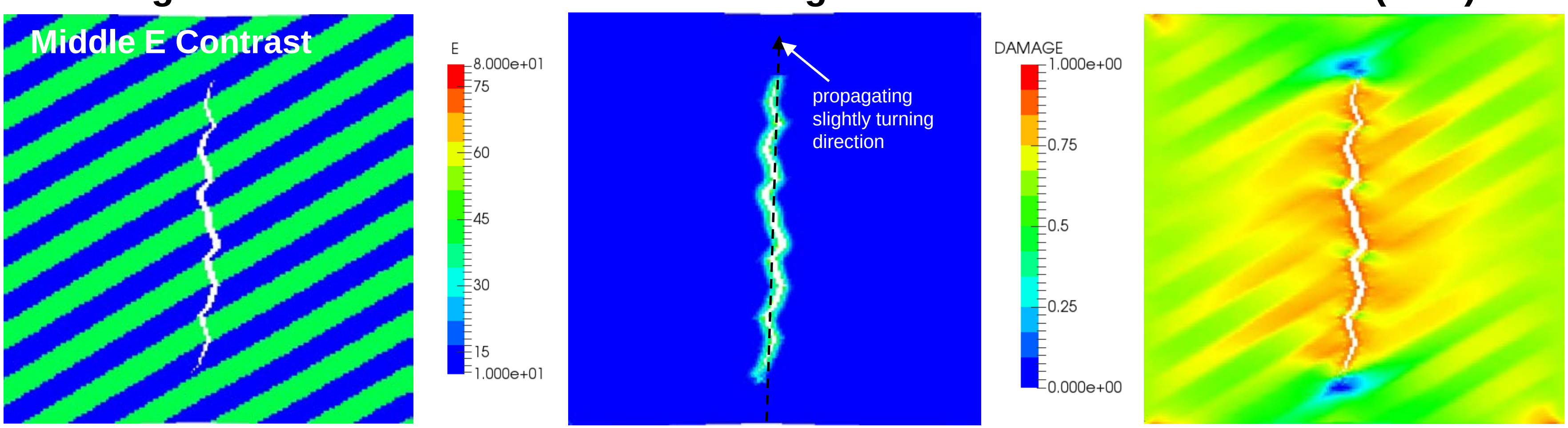

E1/E2 = 40/10; KIC1/KIC2 = 1.0/0.5; Dip angle = 30

Effect of cm scale sub-layers (30 degrees: High E Contrast)

E1/E2 = 80/10; KIC1/KIC2 = 1.4/0.5; Dip angle = 30

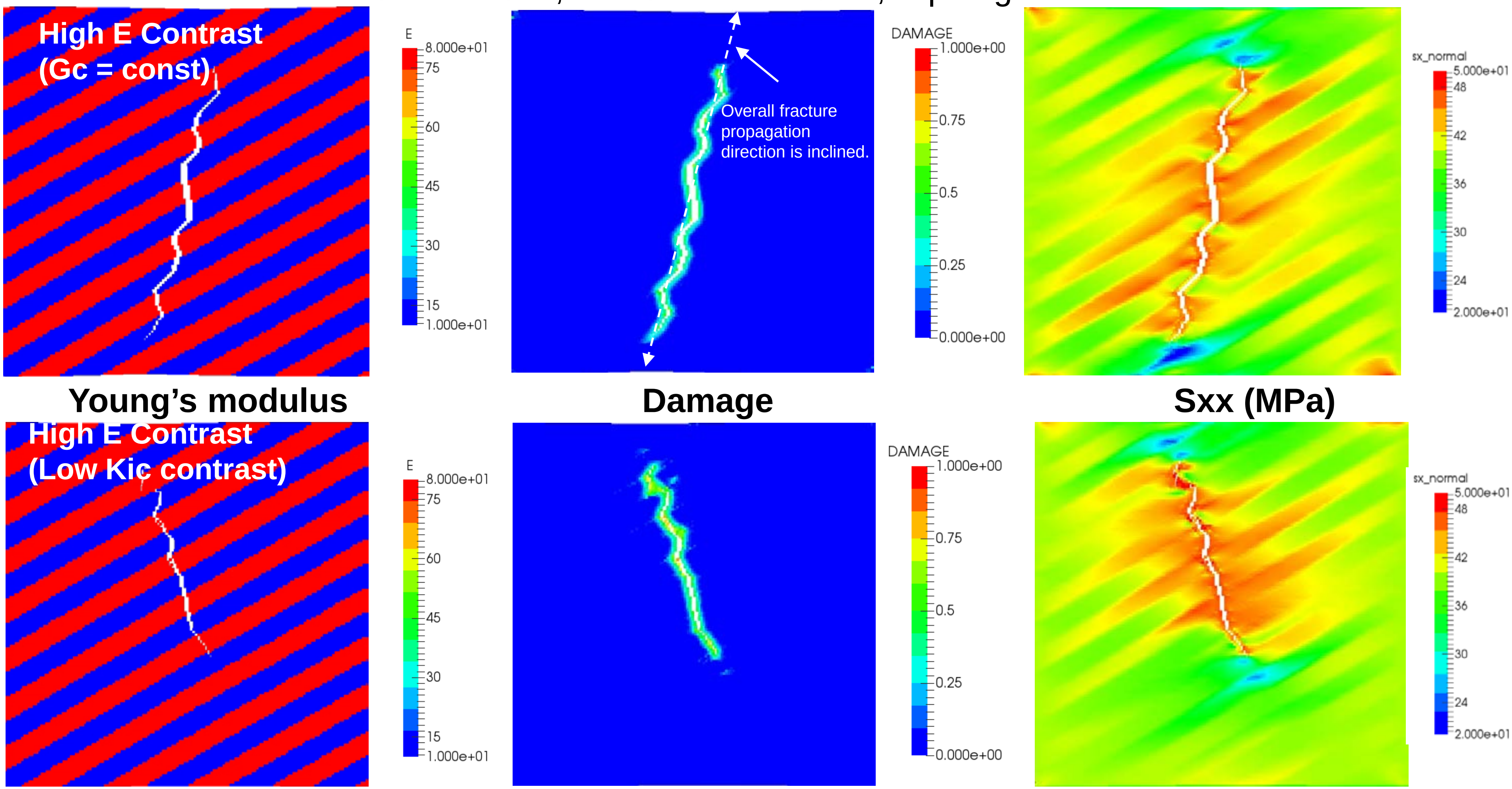

E1/E2 = 80/10; KIC1/KIC2 = 0.7/0.5; Dip angle = 30

Effect of Pore Scale Heterogeneity

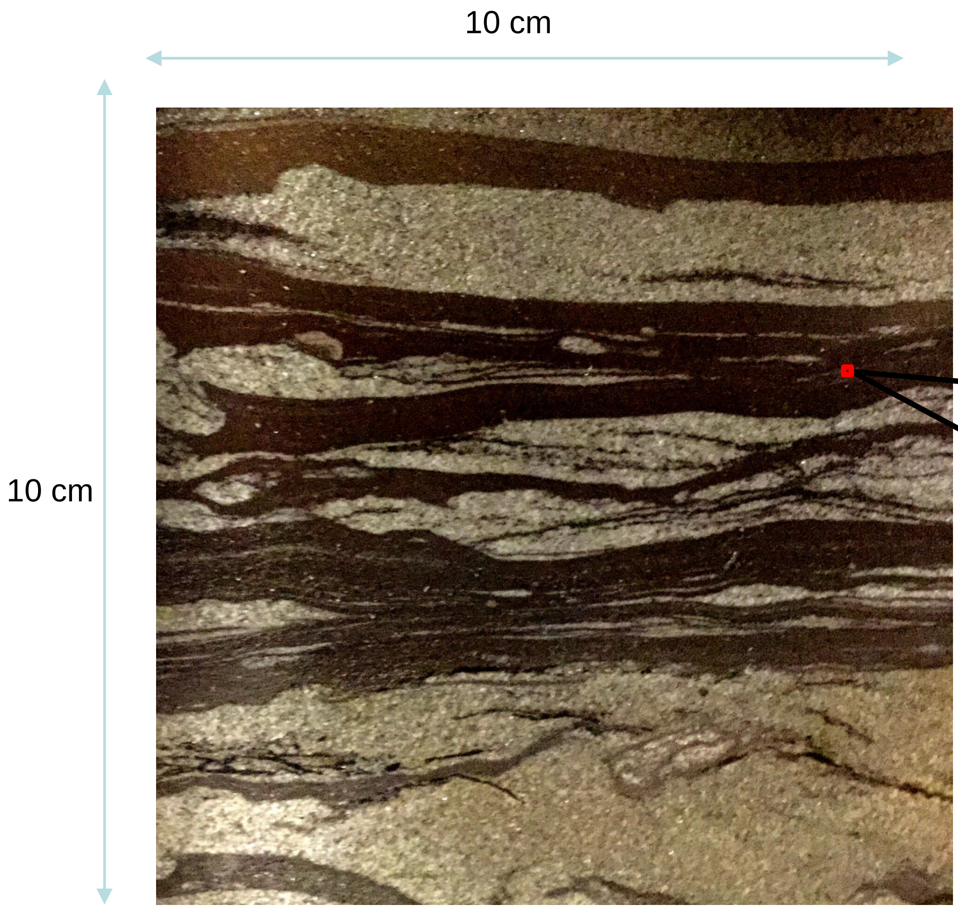

Core scale heterogeneity

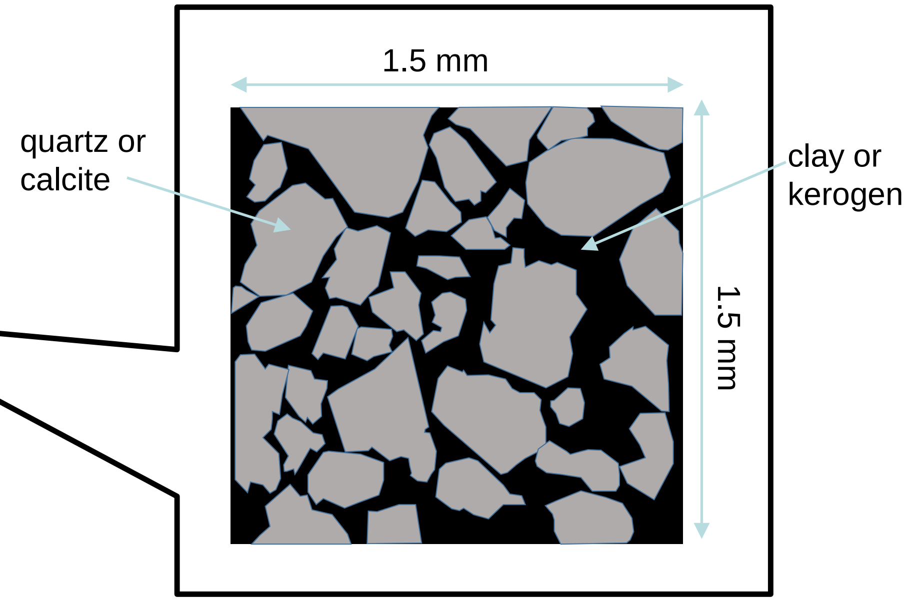

Pore scale heterogeneity

Effect of Pore Scale Heterogeneity (Model Construction)

(1) Borrowing the shape of minerals from the original picture

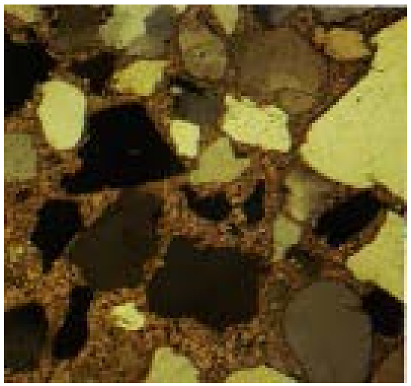

Carozzi (1993)

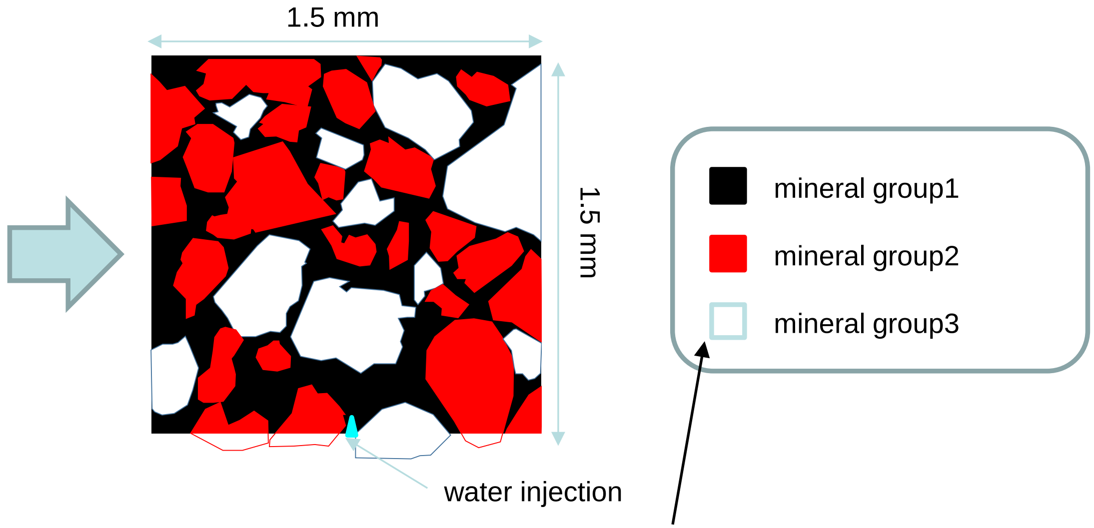

(2) Applying one of these properties to each mineral group

Mineral type	Young's modulus (GPa)	Shear modulus (GPa)	Fracture toughness (MPa $m^{0.5}$)
Quartz	95.6	44.3	2.40
Calcite	83.8	32.0	0.19
Clay	10.0	4	0.50

Effect of Pore Scale Heterogeneity (Case Settings)

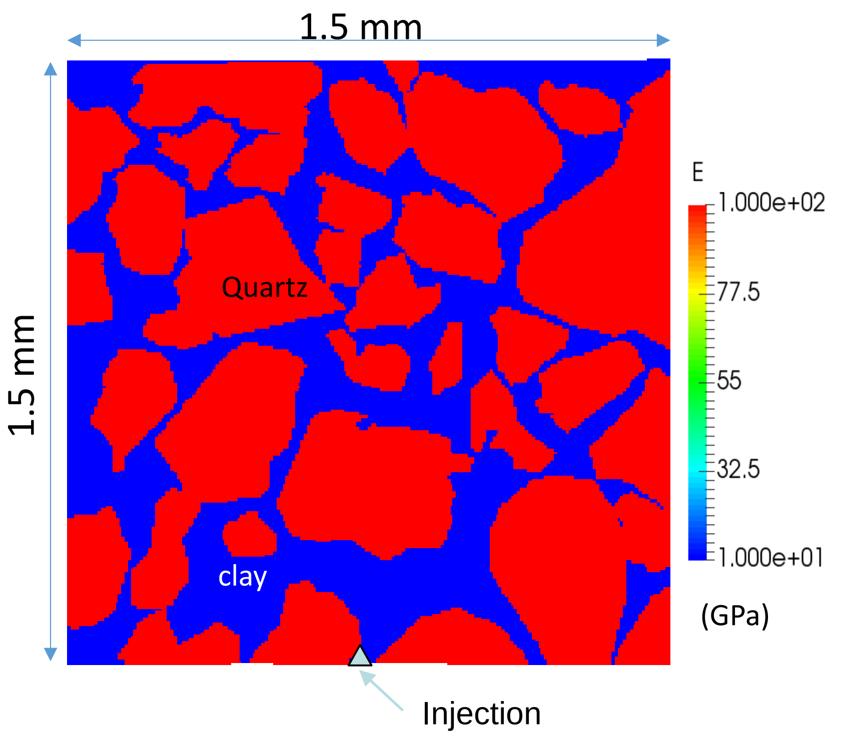

Case 1: **Quartz + Clay**
(mineral connections : **fully bonded**)

Case 2: **Quartz + Clay**
(mineral connections: **damaged**)

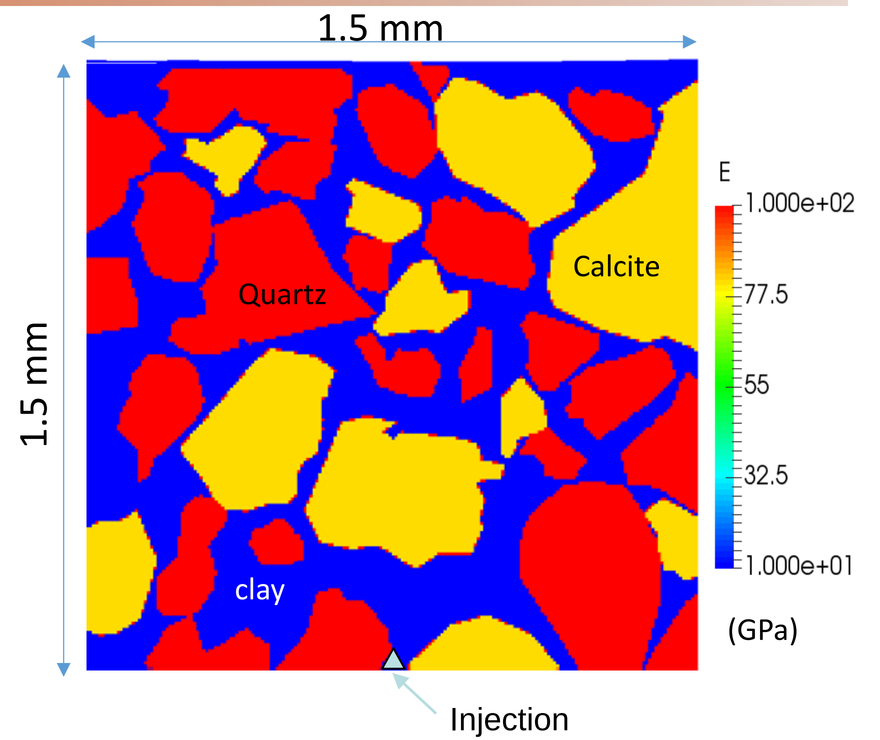

Case 3: **Quartz + Calcite + Clay**
(mineral connections : **fully bonded**)

Case 4: **Quartz + Calcite + Clay**
(mineral connections: **damaged**)

Case 1: Quartz + Clay
No Interface Damage

Fracture initially propagates in the maximum principal stress direction.

Fracture turns along the mineral interface.

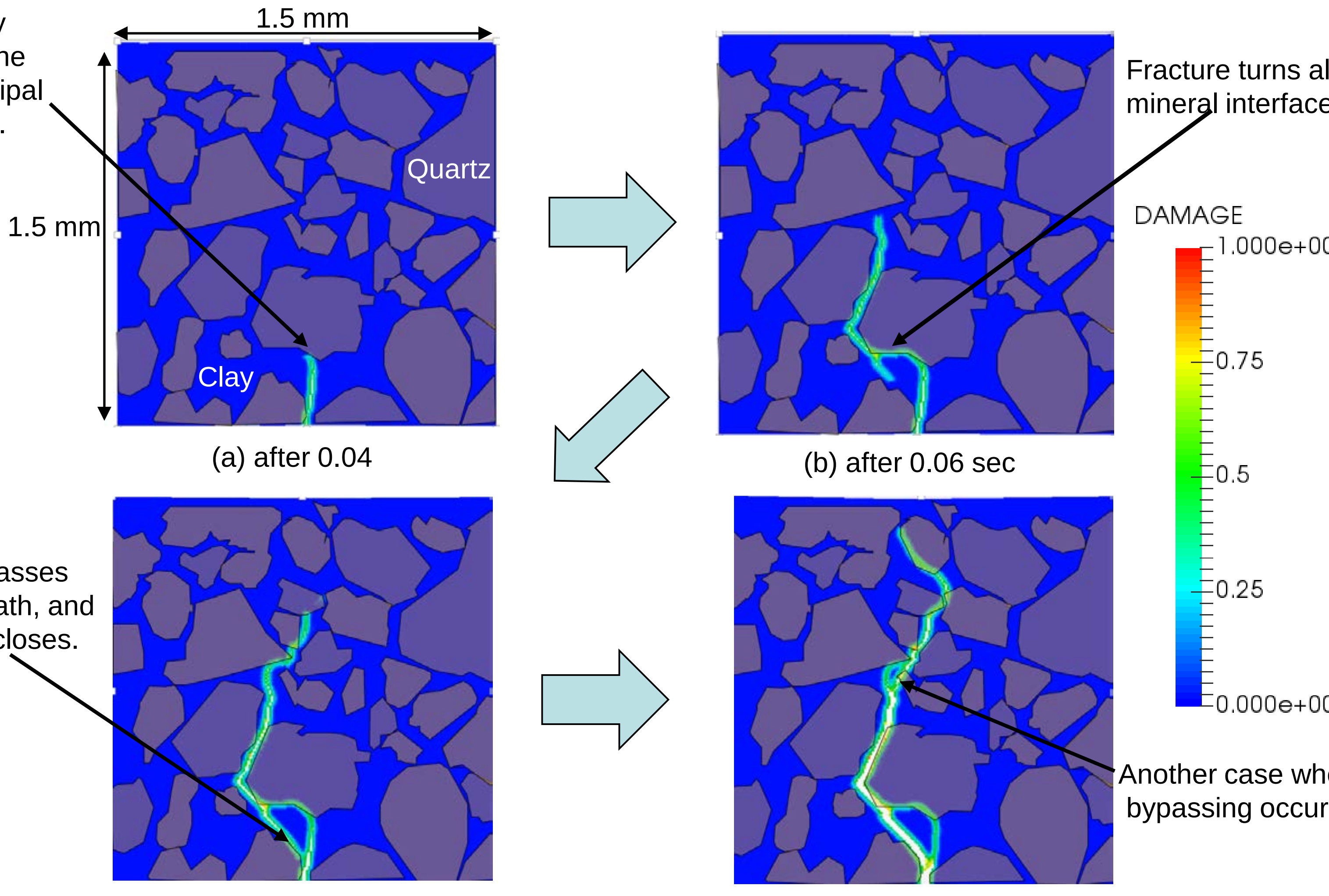

(a) after 0.04

(b) after 0.06 sec

Fracture bypasses the turning path, and the old path closes.

Another case where bypassing occurs.

(c) after 0.23 sec

(d) after 0.3 sec

Case 1: Quartz + Clay
No Interface Damage

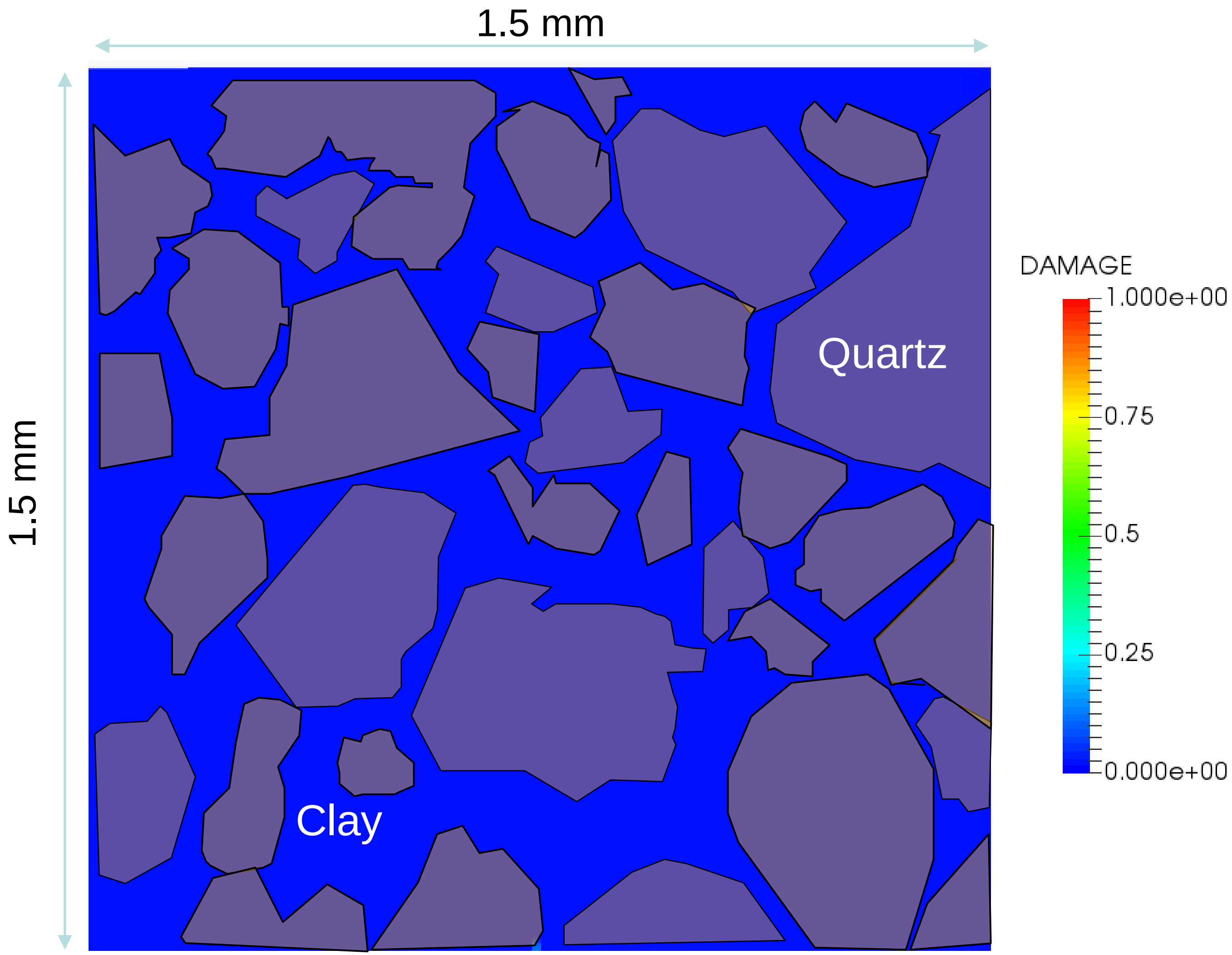

Case 2: Quartz + Clay Interface damage

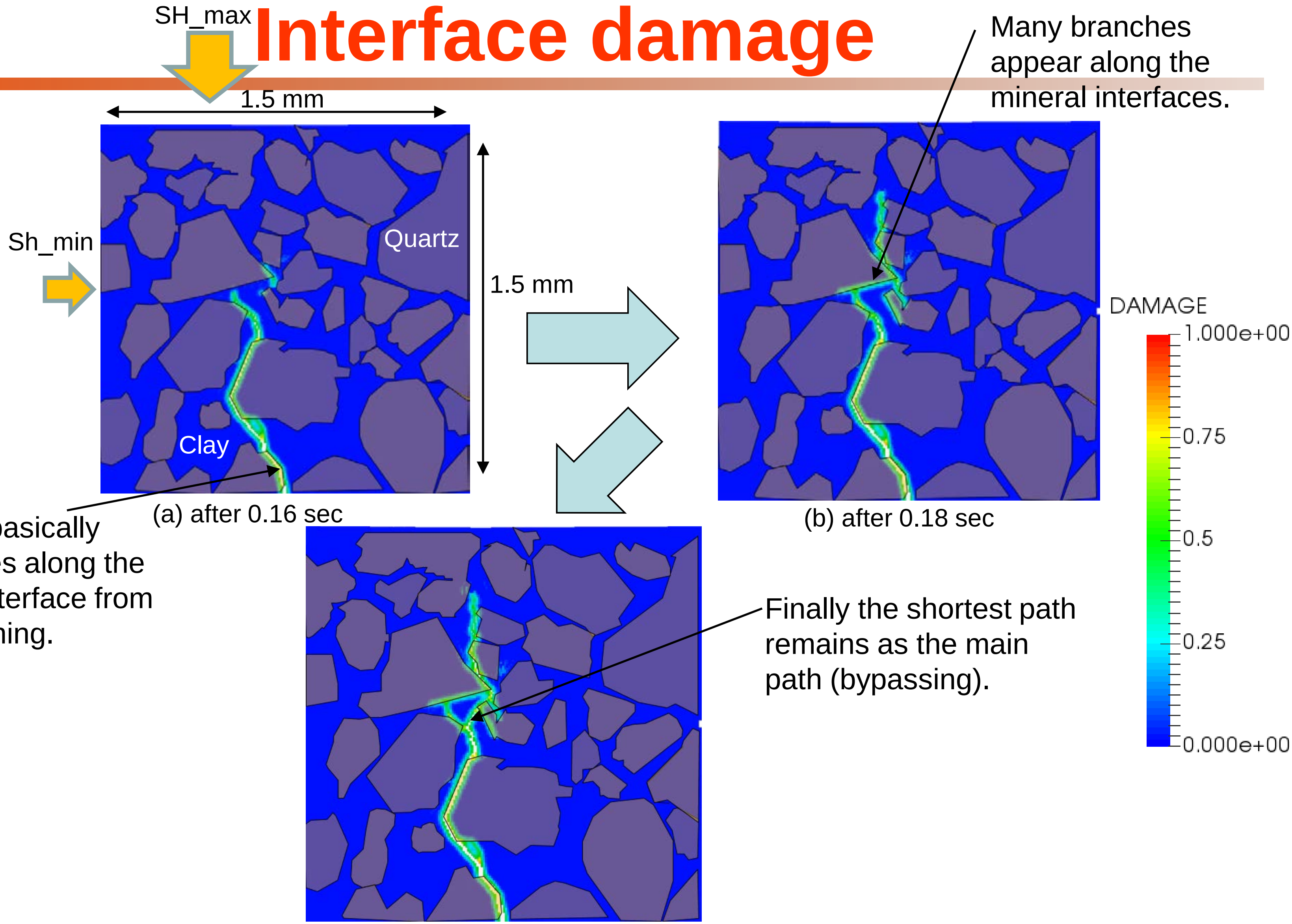

(a) after 0.16 sec

(b) after 0.18 sec

(c) after 0.20 sec

Many branches appear along the mineral interfaces.

Fracture basically propagates along the mineral interface from the beginning.

Finally the shortest path remains as the main path (bypassing).

Case 2: Quartz + Clay
With Interface damage

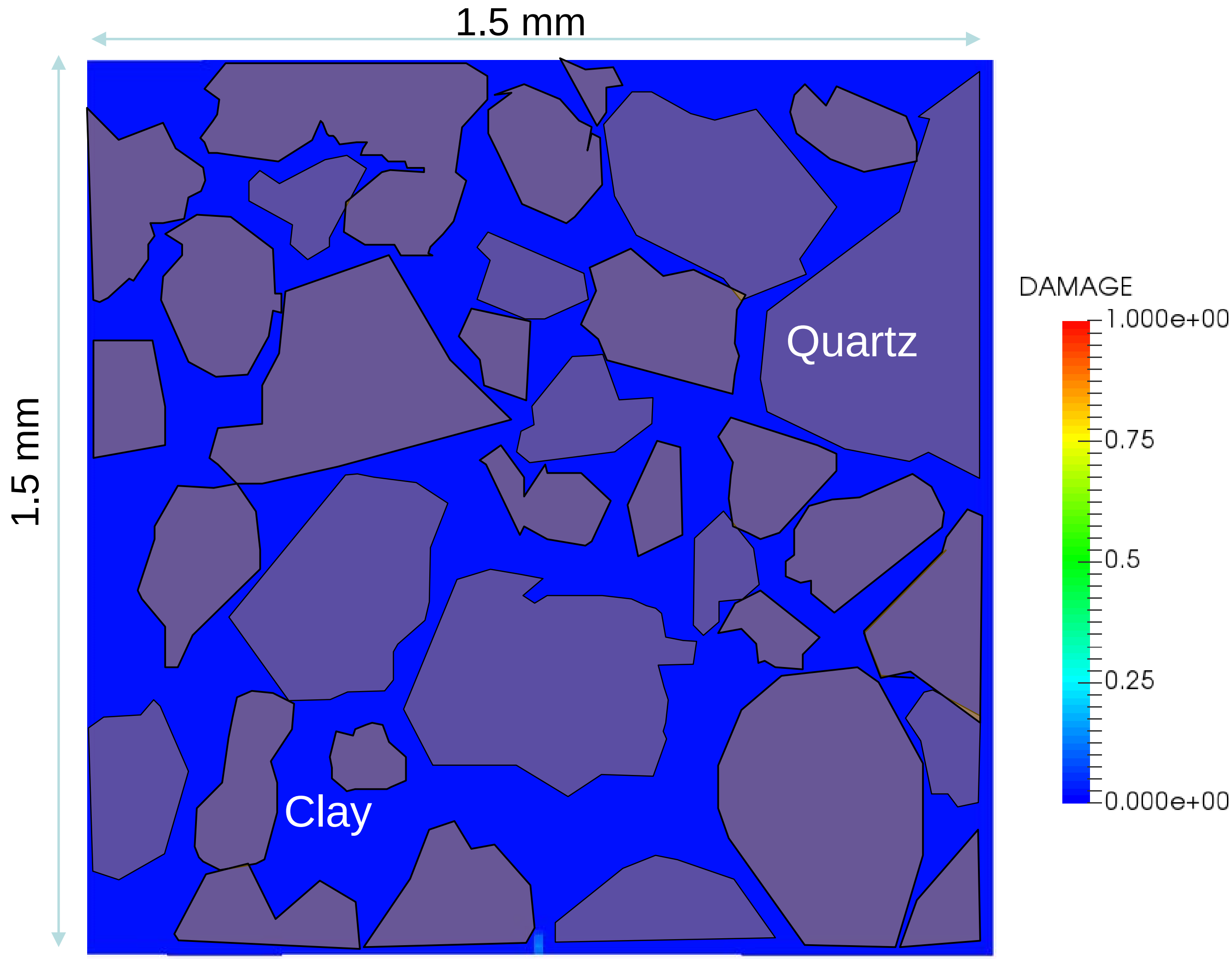

Case 3: Quartz + Calcite + Clay

No Interface Damage

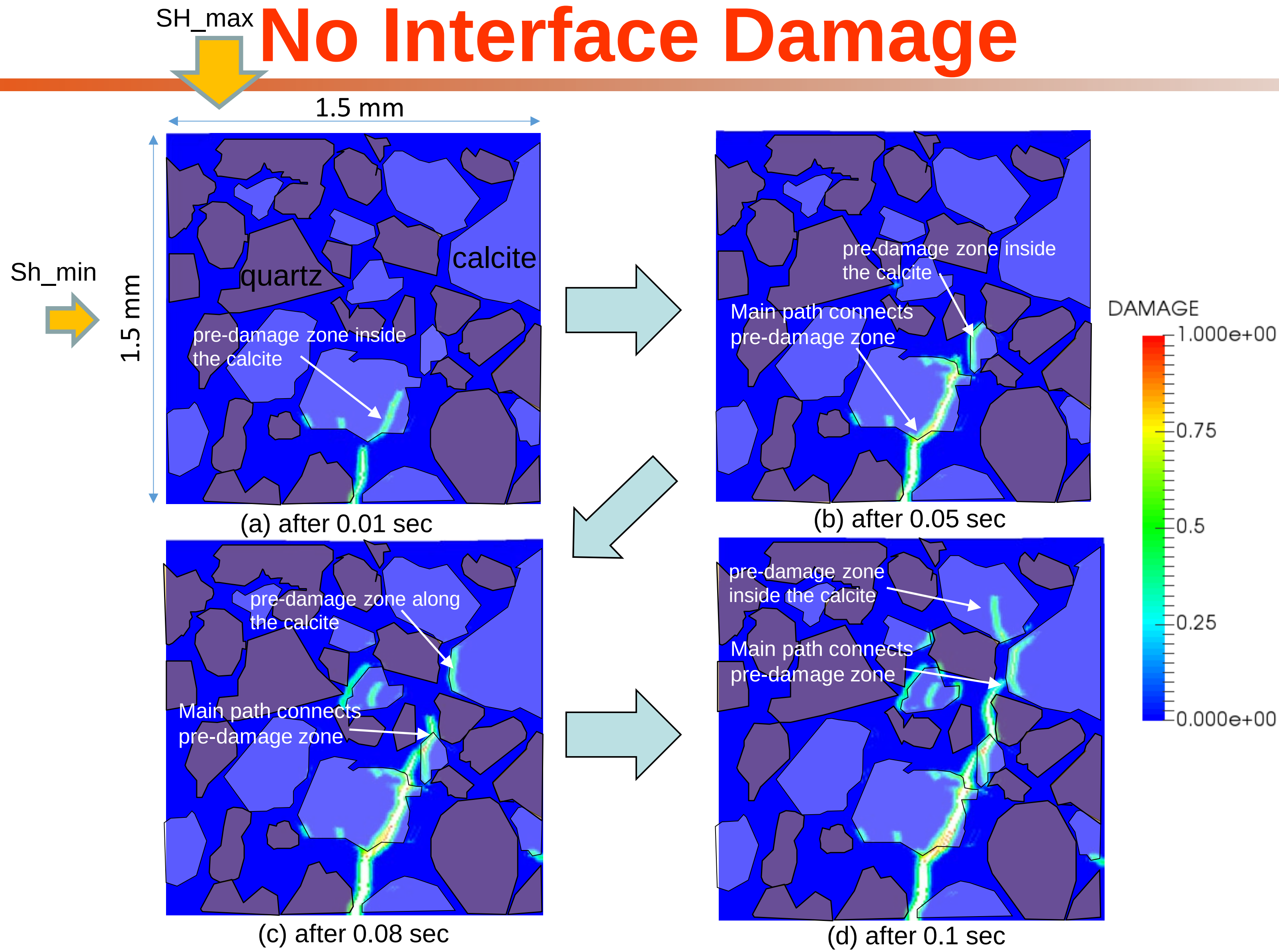

Case 3: Quartz + Calcite + Clay
No Interface Damage

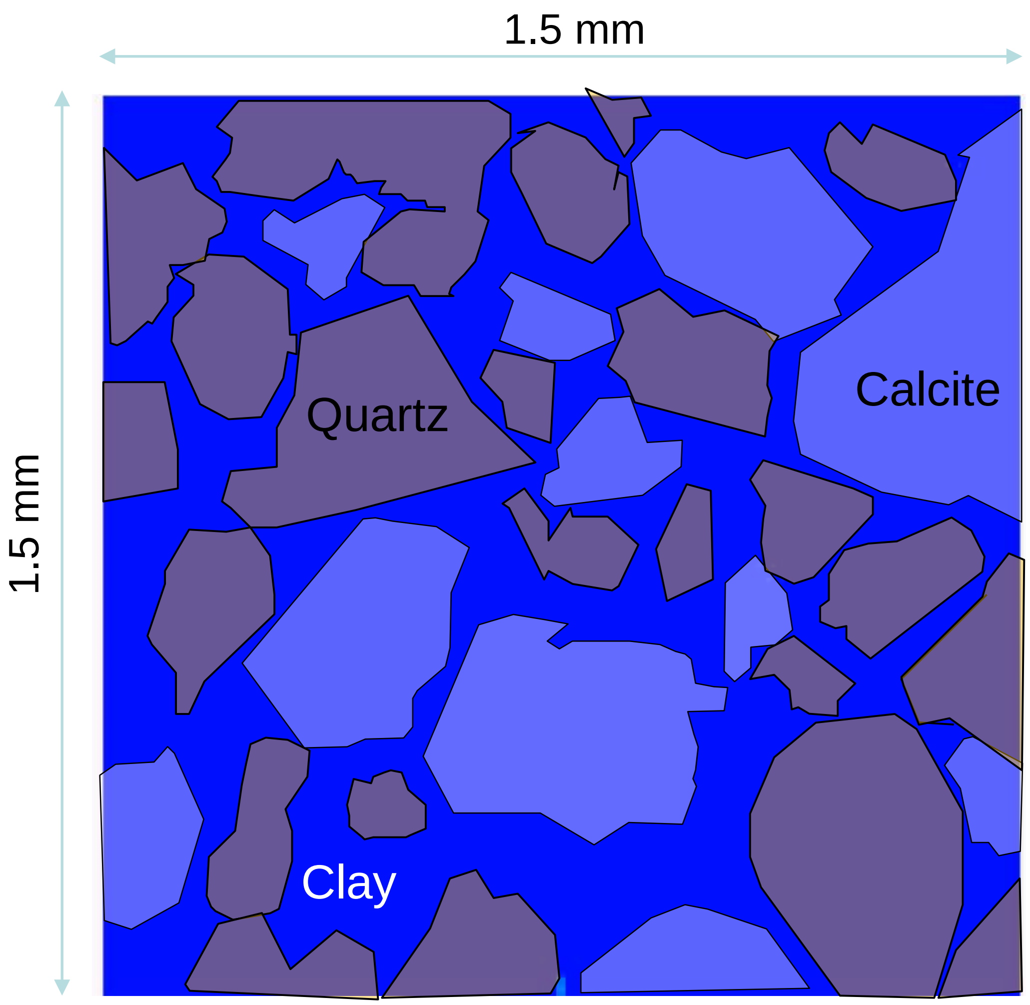

Case 4: Quartz + Calcite + Clay Interface Damage

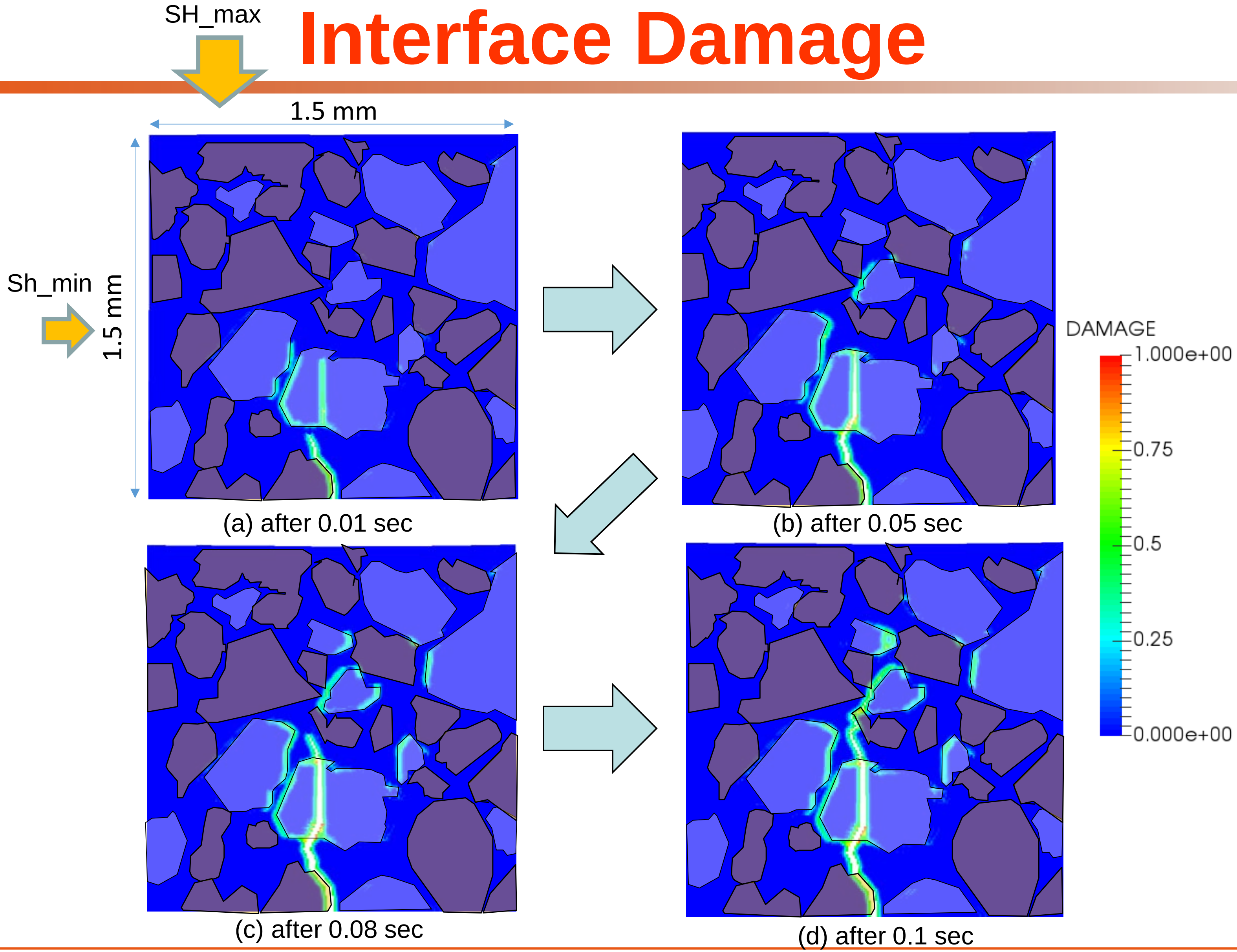

Case 4: Quartz + Calcite + Clay Interface Damage

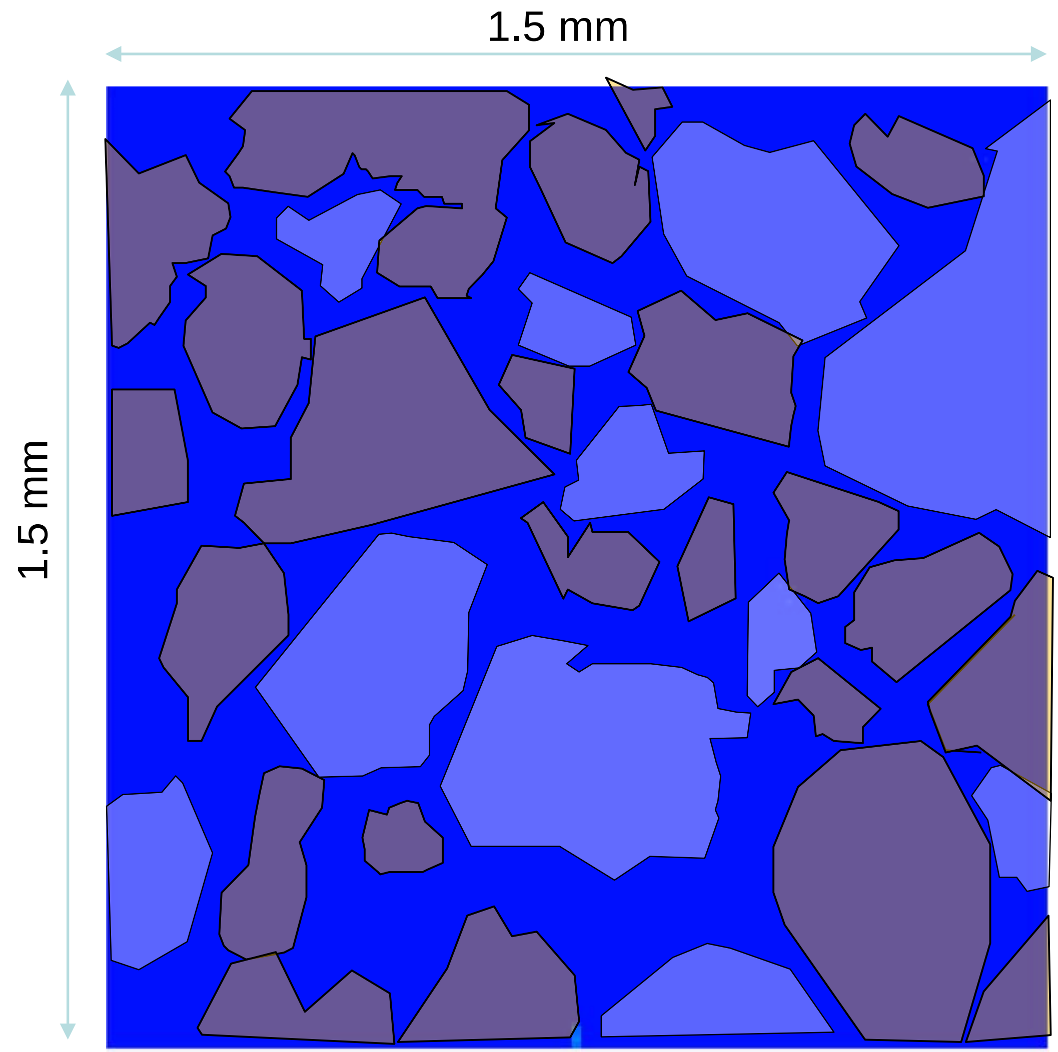

Interaction between Hydraulic and Natural Fractures

Comparison with Experimental Results (Zhou et al. 2008)

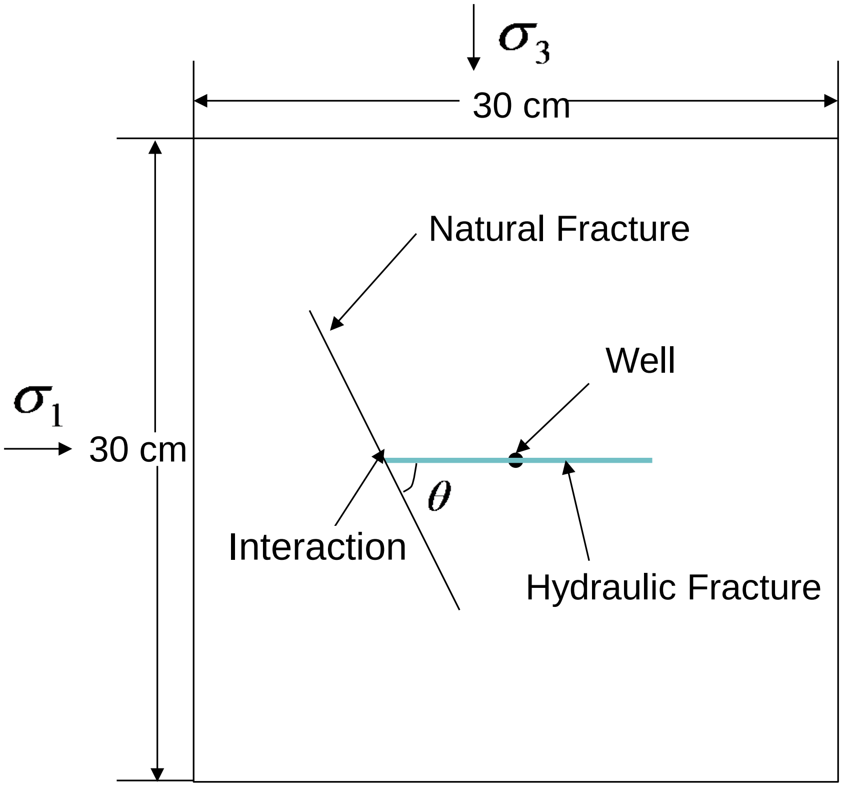

Experimental Setting

Case Parameters

Parameters	Value
θ (degree)	30, 60, 90
$\Delta\sigma$ (MPa)	3, 5, 7, 10

Basic Parameters

Parameters	Value
Young's modulus (GPa)	5.18
Poisson's ratio	0.25
Matrix Permeability (mD)	0.1
Injection rate ($m^3/s/m$)	1.05×10^{-9}
Distance between well and natural fracture (cm)	4.0

Results

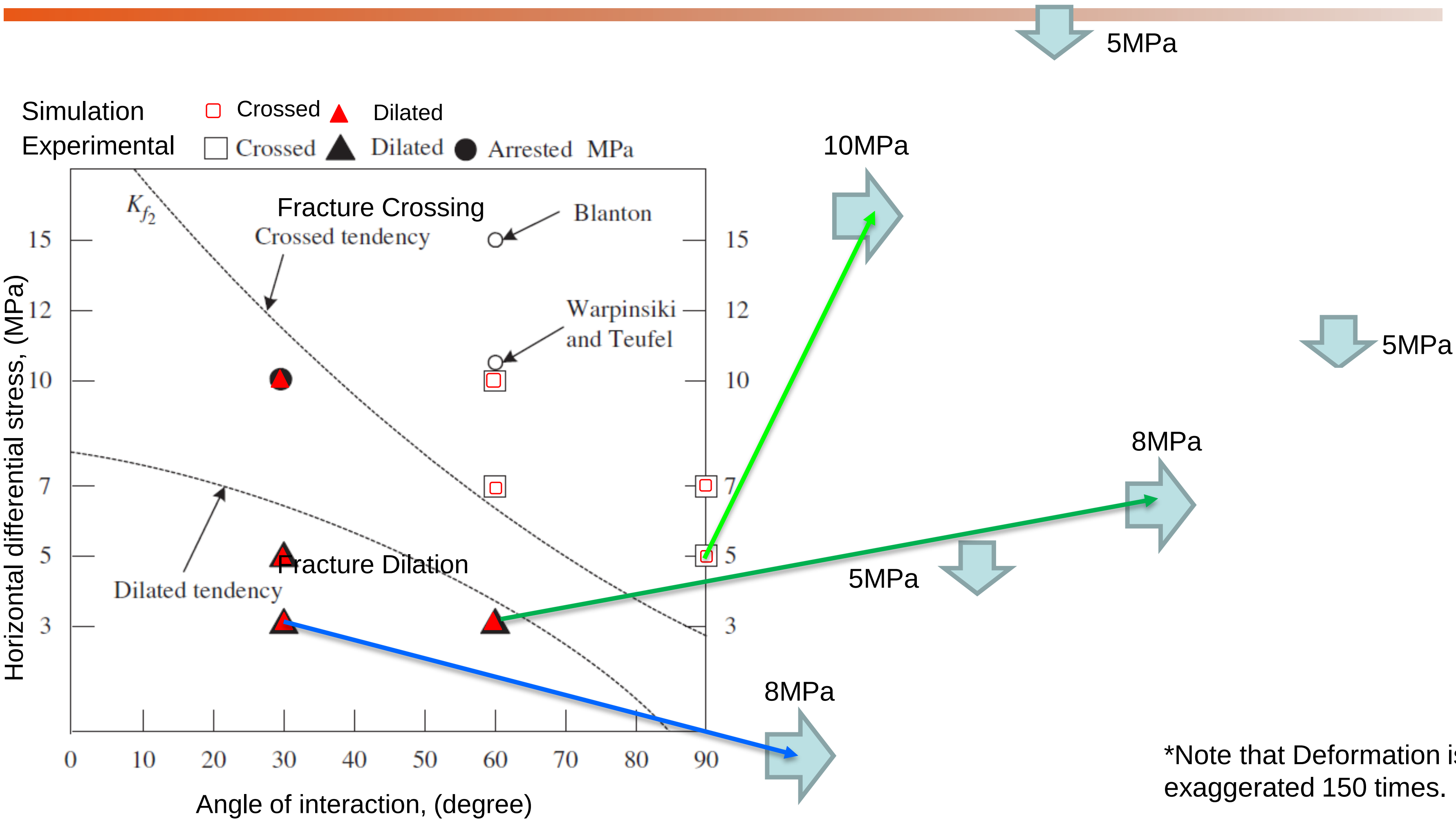

*Note that Deformation is exaggerated 150 times.

Ref: J. Zhou, M. Chen, Y. Jin, G. Zhang, International of Rock Mechanics & Mining Science (2008)

Factors Affecting Interaction of HF with NF Including Poroelastic Effects

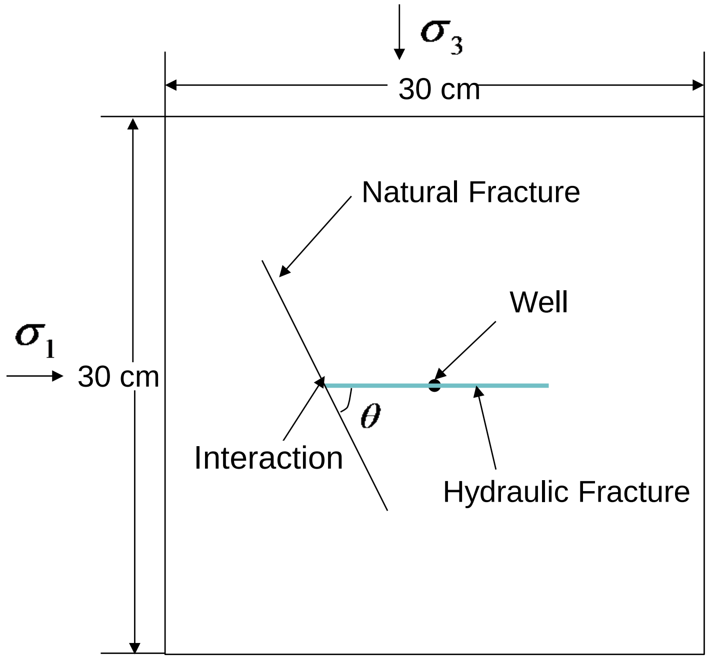

Base Case:

$$\theta = 60\deg \qquad \sigma_1 = 8MPa \qquad \sigma_3 = 5MPa$$

Change the following six parameters for sensitivity analysis:

- **Rock permeability: Poroelastic effects**
- **Shear strength of NF (failure criteria)**
- **NF toughness (NF critical strain)**
- **Rock toughness and Young's modulus**
- Initial Natural Fracture Permeability
- Injection Rate

Effect of Permeability

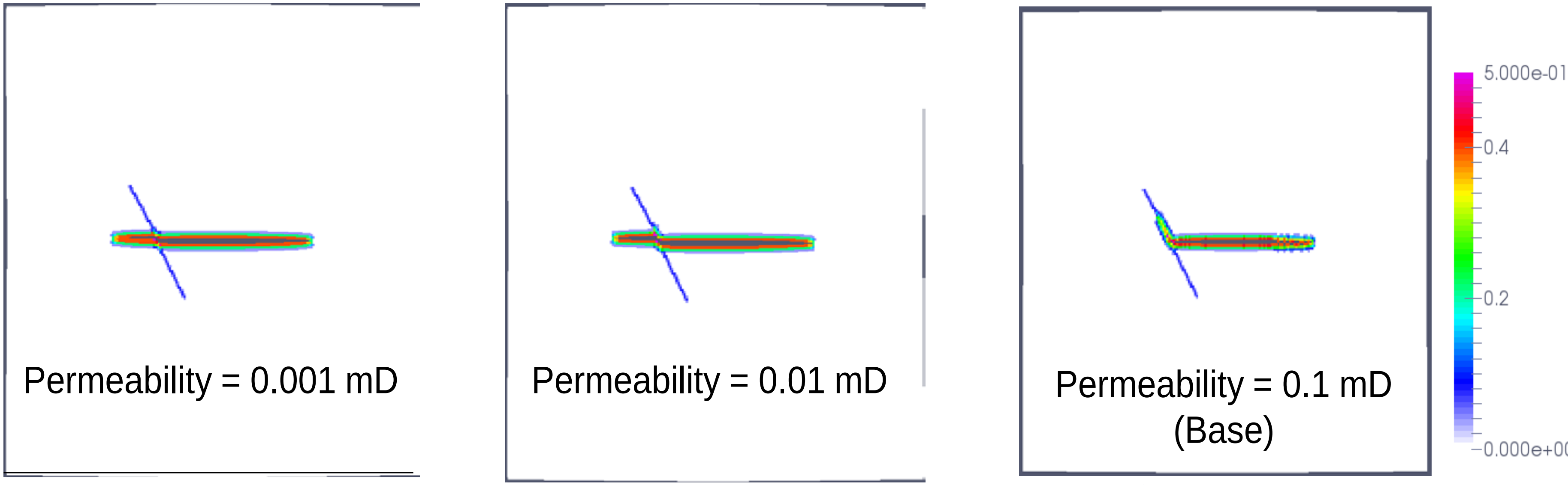

High leak-off

Low effective stress
(shear failure)

Fracture turning

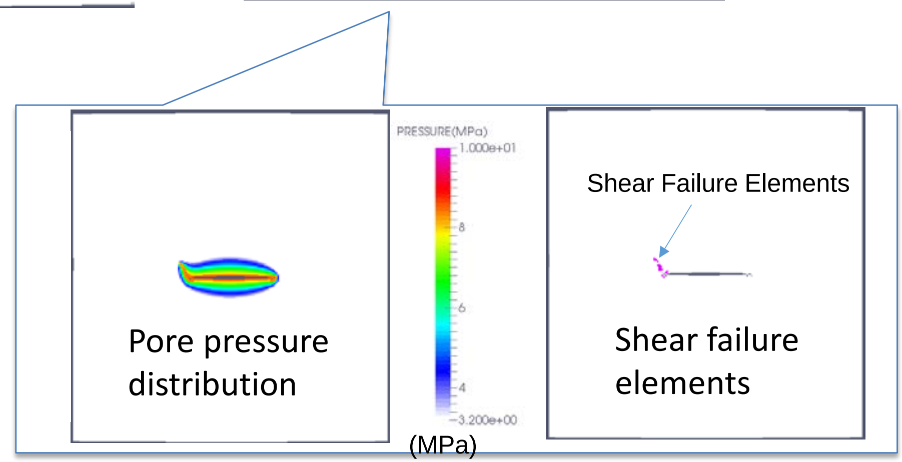

Effect of Shear Strength of Natural Fracture

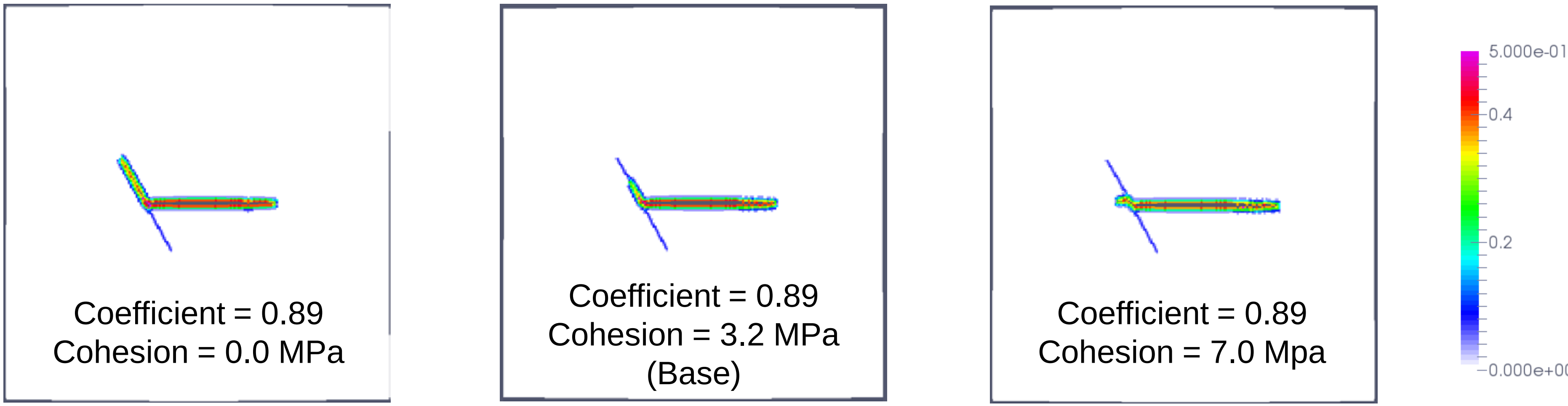

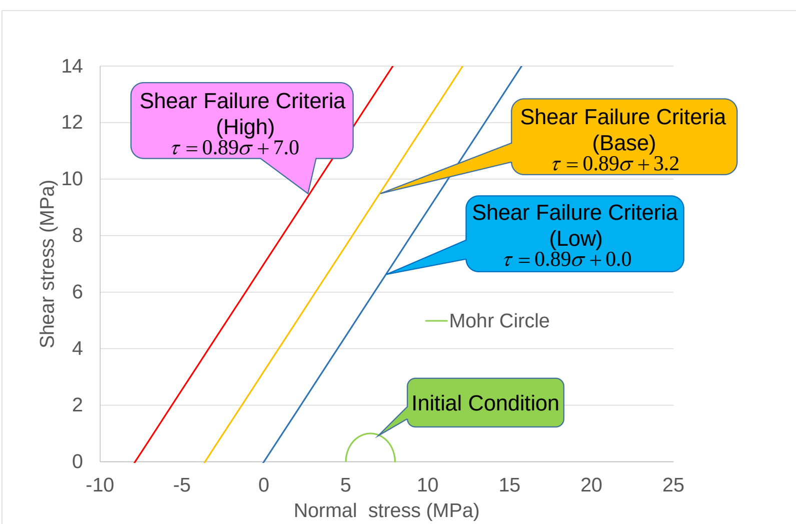

Low shear strength of NF promotes HF turning

Effect of Natural Fracture Toughness

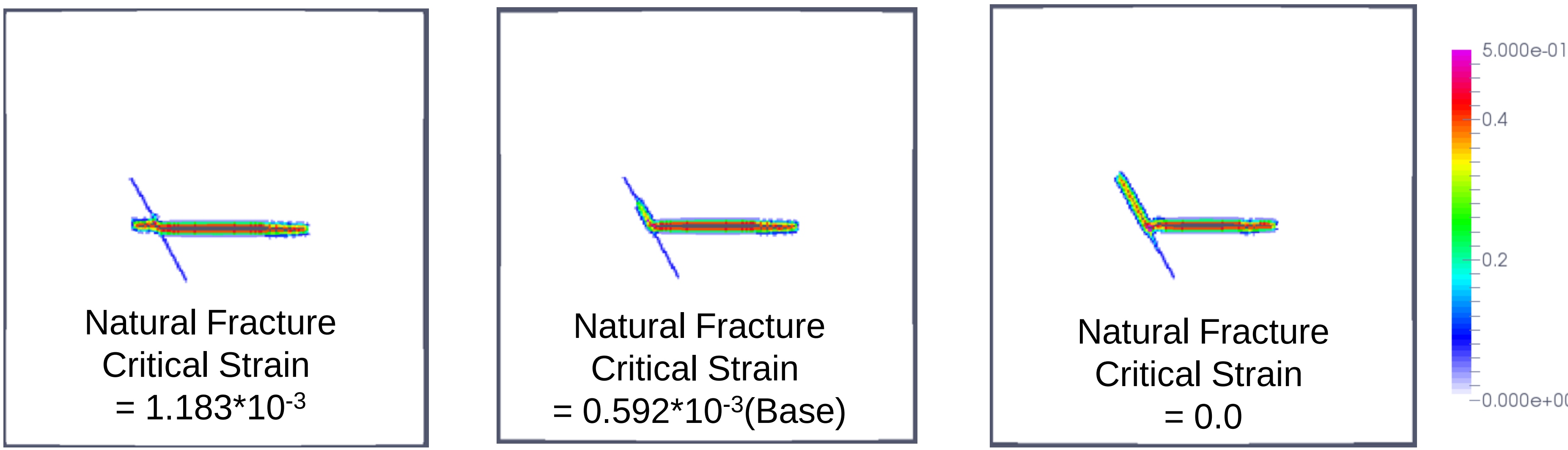

(K_{IC}=1.74 MPa $m^{-1/2}$) (K_{IC}=0.87 MPa $m^{-1/2}$) (K_{IC}=0.0 MPa $m^{-1/2}$)

Fracture toughness of NF also controls Mode I opening.

Low NF toughness → Easier fracture turning

Effect of Matrix Toughness

Assuming $K_{IC} \propto \sqrt{E}$ **in this case**

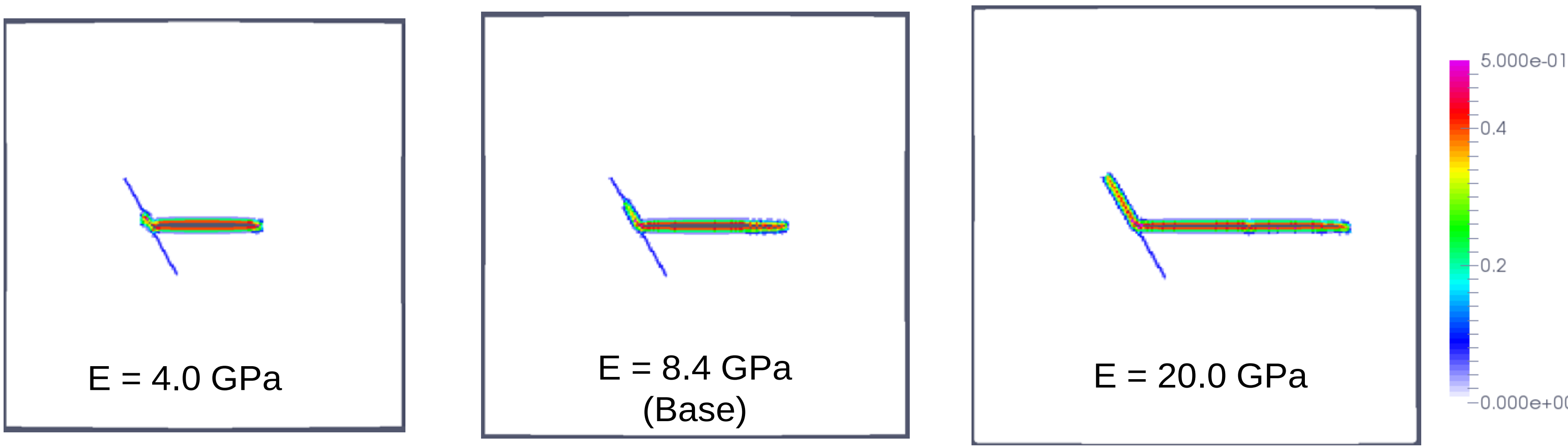

High matrix toughness → Encouraging fracture turning

3-D interaction Behavior

2-D interaction behavior

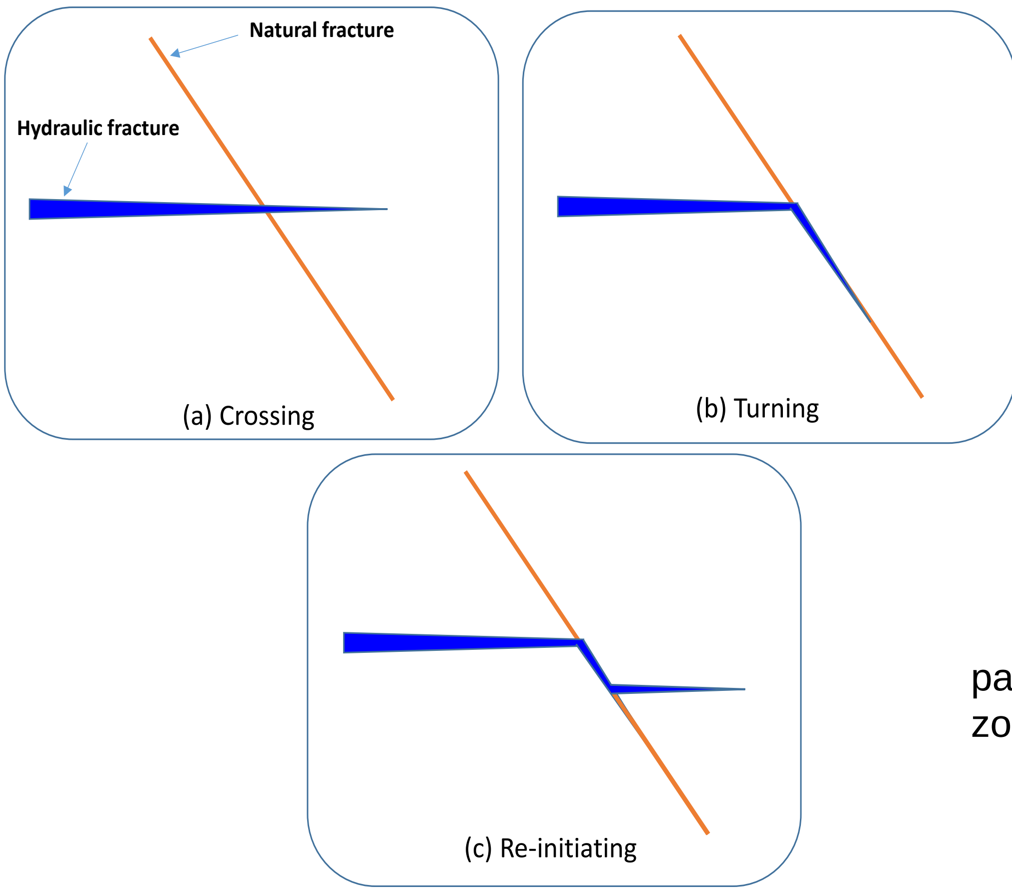

If the NF fills the entire pay zone, these 2-D interactions cover all the patterns of interaction.

However, if

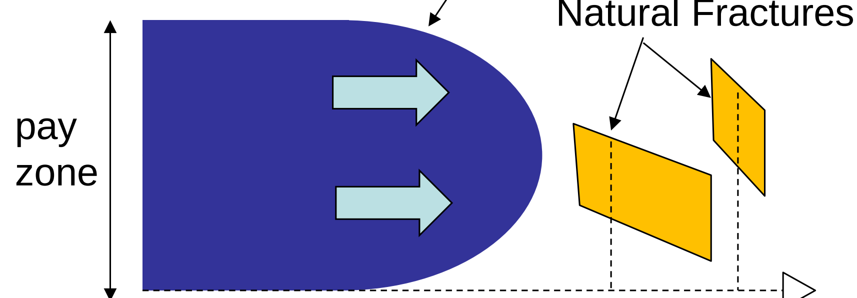

3-D interaction Behavior

Bahorich et. al (2012) showed **more complicated 3-D interaction behavior** could appear in the reservoir.

What kind of parameters affect these characteristic fracture propagation behaviors?

3-D interaction behaviors

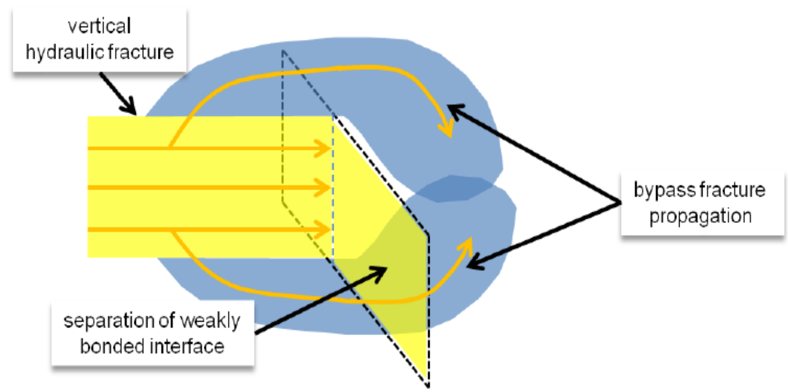

(a) Bypassing + Turning

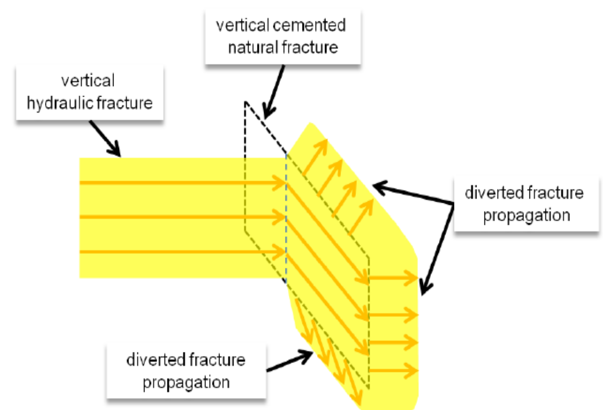

(b) Turning + Diverting propagation from side of NF

Bahorich et al (2012)

Case Settings (Common Parameters)

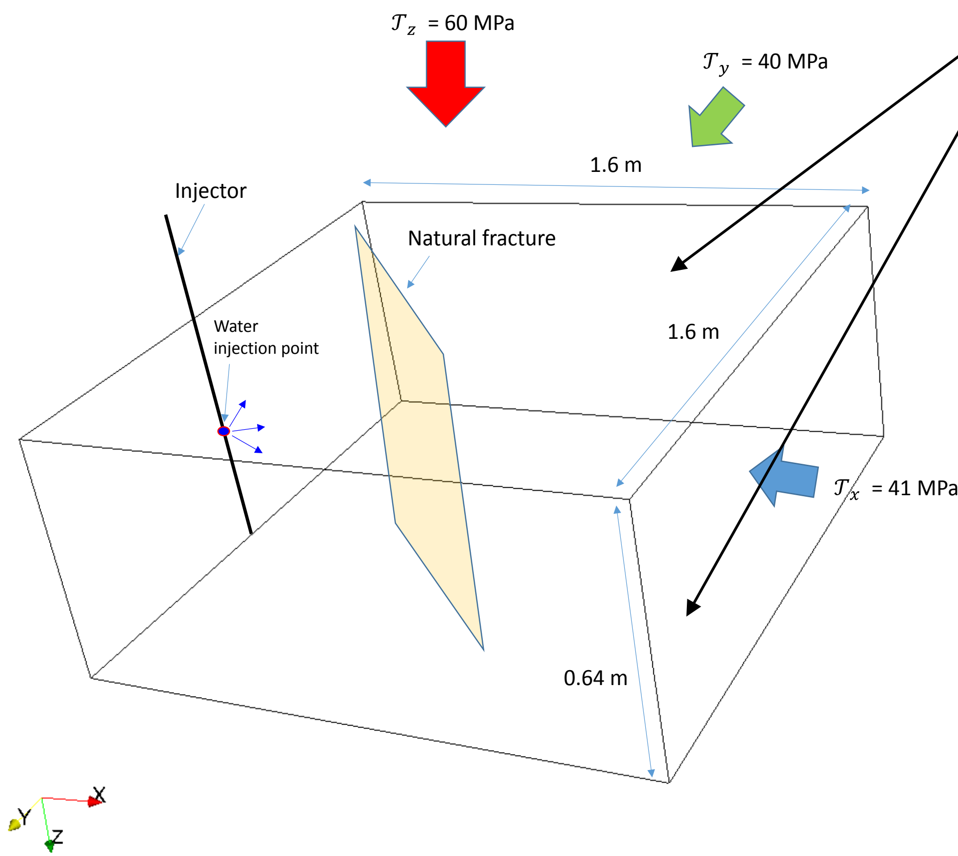

Upper and lower boundary were fixed for mimicking boundary layers.

Common Case Parameters

Parameters	Value
Young's modulus (GPa)	30.0
Poisson's ratio	0.25
Shmax (MPa)	41
Shmin (MPa)	40
NF shear trend	**0.5**
NF cohesion	**0.0**

Case Settings

Effect of NF height, Position, and Tensile Strength

Case 1 (full height)

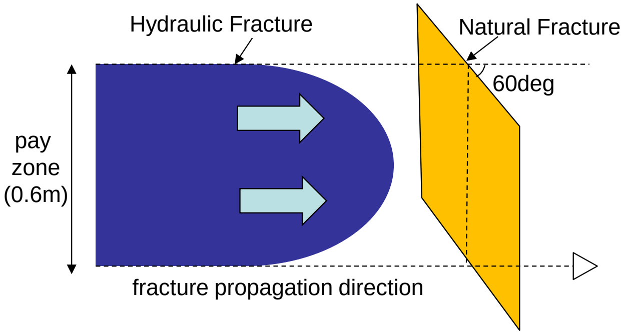

Case 2 (lower half)

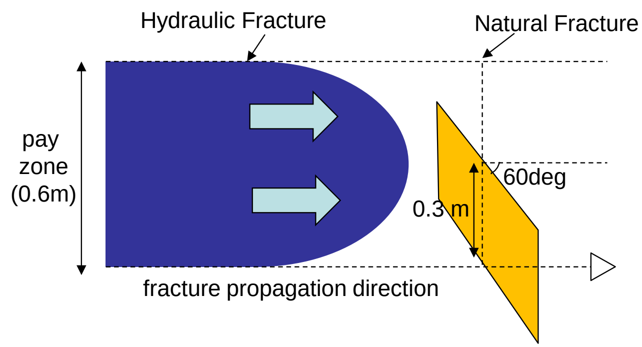

Case 3 (lower half + weak TS)

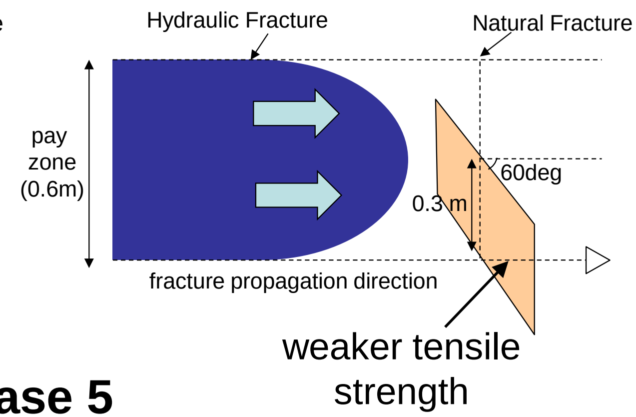

Case 4 (middle half)

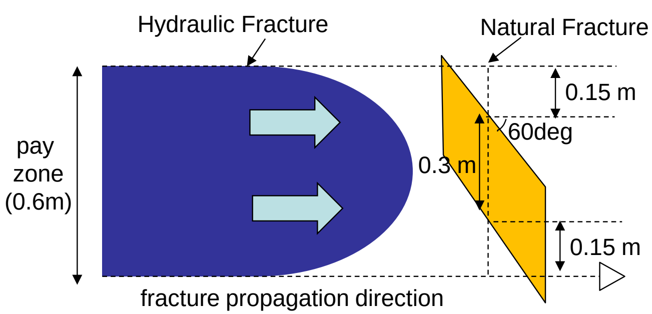

Case 5 (lower one-third)

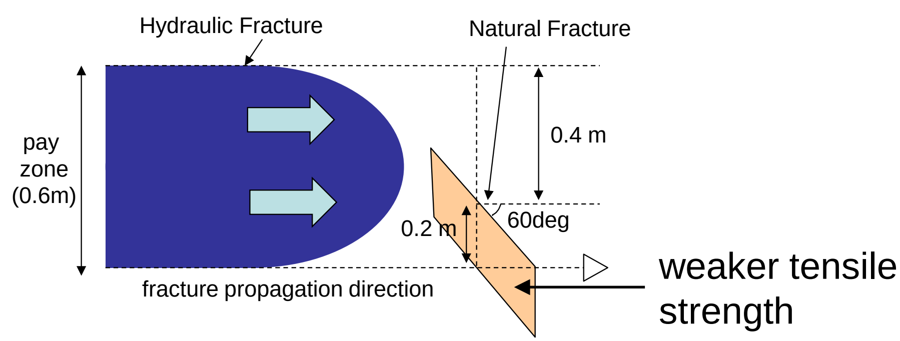

Results (Case 1: Reference)

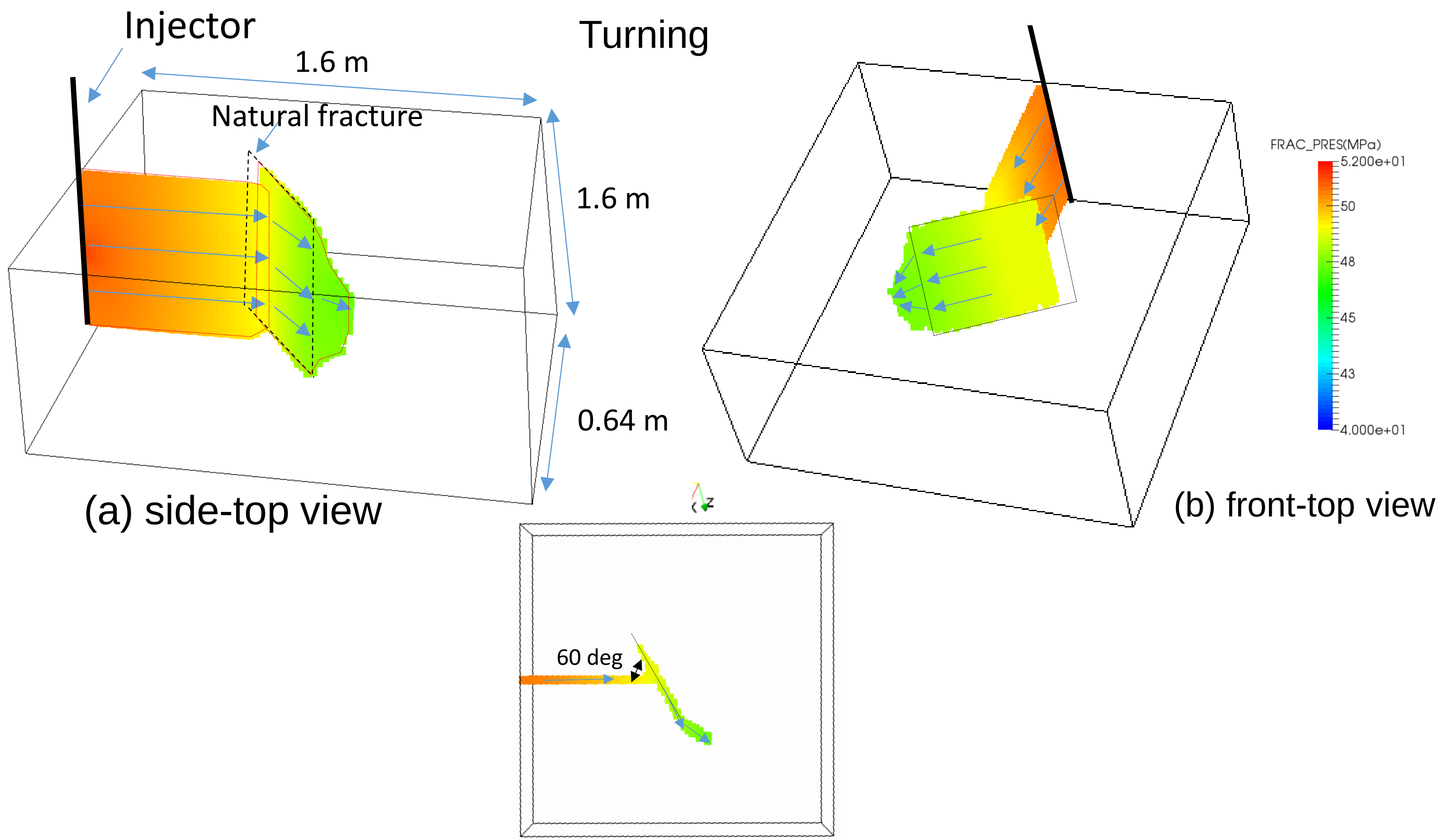

(a) side-top view

(b) front-top view

(c) top view

Results
(Case 2: Lower Half NF)

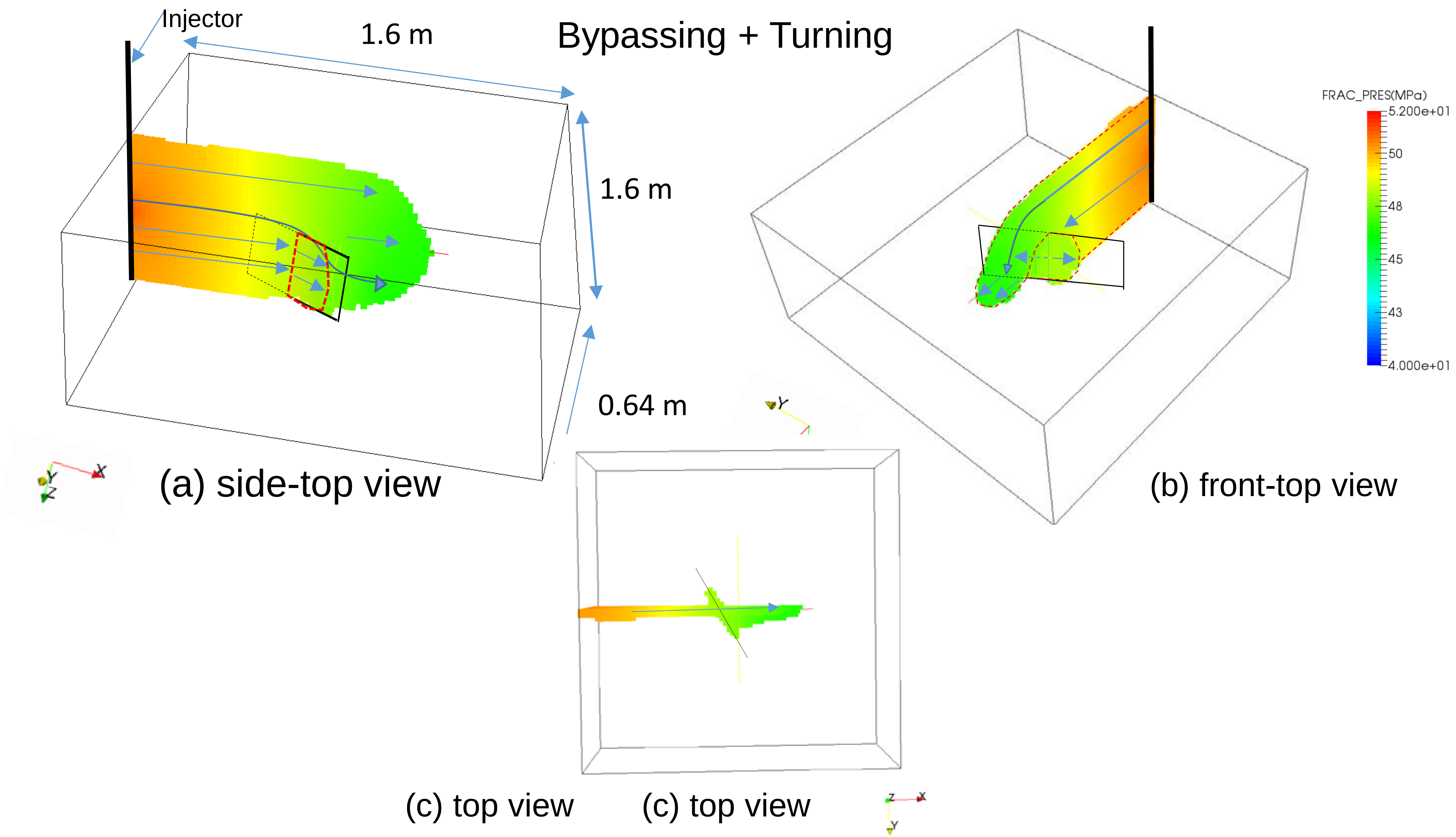

(a) side-top view

(b) front-top view

(c) top view (c) top view

Growth of Multiple Fractures in Naturally Fractured Reservoirs

No-NF model

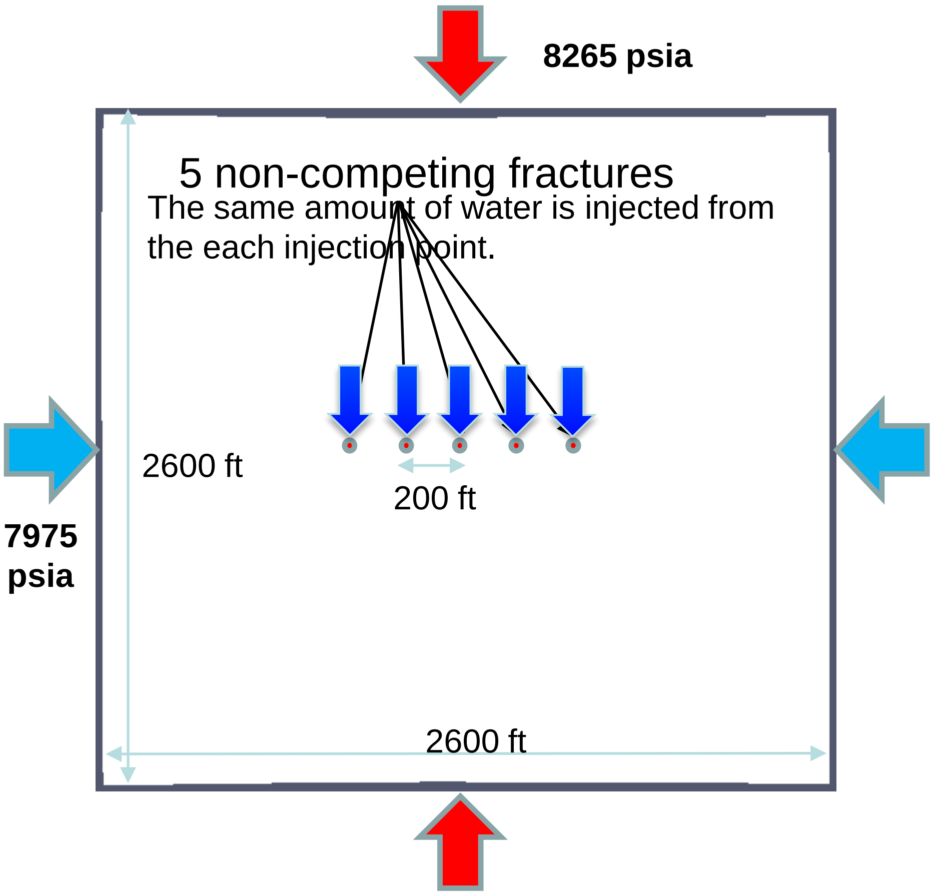

NF model

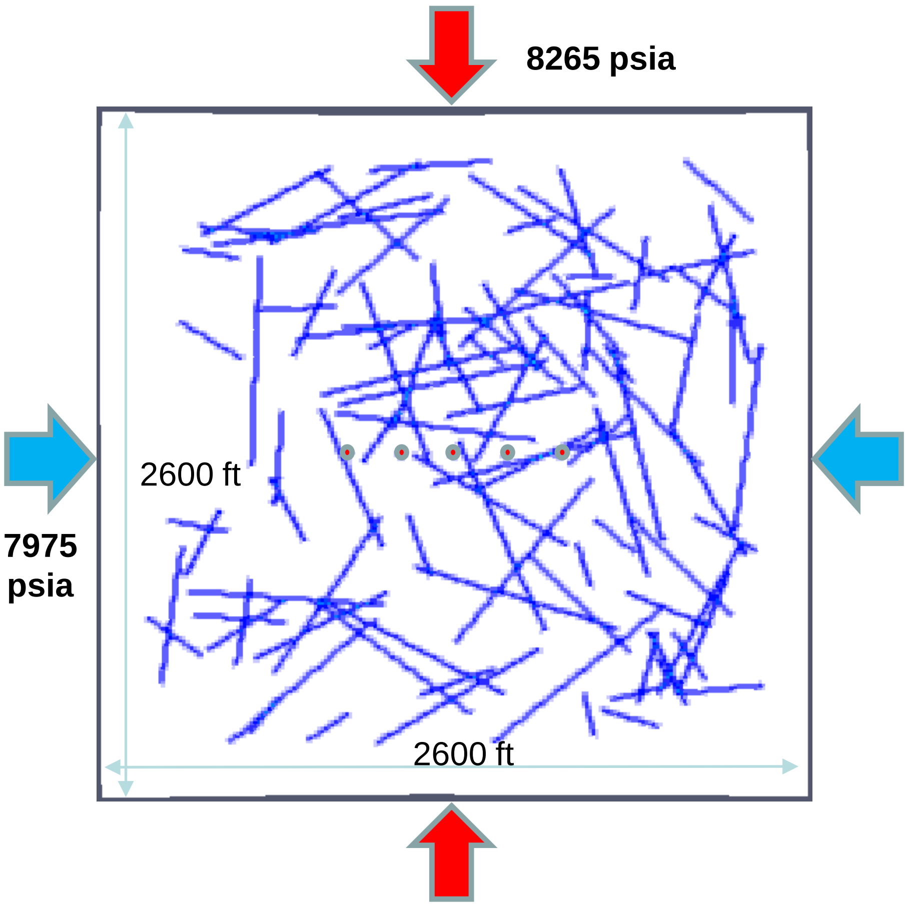

Fracture Growth from 5 Clusters

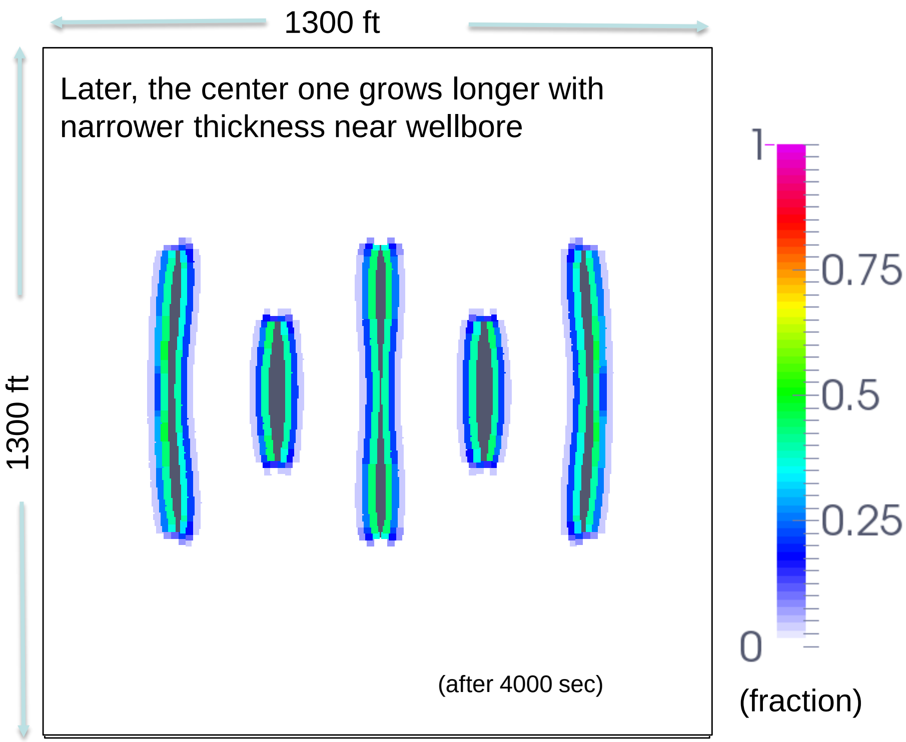

Damage Distribution

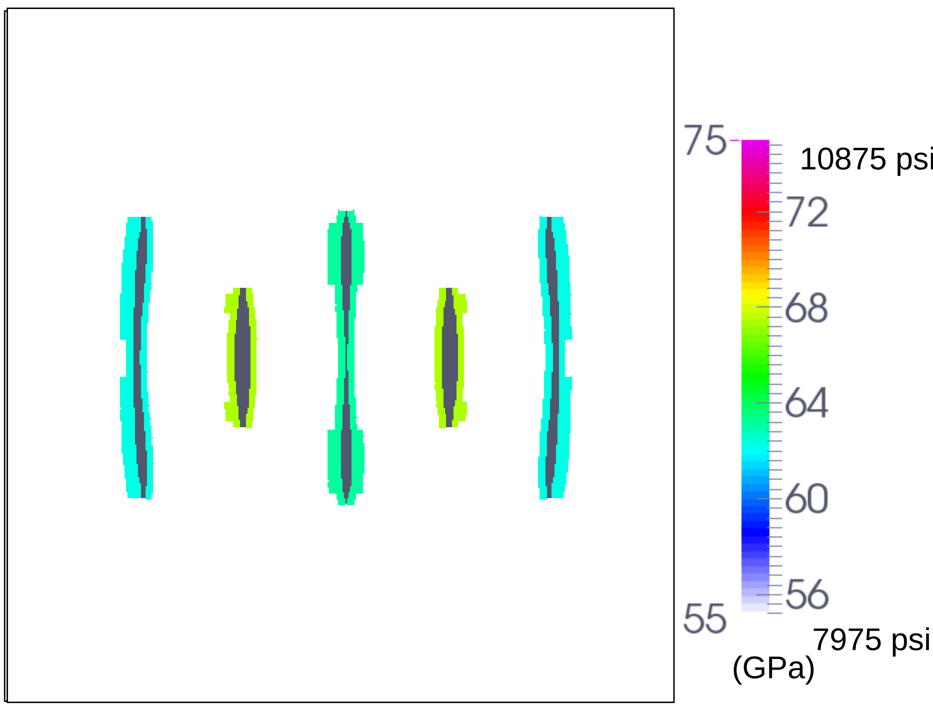

Fracture Pressure Distribution

Multiple Fracture Growth with NF

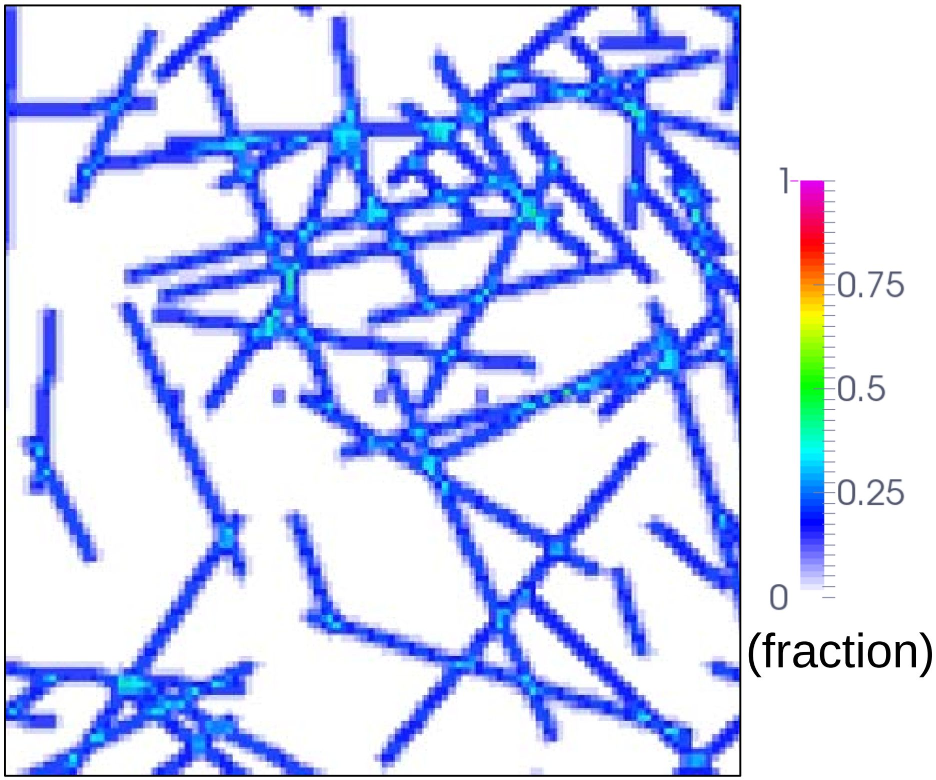

Damage Distribution

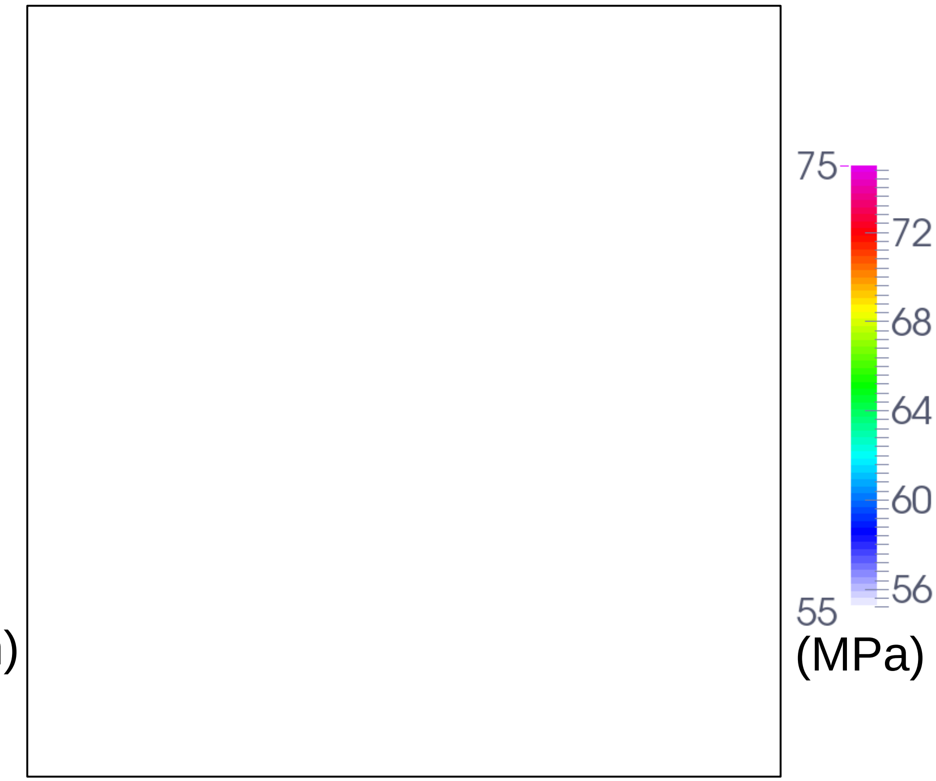

Fracture Pressure Distribution

Conclusions

- **A new peridynamics based hydraulic fracturing model was developed** by modifying the existing elastic formulation to include poroelasticity and coupling it with the new peridynamics formulation for fluid flow.

- This model can simulate **non-planar, multiple fracture growth in arbitrarily heterogeneous reservoirs** by solving deformation of the reservoir, fracturing fluid pressure and pore pressure simultaneously.

- The validity of the model was shown through comparing model results with **analytical solutions** (1-D consolidation problem, the KGD model, the PKN model, and the Sneddon solution) and **experiments**.

Conclusions

- The effects of different types of layer heterogeneity on fracture propagation were systematically investigated.
- The factors controlling characteristic fracture propagation behaviors (“turning”, “kinking”, and “branching”) near the layer interface were quantified.
- In layered systems, the mechanical property contrast between layers, the dip angle, the stress contrast and poroelastic effects all play an important role in controlling the fracture trajectory.
- It was shown that even at the micro-scale, fracture geometry can be quite complex and is determined by the geometry and distribution of mineral grains and their mechanical properties.

Conclusions

- The principal stress difference, the approach angle, the fracture toughness of the rock, the fracture toughness of the natural fracture, and the shear strength of the natural fracture when hydraulic fractures interact with natural fractures.

- The 3-D interaction study elucidated that **the height of the NF, the position of the NF, and the opening resistance of the NF** have a huge impact on the three-dimensional interaction behavior between a HF and a NF.

Publications

- H. Ouchi, A. Katiyar, J.T. Foster, and M.M. Sharma. A Peridynamics Model for the Propagation of Hydraulic Fractures in Heterogeneous, Naturally Fractured Reservoirs. In SPE Hydraulic Fracturing Technology Conference, SPE-173361-MS. Society of Petroleum Engineers, February 2015. doi:10.2118/173361-MS
- H. Ouchi, J.R. York, A. Katiyar, J.T. Foster, and M.M. Sharma. A Peridynamics Model of Fully-Coupled Porous Flow and Geomechanics for Hydraulic Fracturing. Computational Mechanics, 2016. doi:10.1007/s00466-015-1123-8, 2015.
- "A Peridynamic Formulation of Pressure Driven Convective Fluid Transport in Porous Media". Journal of Computational Physics, Vol. 261, pp. 209-229, January, 2014, Amit Katiyar, John T. Foster, Hisanao Ouchi, Mukul M Sharma.
- A Peridynamics Formulation of the Coupled Mechanics-Fluid Flow Problem", Workshop on Nonlocal Damage and Failure: Peridynamics and Other Nonlocal Models, San Antonio, March 2013.
- "A Non-Local Peridynamic Formulation for Convective Flow in Porous Media", USACM's 12th U.S. National Congress on Computational Mechanics, Raleigh, North Carolina, July 2013.

Future Work

- **Improvement of Computation Efficiency**
  - Integration of peridynamics models with finite element models
  - More efficient solvers, pre-conditioners
- **Model Extension/Improvement**
  - Non-Newtonian fluid
  - Proppant transport
- **Effect of heterogeneities at different scales**
  - How smaller scale propagation behavior affects the larger scale propagation behavior

Acknowledgement

This work is supported by **DOE Grant NO. DE-FOA-0000724** and by **the generous support of 35 member companies** participating in **the JIP on Hydraulic Fracturing and Sand Control at The University of Texas at Austin**.

Questions?

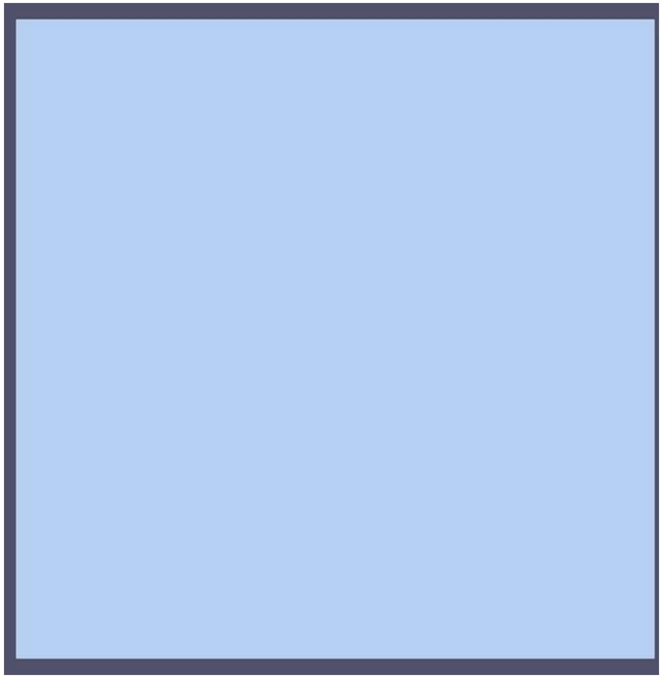

Backup Slides

Project Schedule and Outcomes

Task name	Assigned Resources / year
Task 1 Project Management & Planning	0.5 GRA
Milestones	0.25 PI
Technology Status Assessment Report	
Task 2 Formulation of the Fracturing Problem in Peridynamics	1 GRA
Milestones	1 mo PI
Model completed and documented	0.5 PR
Publication #1	
Publication #2	
Task 3. Development of a New Generation Hydraulic Fracturing Code: UT-MULTIFRAC	1 GRA
Subtask 3.1	
Subtask 3.2	
Milestones	1 mo PI
Alpha version of the code delivered	0.5 PR
Tested final version of the code delivered	
Task 4. Application of the new UT-MULTIFRAC code to field data	
Milestones	
Comparison of code with field data, report	
Publication #3	
Task 5. Development of fracturing guidelines based on new simulation results	
Milestones	
Complete guidelines for fracture designs	
Publication # 4	

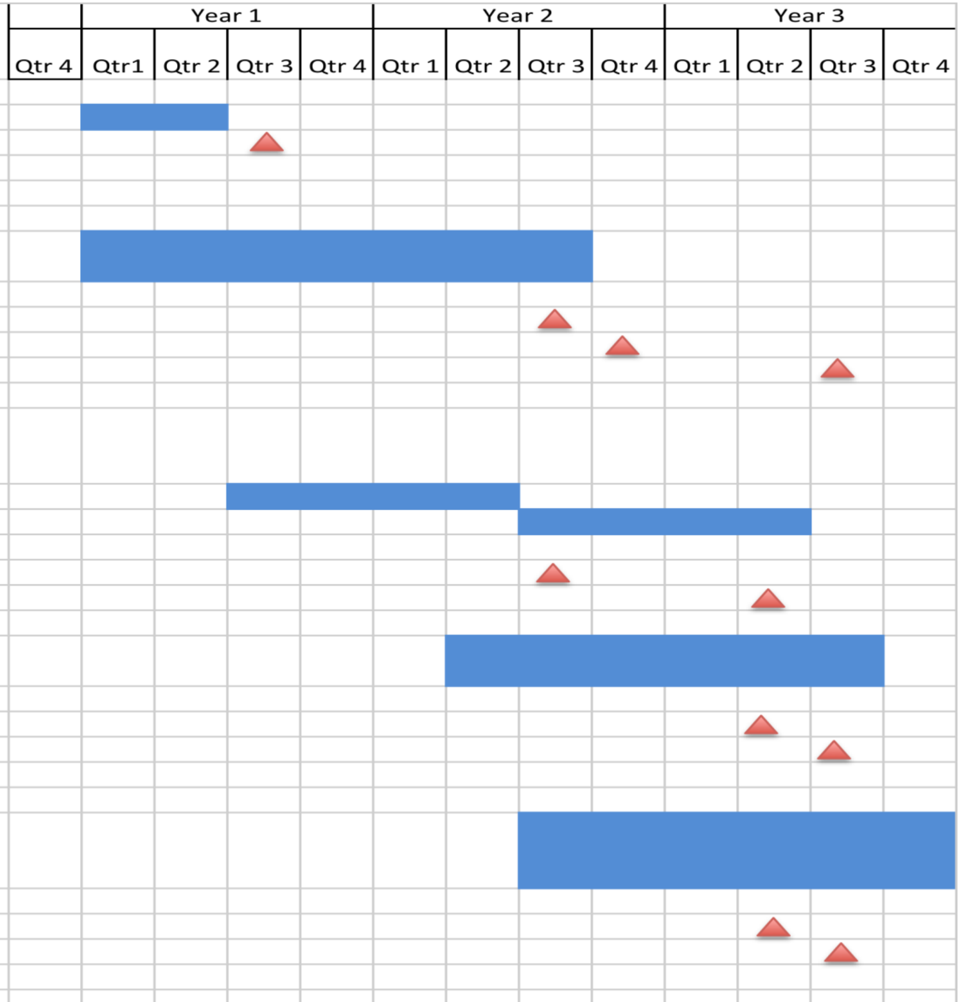

GRA = Graduate Research Assistant; PR = Postdoctoral Research Associate, PI = Principal Investigator

Project Schedule and Outcomes

Milestone Title/Description	Planned Completion Date	Actual Completion Date	Verification Method	Comments (Progress toward achieving milestone, explanation of deviation from plan etc.)
Task 1 Project Management & Planning				
Milestones				
Technology Status Assessment Report	9/30/13	6/28/13	PMP document	
Task 2 Formulation of the Fracturing Problem in Peridynamics				
Milestones				
Model completed and documented	9/30/14			Expected Q2, 2016
Publication #1	11/30/14	1/1/15	Paper publication submitted	DOI: 10.1007/s00466-015-1123-8
Publication #2	8/31/15	8/31/15	Paper publication submitted	Paper SPE # 173361 presented at HFTC 2015, DOI 10.2118/173361-MS, and two technical presentations at the 13th US National Congress on Computational Mechanics. July 2015.
Task 3. Development of a New Generation Hydraulic Fracturing Code: UT-MULTIFRAC				
Milestones				
Alpha version of the code delivered	3/31/16		Provide in quarterly report	Code will be delivered Q1, 2016
Tested final version of the code delivered	9/30/16		Provide in quarterly report	Code will be delivered Q3, 2016
Task 4. Application of the new UT-MULTIFRAC code to field data				
Milestones				
Comparison of code with field data, report	3/31/16		Provide in quarterly report	Currently working on it. Available Q1 2016
Publication #3	6/30/16		Publication available	
Task 5. Development of fracturing guidelines based on new simulation results				
Milestones				
Complete guidelines for fracture designs	6/30/16		Provided in Publication #4 and Final Report	
Publication # 4	6/1/16		Publish results/findings in paper publication	Provided in Publication #4 and Final Report
Final Report	12/31/16		Final report	

Impacts

- Both the modeling and the fracturing recommendations from this work are expected to have an immediate and long-term impact and benefit.

- The developed fracturing model and procedures would be applicable to all shale oil and gas resources that are more likely to have natural fractures and consequently result in more complex fracture patterns.

- This realistic model of hydraulic fracture propagation will allow better understanding of
  - the effects of fracture design on the stimulated rock volume and
  - well performance to potentially improve fracture and well design.

- Both items above should result in significant performance improvements and cost savings thereby allowing more wells to be drilled for the same annual budget.

- Cost reductions and smaller overall footage drilled will result in more economic wells and longer economic well lives resulting in a 5 to 10% increase in the recovery of oil and gas from these unconventional plays.

State-based Peridynamic Formulation Derivation (1)

Classical model: $\nabla.\left(\frac{\rho[\boldsymbol{x}]}{\mu}\boldsymbol{K}[\boldsymbol{x}].\nabla\Phi[\boldsymbol{x}]\right)+r[\boldsymbol{x}]=\mathbf{0}$

Multiplied by Test function

Develop its variational problem and infer the quadratic functional

$$I[\boldsymbol{x}]=\int_{\mathcal{B}} Z\big[\nabla\Phi[\mathbf{x}]\big]\mathrm{dV_x}-\int_{\mathcal{B}} r[\boldsymbol{x}]\Phi[\boldsymbol{x}]dV_x$$

$$Z\big[\nabla\Phi[\boldsymbol{x}]\big]=\frac{1}{2}\nabla\Phi[\boldsymbol{x}].\left(\frac{\rho[\boldsymbol{x}]}{\mu}\boldsymbol{K}[\boldsymbol{x}].\nabla\Phi[\boldsymbol{x}]\right).$$

Remove restrictions on *Z*

- Remove Locality: let Z depend on points $\boldsymbol{x}'$ finite distance away from $\boldsymbol{x}$
- Remove Continuity: let Z admit discontinuities in Φ

$$\begin{aligned}Z\equiv\hat{Z}&=\hat{Z}(\Phi(\boldsymbol{x}'),\Phi(\boldsymbol{x}),\boldsymbol{x}',\boldsymbol{x})\\&=\hat{Z}(\Phi',\Phi,\boldsymbol{x}',\boldsymbol{x})\\&=\hat{Z}\big((\Phi'-\Phi),(\boldsymbol{x}'-\boldsymbol{x})\big)\\&=\hat{Z}\big(\underline{\Phi},\boldsymbol{\xi}\big)\end{aligned}$$

We want to express Z as a function of potential difference and position difference instead of partial differentiation form

State-based Peridynamic Formulation Derivation(2)

Assume peridynamic analogue of the quadratic functional

$$\hat{I}[\boldsymbol{x}] = \int_{\mathcal{B}} \hat{Z}[\underline{\Phi}[\boldsymbol{x}]]dV_x - \int_{\mathcal{B}} r[\boldsymbol{x}]\Phi[\boldsymbol{x}]dV_x, \qquad \underline{\Phi}[\boldsymbol{x}]\langle\boldsymbol{\xi}\rangle = \Phi[\boldsymbol{x}'] - \Phi[\boldsymbol{x}]$$

Minimizing this formulation gives us peridynamic fluid flow formulation

The stationary value of $\hat{I}[x]$ at $\delta\hat{I}[x] = 0$ leads to peridynamic equation

Fréchet derivative: $\delta\hat{Z}\left[\underline{\Phi}[\boldsymbol{x}]\right] = \int_{\mathcal{B}} \underline{\nabla}\hat{Z}\langle\boldsymbol{\xi}\rangle.\,\delta\underline{\Phi}\langle\boldsymbol{\xi}\rangle dV_{x'}$

arbitrary

$$\delta\hat{I}[\boldsymbol{x}] = \int_{\mathcal{B}}\left(\int_{\mathcal{B}}\left(-\underline{\nabla}\hat{Z}[\boldsymbol{x}]\langle\boldsymbol{\xi}\rangle + \underline{\nabla}\hat{Z}[\boldsymbol{x}']\langle-\boldsymbol{\xi}\rangle\right)dV_{x'} + r[\boldsymbol{x}]\right)\delta\Phi[\boldsymbol{x}]dV_x = 0$$

$$\underline{Q}[\boldsymbol{x}]\langle\boldsymbol{\xi}\rangle = -\underline{\nabla}\hat{Z}[\boldsymbol{x}]\langle\boldsymbol{\xi}\rangle$$

Peridynamic model: $\frac{\partial}{\partial t}(\rho[\boldsymbol{x}]\emptyset[\boldsymbol{x}]) = \int_{\mathcal{H}_x}\left(\underline{Q}[\boldsymbol{x}]\langle\boldsymbol{\xi}\rangle - \underline{Q}[\boldsymbol{x}']\langle-\boldsymbol{\xi}\rangle\right)dV_{x'} + R[\boldsymbol{x}]$

$$\int_{\mathcal{B}} \left[\nabla \cdot \left(\frac{\rho_0}{\mu} \boldsymbol{K}[\boldsymbol{x}] \nabla \Phi[\boldsymbol{x}] \right) \right] \delta\Phi[\boldsymbol{x}]\, dV_x + \int_{\mathcal{B}} r[\boldsymbol{x}] \delta\Phi[\boldsymbol{x}]\, dV_x = 0.$$

$$\int_{\mathcal{B}} \left[\nabla\delta\Phi[\boldsymbol{x}] \cdot \left(\frac{\rho_0}{\mu} \boldsymbol{K}[\boldsymbol{x}] \nabla \Phi[\boldsymbol{x}] \right) \right] dV_x - \int_{\mathcal{B}} r[\boldsymbol{x}] \delta\Phi[\boldsymbol{x}]\, dV_x = 0,$$

$$B\left[\delta\Phi[\boldsymbol{x}], \Phi[\boldsymbol{x}]\right] - l\left[\delta\Phi[\boldsymbol{x}]\right] = 0,$$

$$\delta I[\boldsymbol{x}] = B\left[\delta\Phi[\boldsymbol{x}], \Phi[\boldsymbol{x}]\right] - l\left[\delta\Phi[\boldsymbol{x}]\right] = 0,$$

$$\delta I[\boldsymbol{x}] = \frac{1}{2}\delta B\left[\Phi[\boldsymbol{x}], \Phi[\boldsymbol{x}]\right] - \delta l\left[\Phi[\boldsymbol{x}]\right] = \delta\left[\frac{1}{2} B\left[\Phi[\boldsymbol{x}], \Phi[\boldsymbol{x}]\right] - l\left[\Phi[\boldsymbol{x}]\right]\right] = 0,$$

$$I[\boldsymbol{x}] = \frac{1}{2}\int_{\mathcal{B}} \nabla\Phi[\boldsymbol{x}] \cdot \left(\frac{\rho_0}{\mu} \boldsymbol{K}[\boldsymbol{x}] \nabla \Phi[\boldsymbol{x}] \right) dV_x - \int_{\mathcal{B}} r[\boldsymbol{x}] \Phi[\boldsymbol{x}]\, dV_x,$$

$$I[\boldsymbol{x}] = \int_{\mathcal{B}} Z\left[\nabla\Phi[\boldsymbol{x}]\right] dV_x - \int_{\mathcal{B}} r[\boldsymbol{x}] \Phi[\boldsymbol{x}]\, dV_x, \qquad Z\left[\nabla\Phi[\boldsymbol{x}]\right] = \frac{1}{2}\nabla\Phi[\boldsymbol{x}] \cdot \left(\frac{\rho_0}{\mu} \boldsymbol{K}[\boldsymbol{x}] \nabla \Phi[\boldsymbol{x}] \right).$$

Defining peridynamics way of I[x]

$$\hat{I}[\boldsymbol{x}] = \int_{\mathcal{B}} \hat{Z}\left[\underline{\Phi}[\boldsymbol{x}]\right] dV_x - \int_{\mathcal{B}} r[\boldsymbol{x}] \Phi[\boldsymbol{x}]\, dV_x, \qquad \underline{\Phi}[\boldsymbol{x}]\langle\boldsymbol{\xi}\rangle = \Phi\left[\boldsymbol{x}'\right] - \Phi[\boldsymbol{x}].$$

$$\delta\hat{Z}\left[\underline{\Phi}[\boldsymbol{x}]\right] = \hat{Z}\left[\underline{\Phi}[\boldsymbol{x}] + \delta\underline{\Phi}[\boldsymbol{x}]\right] - \hat{Z}\left[\underline{\Phi}[\boldsymbol{x}]\right] = \underline{\nabla}\hat{Z}[\boldsymbol{x}] \bullet \delta\underline{\Phi}[\boldsymbol{x}],$$

$$\delta\hat{Z}\left[\underline{\Phi}[\boldsymbol{x}]\right] = \int_{\mathcal{B}} \underline{\nabla}\hat{Z}[\boldsymbol{x}]\langle\boldsymbol{\xi}\rangle\delta\underline{\Phi}[\boldsymbol{x}]\langle\boldsymbol{\xi}\rangle\, dV_{x'},$$

Same procedure as local mocel with Frechet derivertive

$$\delta\hat{I}[\boldsymbol{x}] = \int_{\mathcal{B}} \delta\hat{Z}\left[\underline{\Phi}[\boldsymbol{x}]\right] dV_x - \int_{\mathcal{B}} \mathrm{r}[\boldsymbol{x}]\delta\Phi[\boldsymbol{x}]\, dV_x,$$

$$= \int_{\mathcal{B}}\int_{\mathcal{B}} \underline{\nabla}\hat{Z}[\boldsymbol{x}]\langle\boldsymbol{\xi}\rangle\delta\Phi\left[\boldsymbol{x}'\right] dV_{x'}\, dV_x - \int_{\mathcal{B}}\int_{\mathcal{B}} \underline{\nabla}\hat{Z}[\boldsymbol{x}]\langle\boldsymbol{\xi}\rangle\delta\Phi[\boldsymbol{x}]\, dV_{x'}\, dV_x - \int_{\mathcal{B}} \mathrm{r}[\boldsymbol{x}]\delta\Phi[\boldsymbol{x}]\, dV_x.$$

$$\delta\hat{I}[\boldsymbol{x}] = \int_{\mathcal{B}}\int_{\mathcal{B}} \left(\underline{\nabla}\hat{Z}\left[\boldsymbol{x}'\right]\langle-\boldsymbol{\xi}\rangle - \underline{\nabla}\hat{Z}[\boldsymbol{x}]\langle\boldsymbol{\xi}\rangle\right)\delta\Phi[\boldsymbol{x}]\, dV_{x'}\, dV_x - \int_{\mathcal{B}} \mathrm{r}[\boldsymbol{x}]\delta\Phi[\boldsymbol{x}]\, dV_x,$$

$$= \int_{\mathcal{B}}\left(\int_{\mathcal{B}} \left(-\underline{\nabla}\hat{Z}[\boldsymbol{x}]\langle\boldsymbol{\xi}\rangle + \underline{\nabla}\hat{Z}\left[\boldsymbol{x}'\right]\langle-\boldsymbol{\xi}\rangle\right) dV_{x'} - \mathrm{r}[\boldsymbol{x}]\right)\delta\Phi[\boldsymbol{x}]\, dV_x.$$

$$\int_{\mathcal{B}} \left(\underline{Q}[\boldsymbol{x}]\langle\boldsymbol{\xi}\rangle - \underline{Q}\left[\boldsymbol{x}'\right]\langle-\boldsymbol{\xi}\rangle\right) dV_{x'} + \mathrm{r}[\boldsymbol{x}] = 0.$$

Local Theory

$$L = L(\dot{u}_i, \varepsilon_{ij}) = T - U = \underbrace{\frac{1}{2}\rho\dot{\mathbf{u}}\cdot\dot{\mathbf{u}}}_{\text{Kinetic}} - \underbrace{\left\{\frac{1}{2}\lambda(\varepsilon_{kk})^2 + G\varepsilon_{ij}\varepsilon_{ij}\right\}}_{\text{Strain Energy Density}}$$

$$\delta\int_{t_1}^{t_2} L dt = \delta\int_{t_1}^{t_2}\int_V L dV dt$$

$$= \int_{t_1}^{t_2}\int_V \frac{\partial L}{\partial \dot{u}_i}\cdot\delta\dot{u}_i + \frac{\partial L}{\partial \varepsilon_{ij}}\delta\varepsilon_{ij} dV dt$$

$$= \int_V\int_{t_1}^{t_2}\frac{\partial L}{\partial \dot{u}_i}\cdot\delta\dot{u}_i dt dV + \int_{t_1}^{t_2}\int_V \frac{\partial L}{\partial \varepsilon_{ij}}\delta\left(\frac{1}{2}\left(\frac{\partial u_i}{\partial x_j} + \frac{\partial u_j}{\partial x_i}\right)\right) dV dt$$

$$= \int_V\int_{t_1}^{t_2}\left\{-\frac{d}{dt}\left(\frac{\partial L}{\partial \dot{u}_i}\right)\cdot\delta u_i\right\} dt dV + \int_{t_1}^{t_2} -\frac{1}{2}\left\{\int_V\sum_{j=1}^{3}\frac{\partial L}{\partial x_j\partial\varepsilon_{ij}}\cdot\delta u_i + \int_V\sum_{i=1}^{3}\frac{\partial L}{\partial x_i\partial\varepsilon_{ij}}\cdot\delta u_j\right\} dV dt$$

$$= \int_{t_1}^{t_2}\int_V\left\{-\frac{d}{dt}\left(\frac{\partial L}{\partial \dot{u}_i}\right) - \sum_{j=1}^{3}\frac{\partial L}{\partial x_j\partial\varepsilon_{ij}}\right\}\delta u_i dV dt$$

finding stationary value

$$-\frac{d}{dt}\left(\frac{\partial L}{\partial \dot{u}_i}\right) - \sum_{j=1}^{3}\frac{\partial L}{\partial x_j\partial\varepsilon_{ij}} = 0$$

$$\Leftrightarrow -\rho\ddot{u}_i - \sum_{j=1}^{3}\left(\lambda\delta_{ij}\frac{\partial\varepsilon_{kk}}{\partial x_j} + 2G\frac{\partial\varepsilon_{ij}}{\partial x_j}\right) = 0$$

$$\Leftrightarrow -\rho\ddot{u}_i - \frac{\partial}{\partial x_j}\left(\lambda\delta_{ij}\varepsilon_{kk} + 2G\varepsilon_{ij}\right) = 0$$

$$\sigma_{ij} = \lambda\varepsilon_{kk}\delta_{ij} + 2G\varepsilon_{ij}$$

$$\rho\ddot{\mathbf{u}} = -\nabla\cdot\boldsymbol{\sigma}$$

Peridynamics Theory

$$L = L(\dot{u}_i, \varepsilon_{ij}) = T - U = \underbrace{\int_B \frac{1}{2}\rho\dot{\mathbf{u}}\cdot\dot{\mathbf{u}} dV}_{\text{Kinetic}} - \underbrace{\int_B \Psi\left(\underline{\mathbf{Y}}(\mathbf{x})\langle\xi\rangle\right) dV_{\mathbf{x}}}_{\text{Strain Energy Density}}$$

$$\delta\int_{t_1}^{t_2} L dt = 0 \int_{t_1}^{t_2}\left(\delta(T-U)\right) dt = 0$$

$$\int_{t_1}^{t_2}\delta T dt = -\int_{t_1}^{t_2}\int_B p\ddot{\mathbf{u}}\cdot\delta\mathbf{u} dV dt$$

$$\int_{t_1}^{t_2}\delta U dt = \int_{t_1}^{t_2}\int_B \delta\Psi\left(\underline{\mathbf{Y}}(\mathbf{x})\langle\xi\rangle\right) dV_{\mathbf{x}} dt$$

Frechet Derivative

Inserting

$$\delta\Psi\left(\underline{\mathbf{Y}}(\mathbf{x})\langle\xi\rangle\right) = \Psi\left(\underline{\mathbf{Y}}(\mathbf{x})\langle\xi\rangle + \Delta\underline{\mathbf{Y}}(\mathbf{x})\langle\xi\rangle\right) - \Psi\left(\underline{\mathbf{Y}}(\mathbf{x})\langle\xi\rangle\right)$$

$$= \underline{\int_B \underline{\nabla}\Psi\left(\underline{\mathbf{Y}}(\mathbf{x})\langle\xi\rangle\right)\cdot\Delta\underline{\mathbf{Y}}(\mathbf{x})\langle\xi\rangle dV_{\xi}} + O\left(\left|\Delta\underline{\mathbf{Y}}(\mathbf{x})\langle\xi\rangle\right|^2\right)$$

$$= \int_{t_1}^{t_2}\int_B\int_B \underline{\nabla}\Psi\left(\underline{\mathbf{Y}}(\mathbf{x})\langle\xi\rangle\right)\cdot\Delta\underline{\mathbf{Y}}(\mathbf{x})\langle\xi\rangle dV_{\mathbf{x}'} dV_{\mathbf{x}} dt$$

$$= \int_{t_1}^{t_2}\int_B\int_B \underline{\nabla}\Psi\left(\underline{\mathbf{Y}}(\mathbf{x})\langle\xi\rangle\right)\cdot\left(\delta\mathbf{u}(\mathbf{x}') - \delta\mathbf{u}(\mathbf{x})\right) dV_{\mathbf{x}'} dV_{\mathbf{x}} dt$$

$$= \int_{t_1}^{t_2}\left\{\int_B\int_B \underline{\nabla}\Psi\left(\underline{\mathbf{Y}}(\mathbf{x})\langle\xi\rangle\right)\cdot\delta\mathbf{u}(\mathbf{x}') dV_{\mathbf{x}'} dV_{\mathbf{x}} - \int_B\int_B \underline{\nabla}\Psi\left(\underline{\mathbf{Y}}(\mathbf{x})\langle\xi\rangle\right)\cdot\delta\mathbf{u}(\mathbf{x}) dV_{\mathbf{x}'} dV_{\mathbf{x}}\right\} dt$$

$$\int_{t_1}^{t_2}\left(\int_B\left(-p\ddot{\mathbf{u}} - \left(\int_B\left(\underline{\nabla}\Psi\left(\underline{\mathbf{Y}}(\mathbf{x}')\langle-\xi\rangle\right) - \underline{\nabla}\Psi\left(\underline{\mathbf{Y}}(\mathbf{x})\langle\xi\rangle\right)\right) dV_{\mathbf{x}'}\right)\right)\cdot\delta\mathbf{u} dV\right) dt = 0$$

finding stationary value

$$\underline{\nabla}\Psi\left(\underline{\mathbf{Y}}(\mathbf{x})\langle\xi\rangle\right) = \underline{t}\frac{\left(\underline{\mathbf{Y}}(\mathbf{x})\langle\xi\rangle\right)}{\sqrt{\left(\underline{\mathbf{Y}}(\mathbf{x})\langle\xi\rangle\right)\cdot\left(\underline{\mathbf{Y}}(\mathbf{x})\langle\xi\rangle\right)}} = t\underline{\mathbf{M}} = \underline{T}(\mathbf{x})\langle\xi\rangle$$

$$p\ddot{\mathbf{u}} = \int_B\left(\underline{T}(\mathbf{x})\langle\xi\rangle - \underline{T}(\mathbf{x}')\langle-\xi\rangle\right) dV_{\mathbf{x}'}$$

# Local Theory	# Peridynamics Theory

$$I[\boldsymbol{x}] = \int_{\mathcal{B}} Z[\nabla\Phi[\mathbf{x}]]\mathrm{dV_x} - \int_{\mathcal{B}} r[\boldsymbol{x}]\Phi[\boldsymbol{x}]dV_x$$

$$Z[\nabla\Phi[\boldsymbol{x}]] = \frac{1}{2}\nabla\Phi[\boldsymbol{x}].\left(\frac{\rho[\boldsymbol{x}]}{\mu}\boldsymbol{K}[\boldsymbol{x}].\nabla\Phi[\boldsymbol{x}]\right).$$

$$\delta I[\mathbf{x}] = 0$$

$$\nabla.\left(\frac{\rho[x]}{\mu}\boldsymbol{K}[x].\nabla\Phi[x]\right) + r[x] = \mathbf{0}$$

$$\hat{I}[\boldsymbol{x}] = \int_{\mathcal{B}} \hat{Z}[\underline{\Phi}[\boldsymbol{x}]]dV_x - \int_{\mathcal{B}} r[\boldsymbol{x}]\Phi[\boldsymbol{x}]dV_x$$

$$\underline{\Phi}[\boldsymbol{x}]\langle\boldsymbol{\xi}\rangle = \Phi[\boldsymbol{x}'] - \Phi[\boldsymbol{x}]$$

$$\delta\hat{Z}\left[\underline{\Phi}[\boldsymbol{x}]\right] = \int_{\mathcal{B}} \underline{\nabla}\hat{Z}\langle\boldsymbol{\xi}\rangle.\,\delta\underline{\Phi}\langle\boldsymbol{\xi}\rangle dV_{x'}$$

arbitrary

$$\delta\hat{I}[\boldsymbol{x}] = \int_{\mathcal{B}}\left(\int_{\mathcal{B}}\left(-\underline{\nabla}\hat{Z}[\boldsymbol{x}]\langle\xi\rangle + \underline{\nabla}\hat{Z}[\boldsymbol{x}']\langle-\xi\rangle\right)dV_{x'} + r[\boldsymbol{x}]\right)\delta\Phi[\boldsymbol{x}]dV_x = 0$$

$$\frac{\partial}{\partial t}(\rho[\boldsymbol{x}]\phi[\boldsymbol{x}]) = \int_{\mathcal{H}_x}\left(\underline{Q}[\boldsymbol{x}]\langle\xi\rangle - \underline{Q}[\boldsymbol{x}']\langle-\xi\rangle\right)dV_{x'} + R[\boldsymbol{x}]$$

Results for a Benchmark Flow Problem

5-spot well pattern

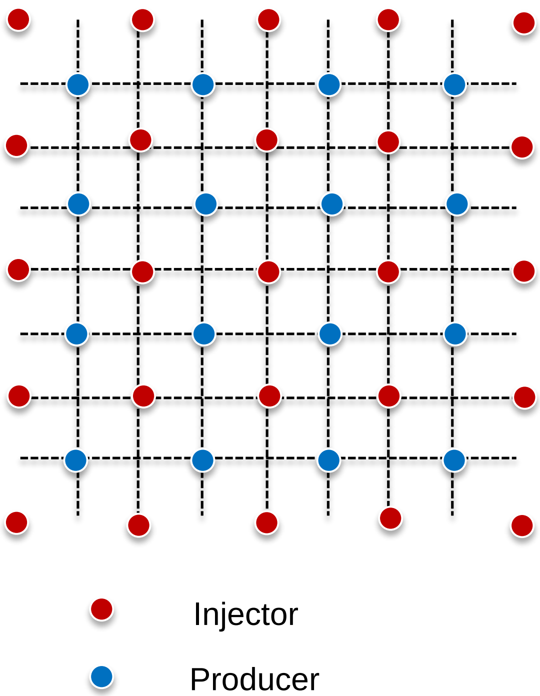

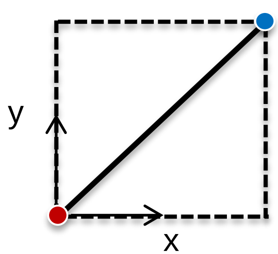

Steady State

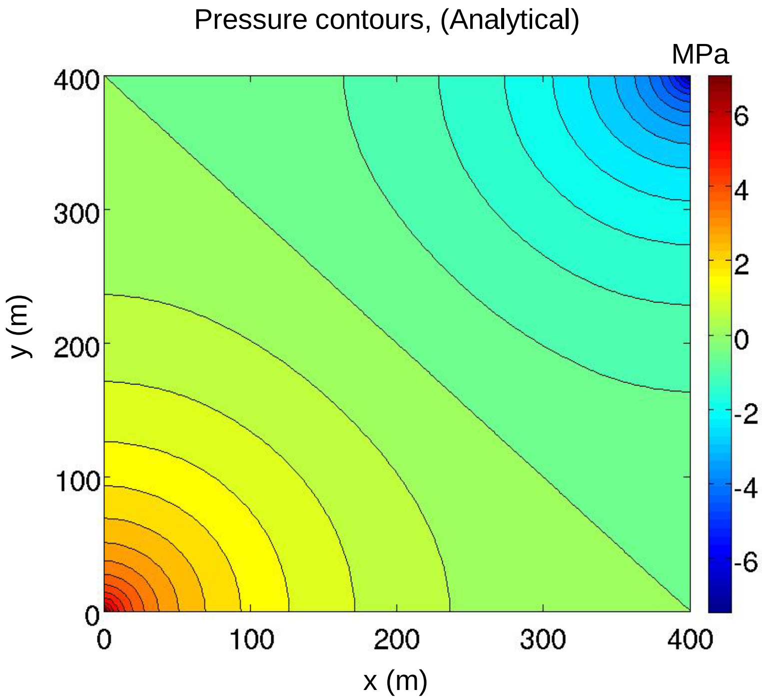

$k = 100\text{ mD} = 10^{-13}\, m^2$

$\mu = 0.001\text{ Pa.s}$

$N = 100$

$$Q_T(\boldsymbol{x}) = 0.001\,\frac{m^3}{s}$$

Results for a Benchmark Flow Problem

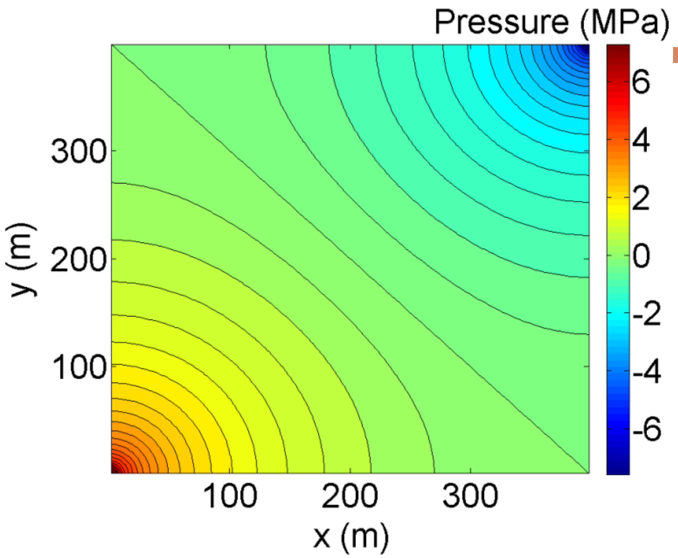

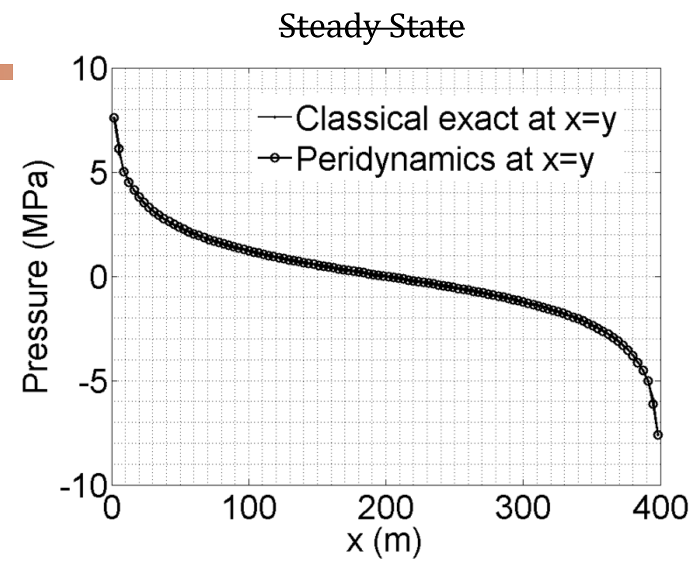

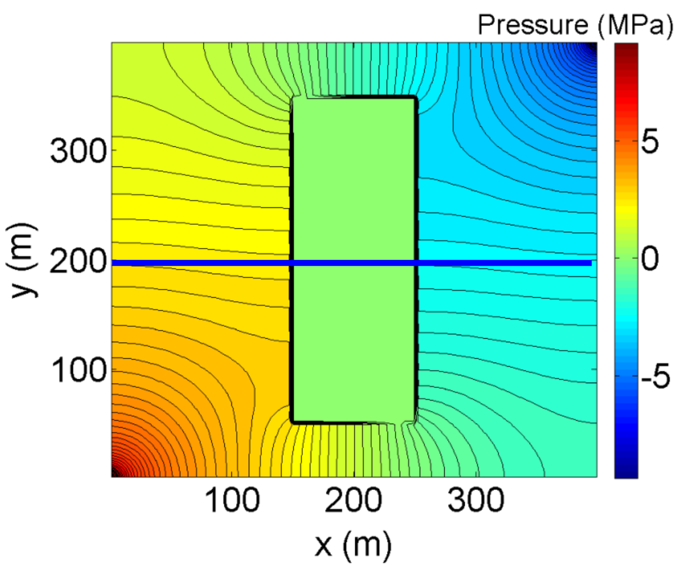

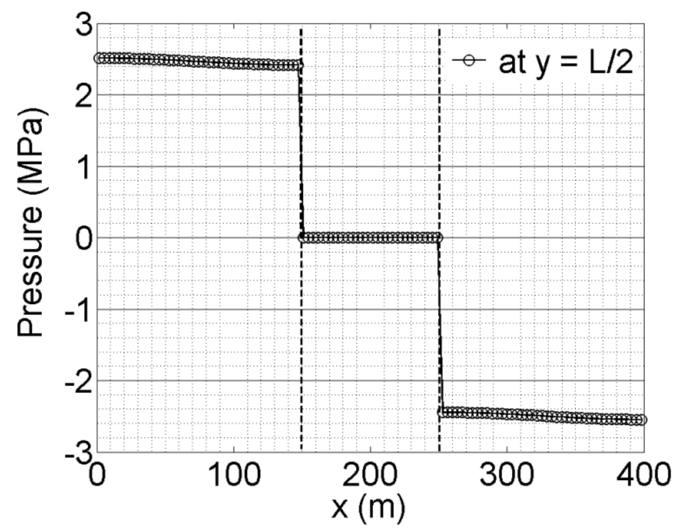

Constitutive Equations

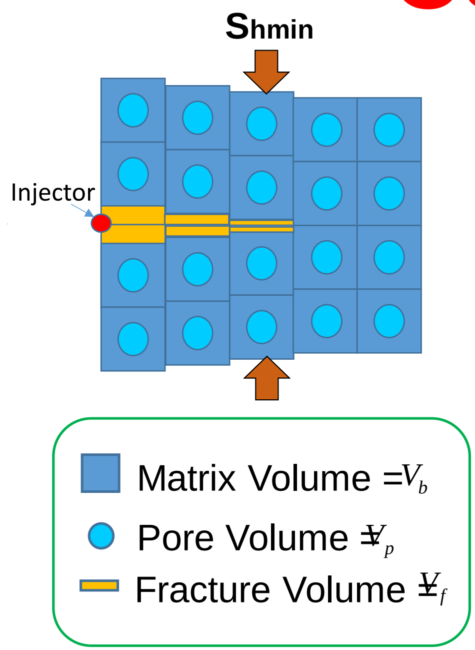

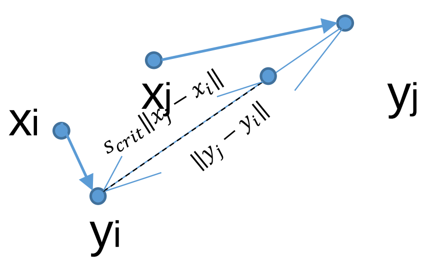

$$e_i^* = \min\left(\left\|\mathbf{y}_j - \mathbf{y}_i\right\|, s_{crit}\left\|\mathbf{x}_j - \mathbf{x}_i\right\|\right) - \left\|\mathbf{x}_j - \mathbf{x}_i\right\|$$

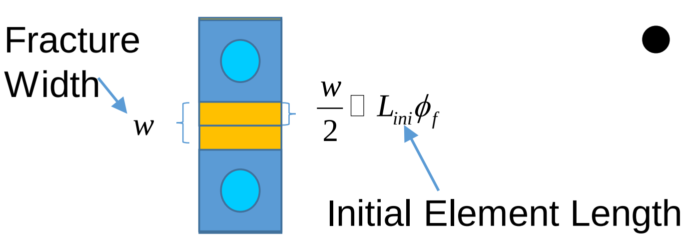

- **Porosity equations**

matrix

$$\phi_i^{(n+1)} = \frac{V_{pi}^{(n+1)}}{V_{bi}} = \phi_i^{(n)}\left\{1 - C_r\left(P_i^{(n+1)} - P_i^{(n)}\right)\right\}$$
$$+\alpha\left(1+\theta_{mlocal\_i}^{(n)}\right)\left\{C_r\left(P_i^{(n+1)} - P_i^{(n)}\right) + \left(\theta_{mlocal\_i}^{(n+1)} - \theta_{mlocal\_i}^{(n)}\right)\right\}$$

fracture

$$\phi_{fi}^{(n+1)} = \frac{V_{fi}^{(n+1)}}{V_{bi}} = \theta_{local\_i}^{(n+1)} - \theta_{local@crit\_damage}$$

where,

$$\theta_{local\_i}^{(n+1)} = \sum_{j=1}^{N_{local}}\left\{\frac{\omega_i\left\|\mathbf{x}_j - \mathbf{x}_i\right\| e_i^{(n+1)} dV_j}{m_{local\_i}}\right\} = \sum_{j=1}^{N_{local}}\left\{\frac{\omega_i\left\|\mathbf{x}_j - \mathbf{x}_i\right\|\left(\left\|\mathbf{y}_j^{(n+1)} - \mathbf{y}_i^{(n+1)}\right\| - \left\|\mathbf{x}_j - \mathbf{x}_i\right\|\right) dV_j}{m_{local\_i}}\right\}$$

$$\theta_{mlocal\_i}^{(n+1)} = \sum_{j=1}^{N_{local}}\left\{\frac{\omega_i\left\|\mathbf{x}_j - \mathbf{x}_i\right\| e_i^{*(n+1)} dV_j}{m_{local\_i}}\right\} = \sum_{j=1}^{N_{local}}\left\{\frac{\omega_i\left\|\mathbf{x}_j - \mathbf{x}_i\right\|\left(\min\left(\left\|\mathbf{y}_j^{(n+1)} - \mathbf{y}_i^{(n+1)}\right\|, s_{crit}\left\|\mathbf{x}_j - \mathbf{x}_i\right\|\right)\right) dV_j}{m_{local\_i}}\right\}$$

$$m_{local\_i} = \sum_{j=1}^{N_{local}}\left\{\omega_i\left\|\mathbf{x}_j - \mathbf{x}_i\right\|^2 dV_j\right\}$$

- **Fracture Permeability Equation**

$$k_f = 0 \qquad (if\ \ d < d_{crit})$$

$$= \frac{w^2}{12} = \frac{\left(2L_{ini}\phi_f\right)^2}{12} \qquad (if\ \ d \ge d_{crit})$$

Constitutive Equations

- **Flow between pore and fracture in a element**

$$I\left(x_i,t\right)=\frac{q_{i\_inner}}{V_{bi}}=\frac{k_{mi}A_i\left(P_{fi}-P_{mi}\right)}{V_{bi}\mu\Delta l_i}$$

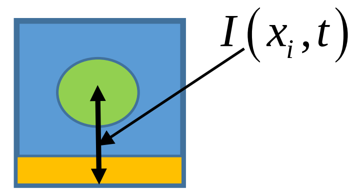

- **Force Scalar State**

For bonds not passing through fracture surface

$$T\left[\mathbf{x}_i,t\right]\left\langle \mathbf{x}_j-\mathbf{x}_i\right\rangle - T\left[\mathbf{x}_j,t\right]\left\langle \mathbf{x}_i-\mathbf{x}_j\right\rangle = \left[\left\{(3K-5G)\left(\frac{\theta_i\omega_i}{m_i}+\frac{\theta_j\omega_j}{m_j}\right)-3\alpha\left(\frac{P_i\omega_i}{m_i}+\frac{P_j\omega_j}{m_j}\right)\right\}\left\|\mathbf{x}_j-\mathbf{x}_i\right\|+15G\left(\frac{\omega_i}{m_i}+\frac{\omega_j}{m_j}\right)e_i\right]\frac{\left(\mathbf{y}_j^{(n+1)}-\mathbf{y}_i^{(n+1)}\right)}{\left\|\mathbf{y}_j^{(n+1)}-\mathbf{y}_i^{(n+1)}\right\|}$$

For bonds passing through fracture surface

$$T\left[\mathbf{x}_i,t\right]\left\langle \mathbf{x}_j-\mathbf{x}_i\right\rangle - T\left[\mathbf{x}_j,t\right]\left\langle \mathbf{x}_i-\mathbf{x}_j\right\rangle = 3P_{fk}\left(\frac{\omega_i}{m_i}+\frac{\omega_j}{m_j}\right)\left\|\mathbf{x}_j-\mathbf{x}_i\right\|\frac{\left(\mathbf{y}_j^{(n+1)}-\mathbf{y}_i^{(n+1)}\right)}{\left\|\mathbf{y}_j^{(n+1)}-\mathbf{y}_i^{(n+1)}\right\|}$$

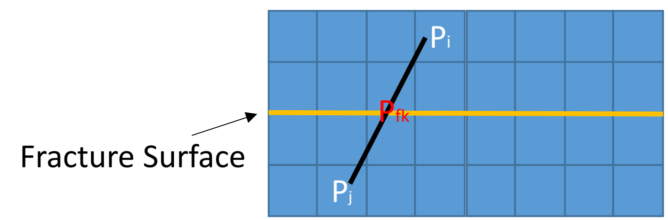

- **Flow Scalar State**

For matrix

$$Q_m\left[\mathbf{x}_i,t\right]\left\langle \mathbf{x}_j-\mathbf{x}_i\right\rangle - Q_m\left[\mathbf{x}_j,t\right]\left\langle \mathbf{x}_i-\mathbf{x}_j\right\rangle = \frac{\gamma\rho_{mi}}{\mu}\frac{\xi\left(\mathbf{K}_{mi}-0.25\,trace\left(\mathbf{K}_{mi}\right)\mathbf{I}\right)\xi}{\left\|\xi\right\|^4}\left(P_{mj}-P_{mi}\right)$$

For fracture

$$Q_f\left[\mathbf{x}_i,t\right]\left\langle \mathbf{x}_j-\mathbf{x}_i\right\rangle - Q_f\left[\mathbf{x}_j,t\right]\left\langle \mathbf{x}_i-\mathbf{x}_j\right\rangle = \frac{\gamma\rho_{fi}}{2\mu}\frac{k_{i\_ij}}{\left\|\xi\right\|^2}\left(P_{fj}-P_{fi}\right)$$

How to apply constant stress boundary condition?

Constant stress boundary condition is given as a body force in the elements which distance from the boundary is less than horizon size.

<u>Example case: horizon size = 3 delta (boundary forces are given to three layers from the boundary)</u>

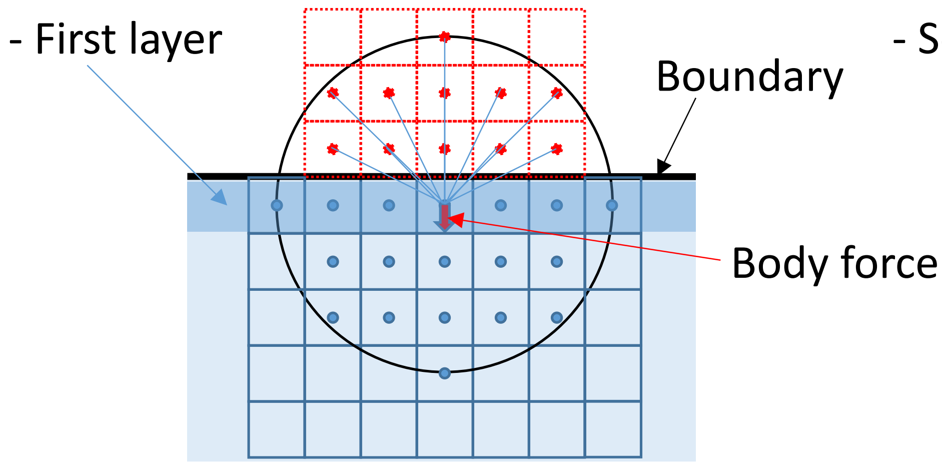

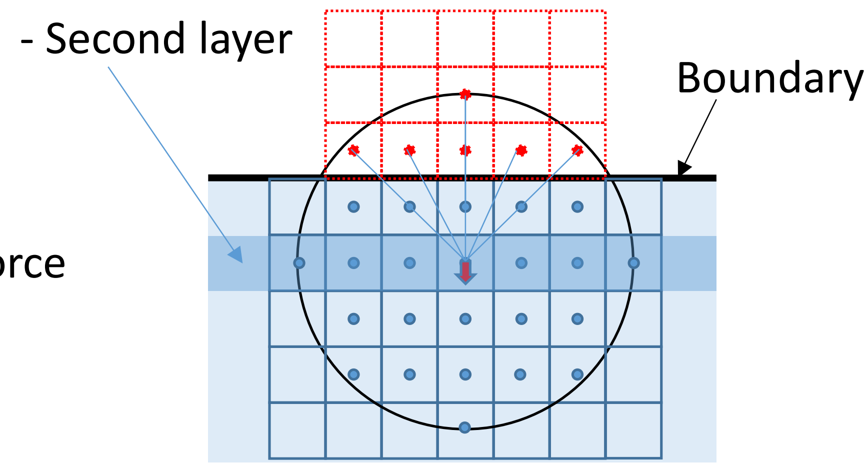

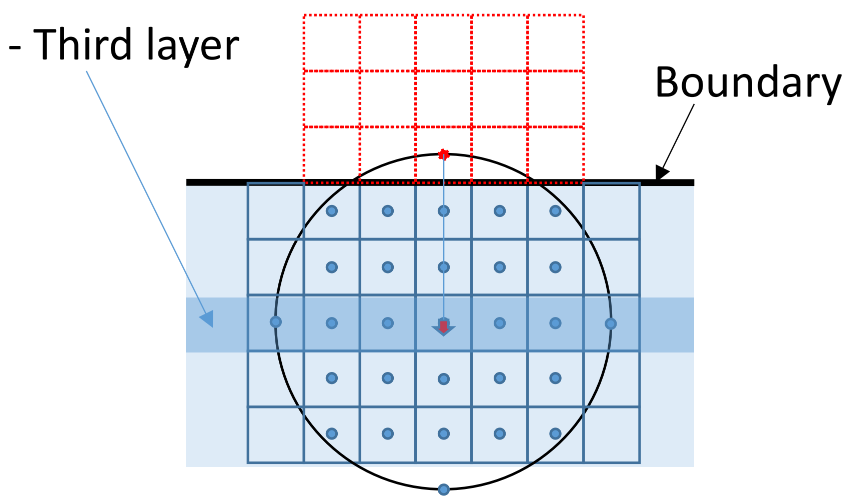

$$\vec{b}_{boundary} = \sum_{j=1}^{N_{ghost}} \left\{ -3\tau_{bounary} \left(\frac{\omega_i}{m_i} + \frac{\omega_j}{m_j} \right) \left\| x_j - x_i \right\| V_j \frac{\vec{\xi}}{\left\| \xi \right\|} \right\}$$

*note that the equation above is for 3D.

(for 2D) $\vec{b}_{boundary} = \sum_{j=1}^{N_{ghost}} \left\{ -2\tau_{bounary} \left(\frac{\omega_i}{m_i} + \frac{\omega_j}{m_j} \right) \left\| x_j - x_i \right\| V_j \frac{\vec{\xi}}{\left\| \xi \right\|} \right\}$

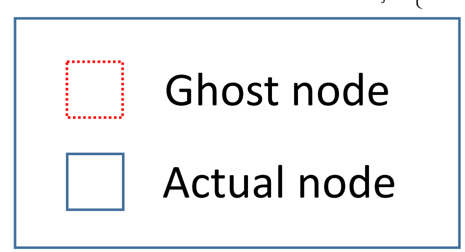

Fracture Surface Connection

We want to limit our fracture elements in 1st line even if 2nd line damage exceeds a critical damage. How?

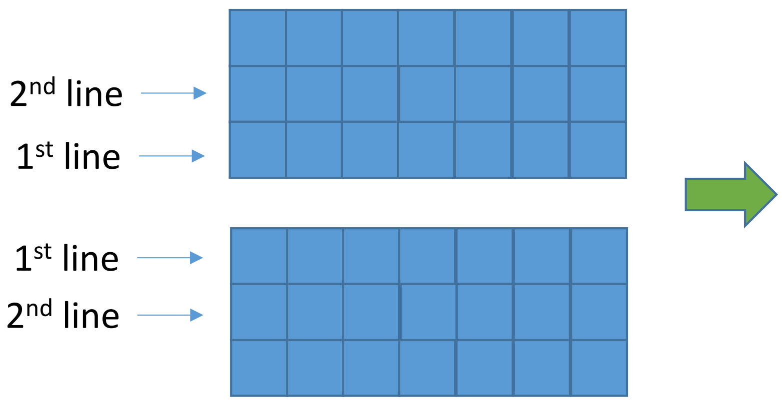

Additional constraints for fracture flow

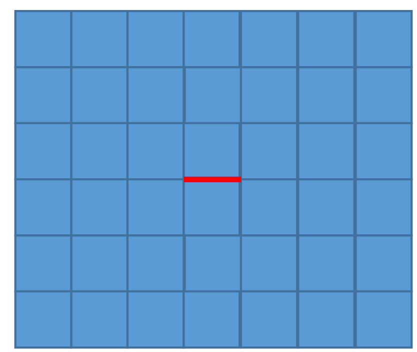

- Defining which surface has fracture in each element
- One element cannot have two independent frac. Surface
- New fracture surface must connecting pre existing fracture surface

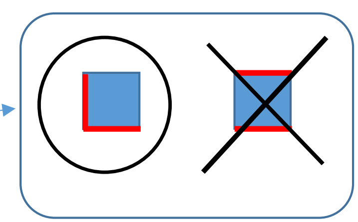

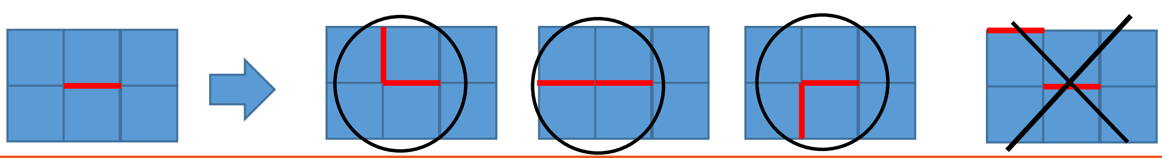

Comparison with KGD solution

(Fracture Pressure Distribution after 80 sec)

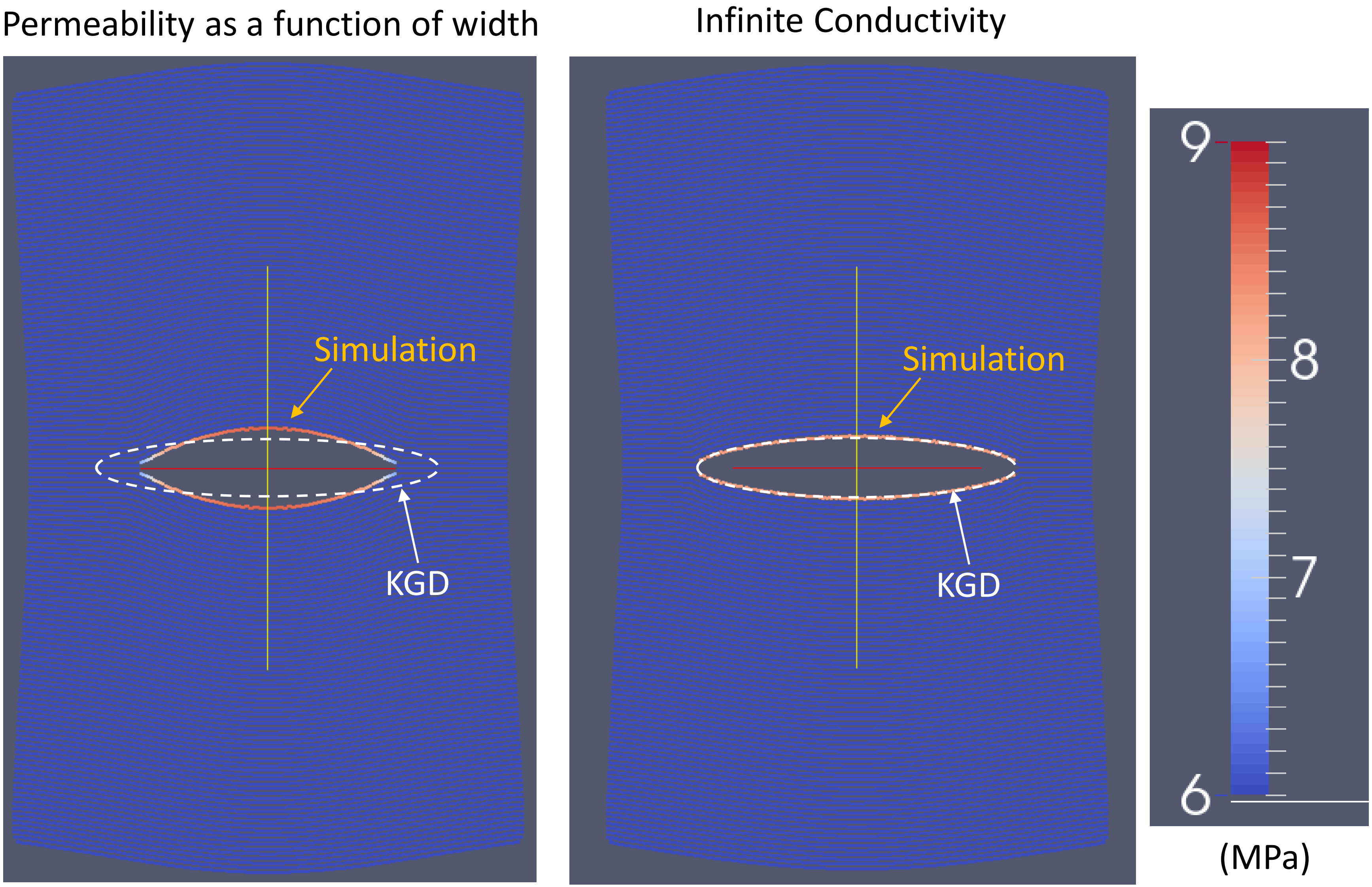

*note that Shmin = 8 MPa, Deformation is exaggerated 2000 times.

ervoir rock requires a particular boundary condition at the tip of the fracture. This condition, for the first time suggested by Zheltov and Khristianovitch,[3] and later clarified by Barenblatt,[4] states that, in the case of a fracture in mobile equilibrium propagating in a brittle solid, the distribution of normal pressure exerted by the fracturing fluid on the fracture walls must be such that the faces of the fracture close smoothly at the edges. The condition of smooth closing implies that

$$\left(\frac{dw}{df_L}\right)_{f_L=1} = 0 \quad \text{and} \quad \left(\frac{dw}{df_R}\right)_{f_R=1} = 0, \text{ respectively.}$$

Barenblatt proved that this ensures that the normal-stress component at the tip of the fracture is finite and equal to the tensile strength of the rock. The tensile strength can be assumed to be of negligible influence for large-sized fractures in the practical range of overburden pressures (see Perkins and Krech[5]). Substitution of the above boundary condition in Eqs. 3 and 4 leads to

$$\int_0^1 \frac{p(f_L)\, df_L}{\sqrt{1-f_L^2}} = \frac{\pi}{2} S \quad , \quad . \quad . \quad . \quad . \quad (5)$$

for the linear configuration, and

$$\int_{f_{Rw}}^1 \frac{f_R\, p(f_R)\, df_R}{\sqrt{1-f_R^2}} = S \quad , \quad . \quad . \quad . \quad . \quad (6)$$

for the circular.

(Note that if the tensile strength had been taken into account, Eqs. 5 and 6 would have been found to be

$$\int_0^1 \frac{p(f_L)\, df_L}{\sqrt{1-f_L^2}} = \frac{\pi}{2} S + \frac{K}{\sqrt{2L}} ,$$

and

$$\int_{f_{Rw}}^1 \frac{f_R\, p(f_R)\, df_R}{\sqrt{1-f_R^2}} = S + \frac{K}{\sqrt{2R}} ,$$

respectively,

in which $K = \sqrt{\frac{\pi E a}{1-\nu^2}}$ = Barenblatt's cohesion modulus. In this expression E = Young's modulus and a the specific surface energy. Our theory thus assumes that $2L \geq \frac{4}{\pi^2}\frac{K^2}{S^2}$ and that $2R \geq \frac{K^2}{S^2}$, respectively.)

Equations for Fracture Width and Shape

In Appendices A and B approximate solutions for the sets of equations (Eqs. 1, 3, 5 and Eqs. 2, 4, 6) are derived. For a linearly propagating fracture the maximum width at the origin amounts approximately to

$$w_w = 2.1 \sqrt[4]{\frac{\mu Q L^2}{G h}} \quad , \quad . \quad . \quad . \quad . \quad . \quad . \quad (7)$$

for an average value of Poisson's ratio, $\nu = 0.25$; and the shape of the fracture, except in a narrow wedge-like zone near the tip, is more or less elliptical:

$$w^2 = w_w^2 (1 - f_L^2) \quad . \quad . \quad . \quad . \quad . \quad . \quad . \quad (8)$$

Eq. 7 is valid for

$$\sqrt{\frac{\mu Q G^3}{S^4 L^2 h}} << 1, \text{ say } < 0.05 \quad . \quad . \quad (9)$$

This means that by combining condition (9) with Eq. 7, the theory is valid at least for $w_w < \frac{SL}{G}$ or $\frac{w_w}{L} < \frac{S}{G}$. For instance if $G = 10^5$ kgf/sq cm, at a depth where $S = 200$ kg/sq cm, w_w must be smaller than 20 mm for $L = 10$ m.

Under these conditions, it develops that the fluid-injection pressure with respect to the tectonic stress perpendicular to the fracture walls, S, is

$$p_w = S + \frac{2\, G\, w_w}{3L} . \quad . \quad . \quad . \quad . \quad . \quad . \quad (10)$$

Because according to Eq. 7 w_w increases in proportion to $\sqrt{L}$, it is found that p_w decreases with increasing fracture length and approaches S for large values of L. Such pressure behavior is in agreement with reported field observations. A check for the validity of the assumption of laminar flow is that the Reynolds number, N_{Re} equals $Q\, \rho / h\, \mu$ less than 1,000, where ρ is the liquid density.

For a radially propagating fracture, the maximum width at the wellbore, again for $\nu = 0.25$, is approximately

$$w_w = 2 \sqrt[4]{\frac{\mu Q R}{G}} \quad , \quad . \quad . \quad . \quad . \quad . \quad . \quad (11)$$

and the shape is parabolic except for a narrow zone near the tip:

$$w^2 = w_w^2 (1 - f_R) \quad . \quad . \quad . \quad . \quad . \quad . \quad . \quad (12)$$

Eq. 12 is valid for $\sqrt{\frac{\mu Q G^3}{S^4 R^3}} << 1$, again say < 0.05, or $w_w < \frac{SR}{G}$.

The fluid pressure at the entrance of the fracture ($r = R_w$) decreases with increasing fracture radius R according to

$$p_w = S - \frac{5}{4\pi} \frac{G w_w}{R} \ln f_{Rw} .$$

In terms of the Reynolds number, laminar flow conditions are now fulfilled provided N_{Re} equals $Q\, \rho / 2\, \pi\, r\, \mu$ less than 1,000. The fracturing fluid will usually behave in a laminar fashion, except in a certain area near the wellbore. As long as this area is limited to a few well radii, it will hardly invalidate the theory given.

Effect of Formation Permeability on Fracture Dimensions

Communication between fracture volume and the

r = radial distance
S = tectonic stress normal to fracture plane
S_p = spurt loss
t = pumping time
Δt = time of exposure to fluid loss
u = rate of fluid loss per unit surface area
V = fracture volume
w = fracture width
x = longitudinal distance
δ = penetration depth of fracturing fluid in formation
μ = fluid viscosity
ν = Poisson's ratio of formation
ρ = fluid density
$\tau = t - \Delta t$

Acknowledgments

We wish to thank A. C. van der Vlis for providing the data on the field application mentioned in the last section, and the management of Shell Research N.V., The Hague, The Netherlands, for permission to publish this paper.

References

1. England, A. H. and Green, A. E.: "Some Two-Dimensional Punch and Crack Problems in Classical Elasticity", *Proc.*, Cambridge Phil. Soc. (1963) **59**, 489.
2. Sneddon, I. N.: "The Distribution of Stress in the Neighbourhood of a Crack in an Elastic Solid", *Proc.*, Royal Society of London (1946) A 187, 229.
3. Zheltov, Yu. P. and Khristianovitch, S. A.: "The Hydraulic Fracturing of an Oil-Producing Formation", Izvest. Akad. Nauk SSSR, Otdel Tekh Nauk (1955) No. 3, 41.
4. Barenblatt, G. I.: "The Mathematical Theory of Equilibrium Cracks in Brittle Fracture", *Advances in Applied Mechanics* (1962) **7**, 56.
5. Perkins, T. K. and Krech, W. W.: "The Energy Balance Concept of Hydraulic Fracturing", *Soc. Pet. Eng. J.* (March, 1968) 1-12.
6. Geertsma, J.: "Problems of Rock Mechanics in Petroleum Production Engineering", *Proc.*, First Cong. Intl. Soc. of Mech., Lisbon (1966) **I**, 585.
7. Sadowsky, M. A.: "Thermal Shock on a Circular Surface of Exposure of an Elastic Half Space", *J. Appl. Mech.* (1955) **22**, 177.
8. Howard, G. C. and Fast, C. R.: "Optimum Fluid Characteristics for Fracture Extension", *Drill. and Prod. Prac.*, API (1957) 261.
9. *Handbook of Mathematical Functions*, M. Abramowitz and I. A. Stegun, eds., Natl. Bureau of Standards, New York (1964).
10. Perkins, T. K. and Kern, L. R.: "Widths of Hydraulic Fractures", *J. Pet. Tech.* (Sept., 1961) 937-949.
11. Baron, G. *et al.*: "Fracturation hydraulique; bases théoriques, études de laboratoire, essais sur champ", *Proc.*, Seventh World Pet. Cong. (1967) **3**, 371.
12. Khristianovitch, S. A. and Zheltov, Yu. P.: "Formation of Vertical Fractures by Means of Highly Viscous Fluid", *Proc.*, Fourth World Pet. Cong. (1955) **II**, 579.

APPENDIX A

Fracture Width Determination for a Linear Mode of Propagation

The behavior of a linearly propagating fracture has been considered in some detail by Khristianovitch and Zheltov.[12] A conformal mapping technique was used for finding the displacement field. We give here a simplified approach that leads to the practical formula, Eq. 7. To this end, we assume a plausible pressure distribution in the fracture and calculate from Eq. 3 the fracture shape, and from Eq. 1 the pressure distribution in such a fracture. This will show whether or not the assumption is acceptable.

Barenblatt's condition that closure must be smooth implies infinite flow resistance at the very tip of the fracture, so that pressure here must be zero. Since with smooth closure the increase in fracture width is more than proportional to the distance from the tip, the pressure gradient decreases by at least the third power of the distance (see Eq. 1). It therefore rapidly becomes very small, and it is plausible to approximate the pressure distribution in the fracture by the discontinuous one*

$$p = \bar{p} \text{ for } 0 \leqslant f_L \leqslant f_{Lo}$$
$$p = 0 \text{ for } f_{Lo} \leqslant f_L \leqslant 1,$$

where we suppose, *a priori*, $f_{Lo} \to 1$. Barenblatt's condition equation (Eq. 5) gives, with such a distribution,

$$f_{Lo} = \sin \frac{\pi}{2} \frac{S}{\bar{p}} \quad . \quad . \quad . \quad . \quad . \quad . \quad . \quad . \quad \text{(A-1)}$$

The fracture shape resulting from this pressure distribution follows from Eq. 3

$$w = \frac{2(1-\nu)}{\pi G} \bar{p} L \left[f_L \ln \frac{\left| 1 - \frac{f_{Lo}}{f_L} \left(\frac{1-f_L^2}{1-f_{Lo}^2} \right)^{1/2} \right|}{1 + \frac{f_{Lo}}{f_L} \left(\frac{1-f_L^2}{1-f_{Lo}^2} \right)^{1/2}} - f_{Lo} \ln \frac{\left| 1 - \left(\frac{1-f_L^2}{1-f_{Lo}^2} \right)^{1/2} \right|}{1 + \left(\frac{1-f_L^2}{1-f_{Lo}^2} \right)^{1/2}} \right] \quad . \quad . \quad \text{(A-2)}$$

This shows that the maximum fracture width at the wellbore amounts to

$$w_w = \frac{2(1-\nu)}{\pi G} \bar{p} L f_{Lo} \ln \frac{(1-f_{Lo}^2)^{-1/2} + 1}{(1-f_{Lo}^2)^{-1/2} - 1} .$$

For $f_{Lo} \to 1$ this reduces to

$$w_w \sim \frac{4(1-\nu)}{\pi G} \bar{p} L f_{Lo} \sqrt{1 - f_{Lo}^2} ,$$

whereas a good approximation of the equilibrium condition (Eq. A-1) is

$$(\bar{p} - S) \sim \frac{2}{\pi} \bar{p} f_{Lo} \sqrt{1 - f_{Lo}^2} .$$

Combining the last two approximations leads to

$$w_w \sim \frac{2(1-\nu)}{G} L (\bar{p} - S) .$$

For a given pressure in the fracture in excess of the tectonic stress, the fracture width at the origin is thus to a first approximation independent of f_{Lo}; i.e., it does not depend on the extent of the region of zero

*This approach to solve the problem, proposed for the first time in Ref. 12 is frequently misinterpreted as assuming a void near the tip of the fracture. However, only the pressure is off, at least in our theory. The fracturing extends right to the tip of the fracture with a local steep pressure gradient.

Ref: Geertsma, J., and de Klerk, F. 1969. A rapid method of predicting width and extent of hydraulically induced fractures. *J. Pet. Tech.* 21:1571–1581.

Parallel Performance

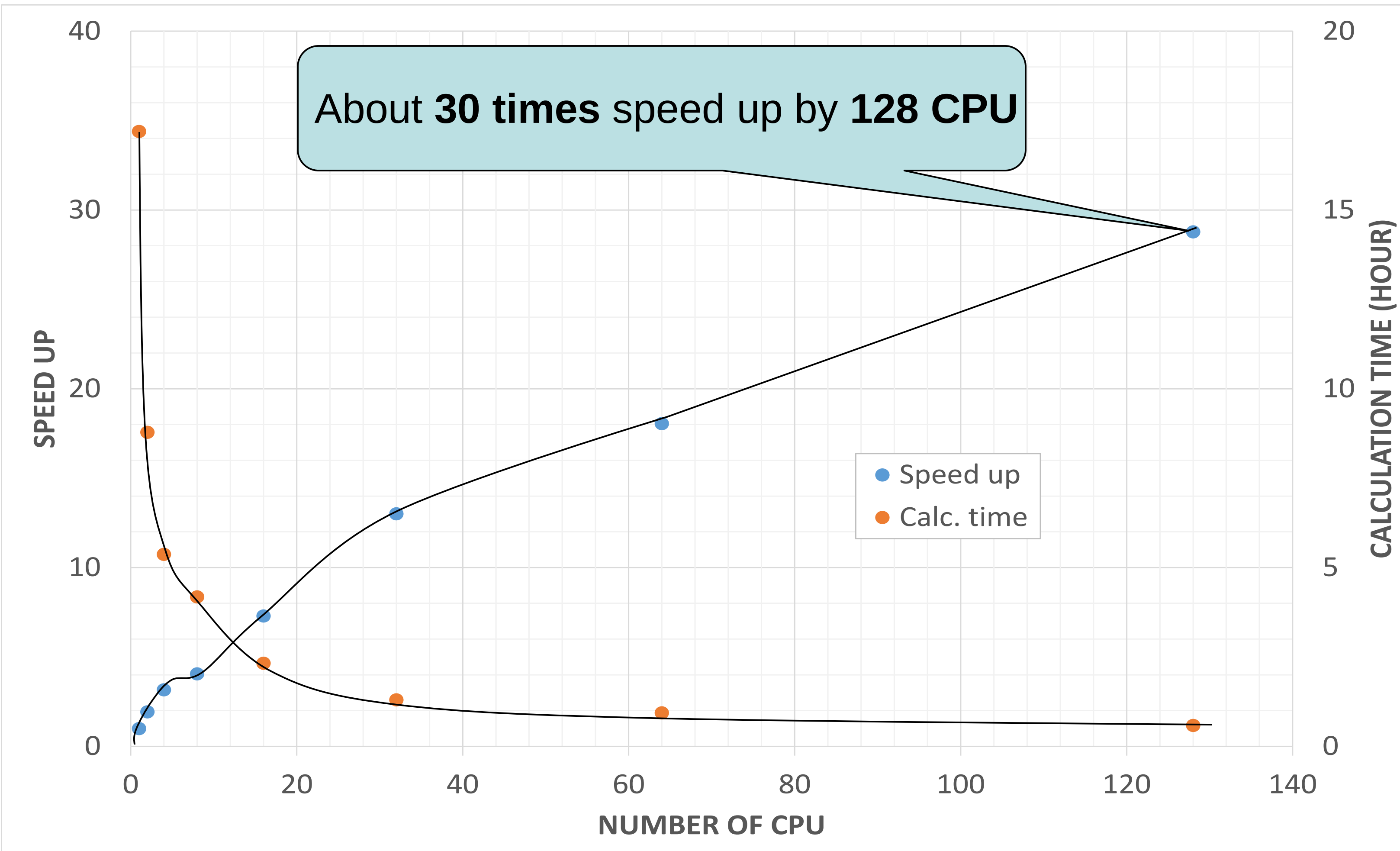

Biot Consolidation Validation

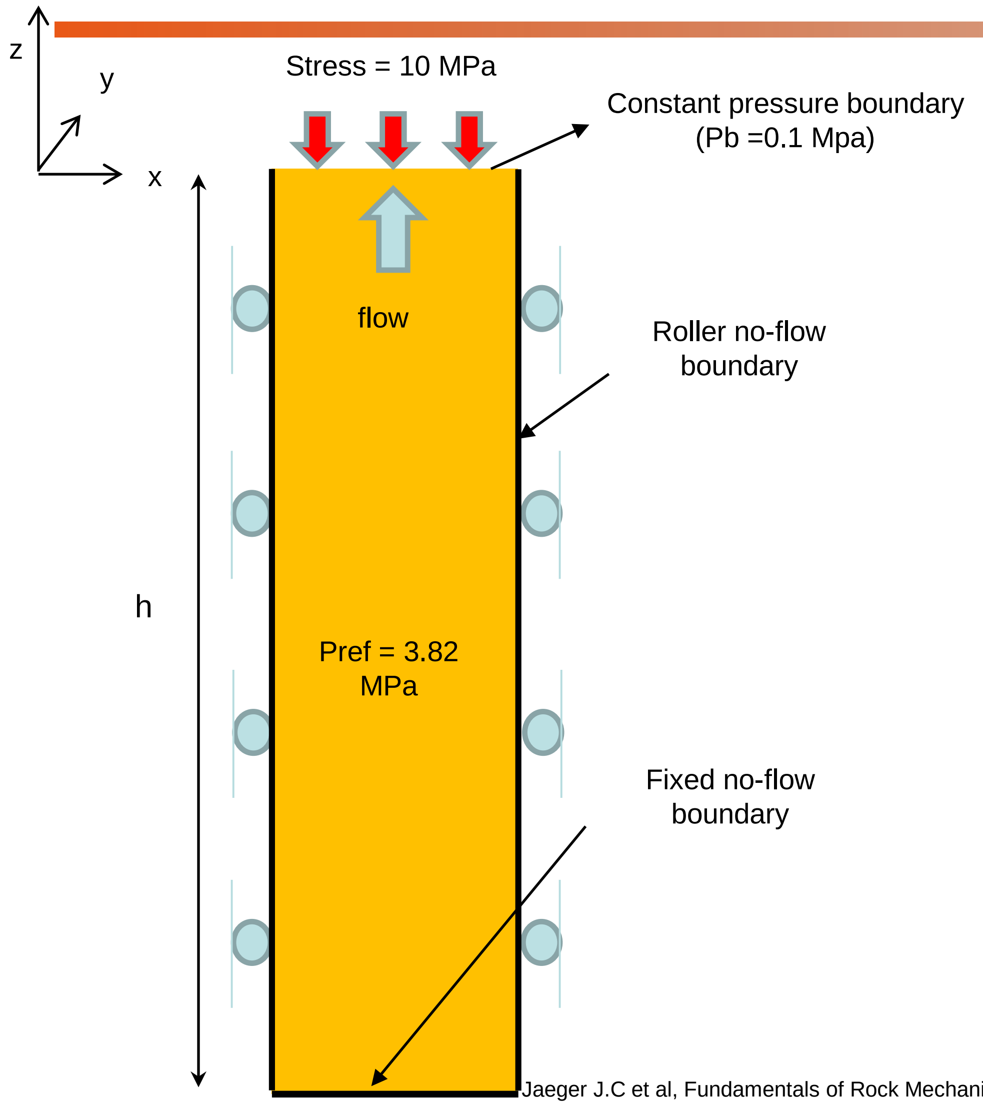

- Young's modulus (GPa) = 30
- Poisson's ratio = 0.25
- Porosity = 0.02
- Permeability (mD) = 6
- Biot coefficient = 0.6667
- Initial pore pressure (MPa) = 3.82
- Fluid: Water

Jaeger J.C et al, Fundamentals of Rock Mechanics, forth edition, 189-P194

Results: Pressure and Deformation

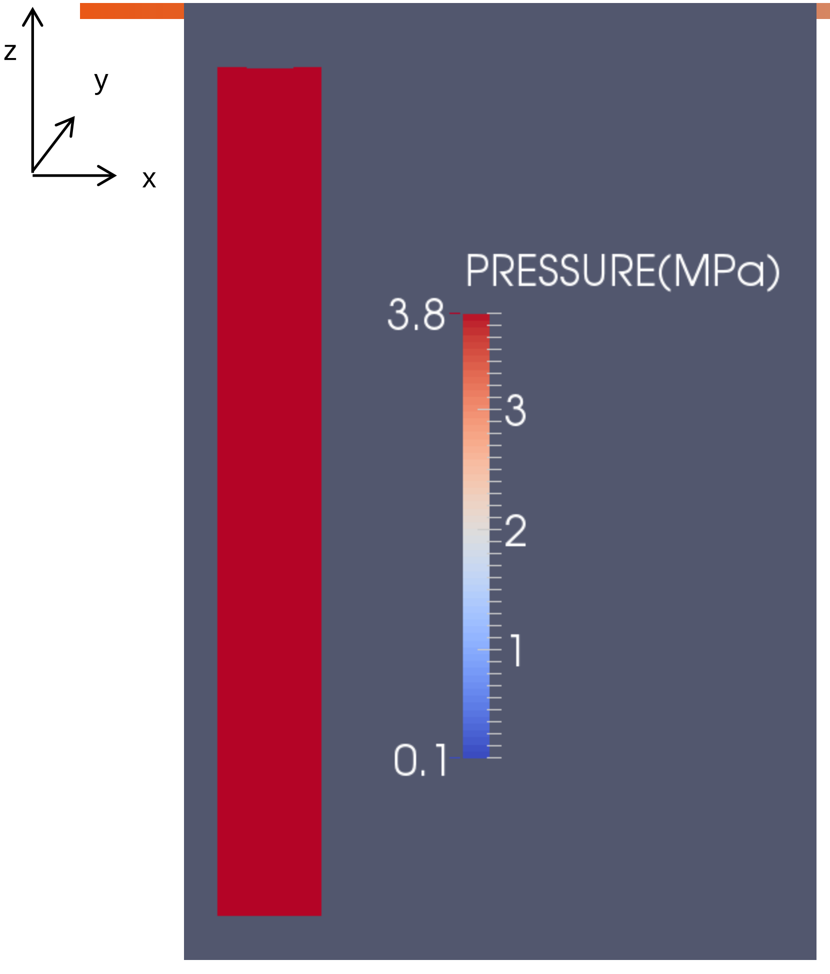

time < 0

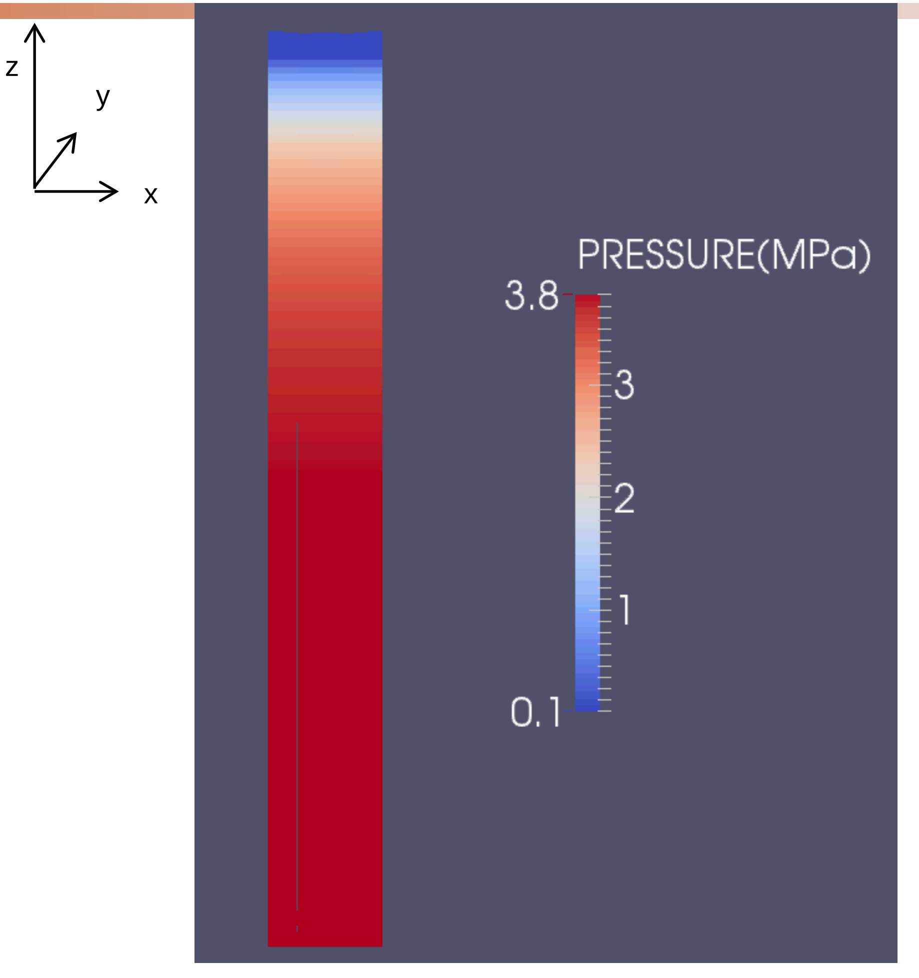

time > 0

Shear Failure Model in Peridynamics

Disassembling original force vector state into two directions

Deleting tangential force vector state once shear failure criteria is satisfied

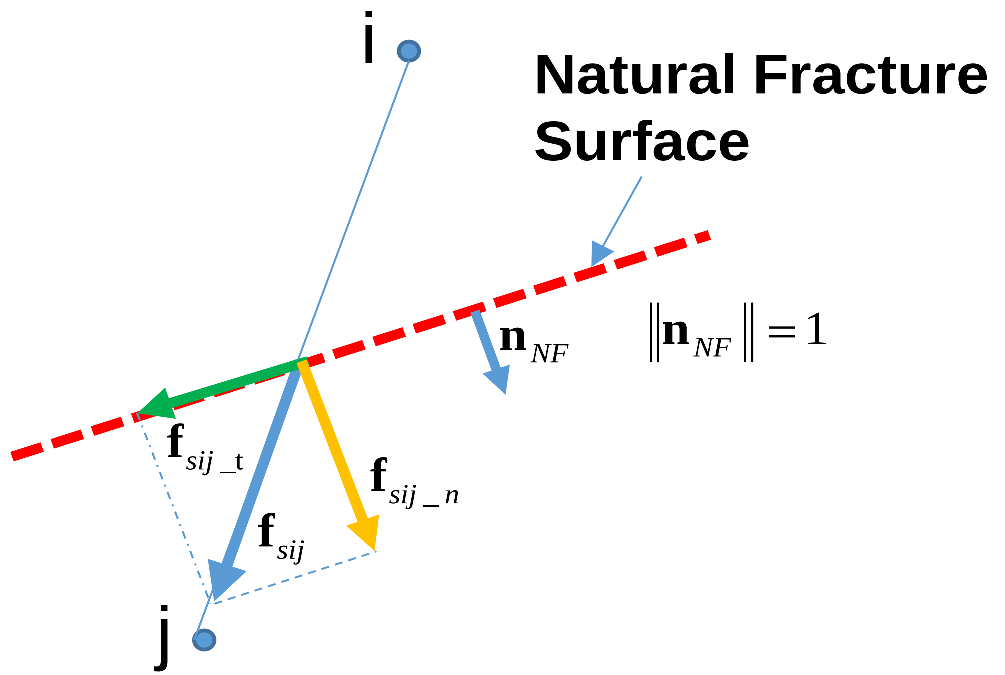

Results
(Case 2: Lower Half NF)

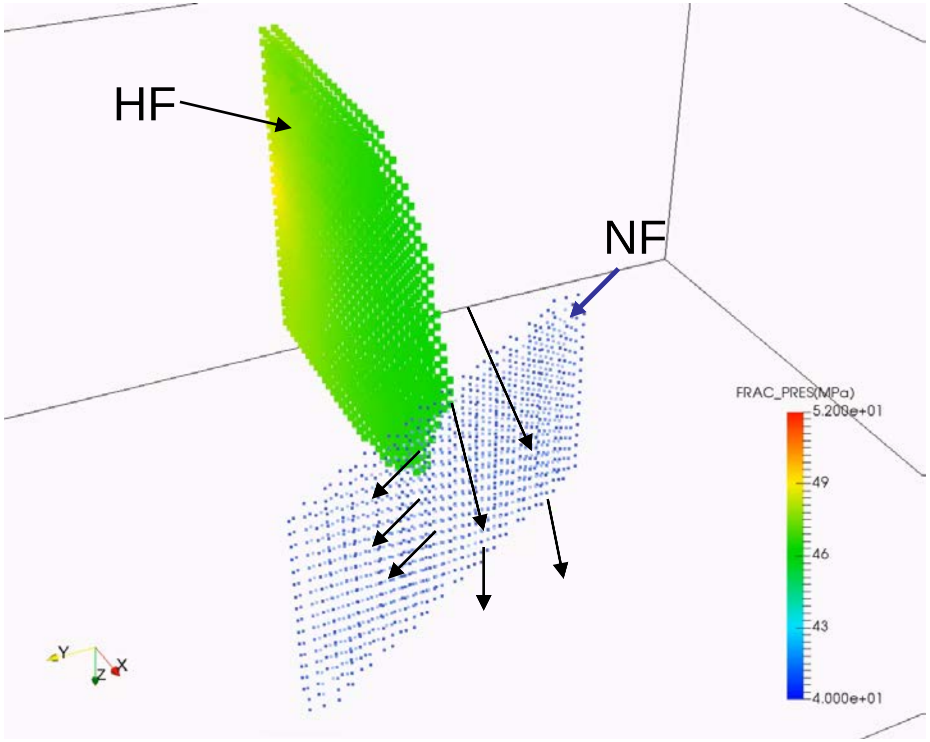

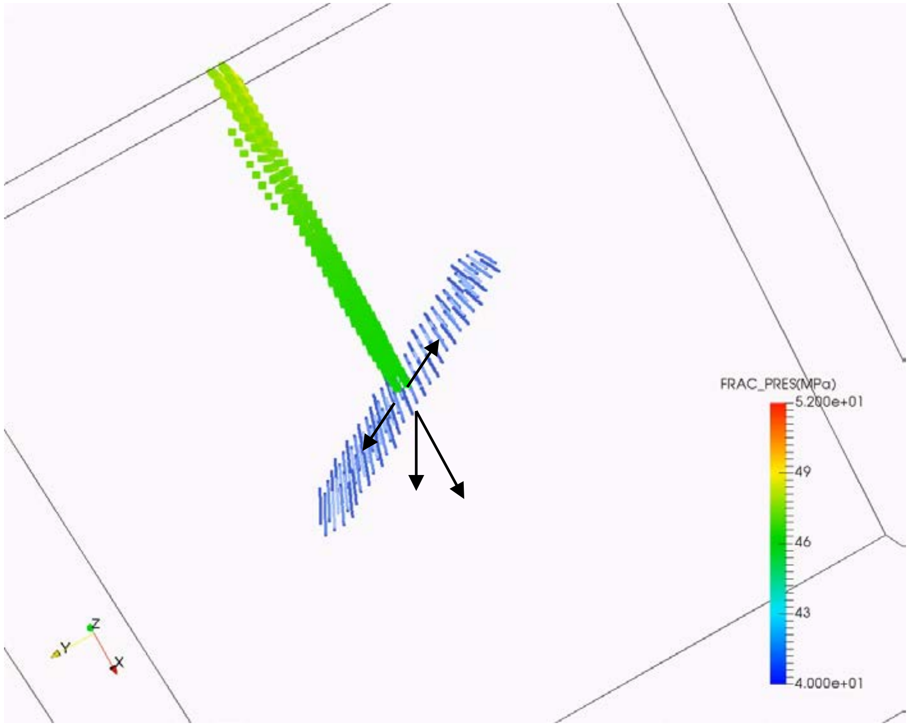

Results
(Case 4: Middle Half NF)

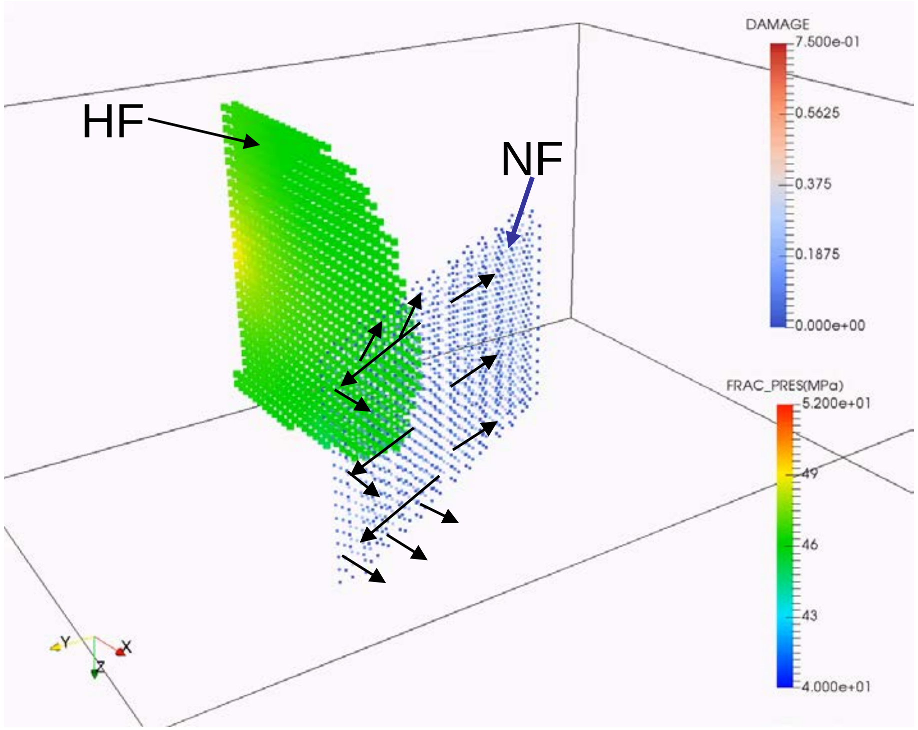

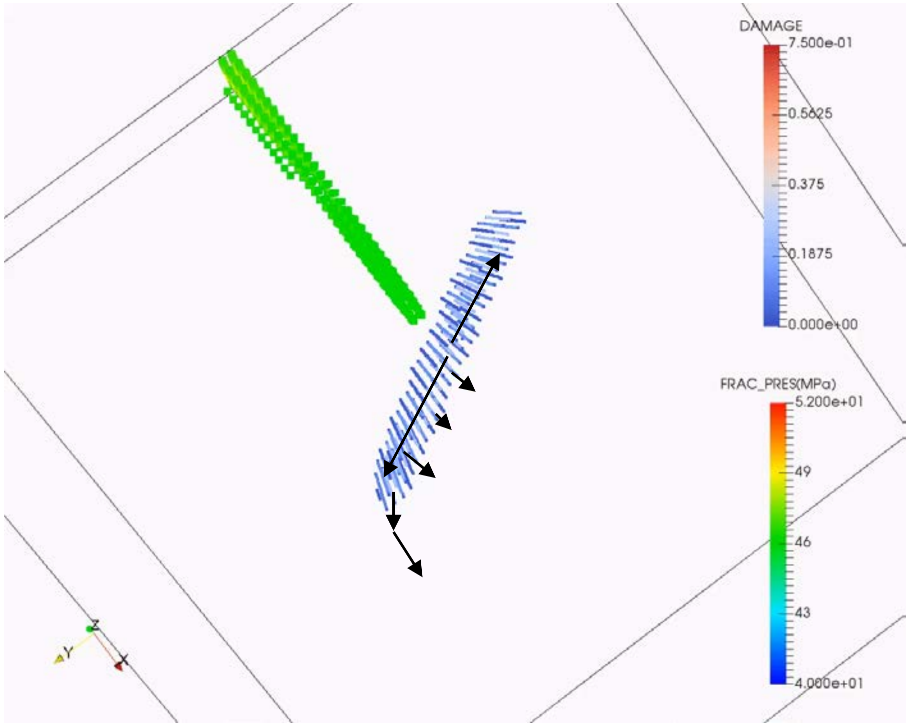

Investigation of Fracture Propagation Behavior in 3 Layers

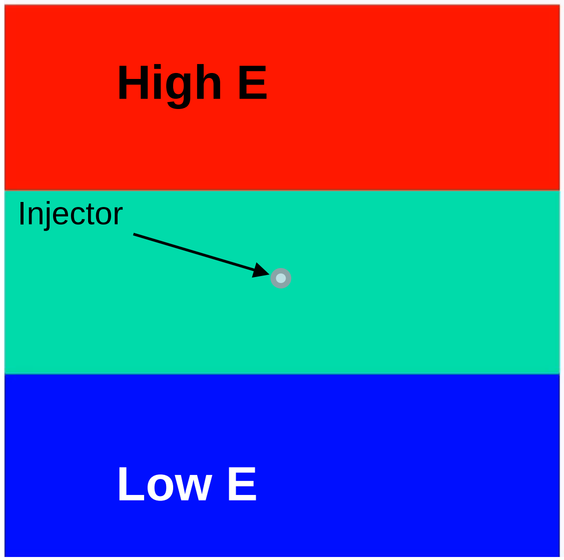

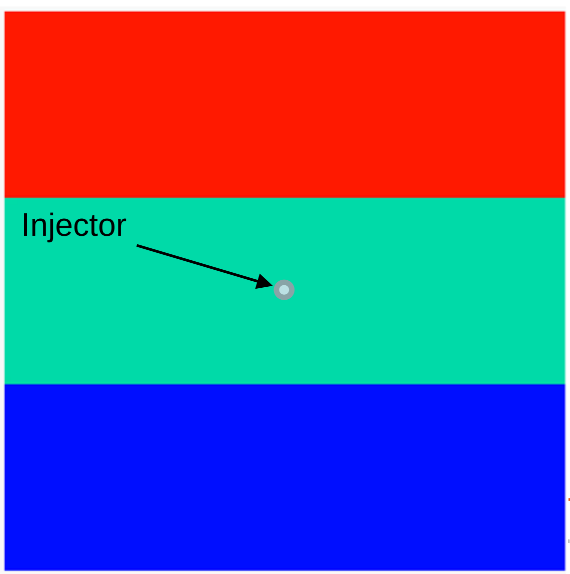

If the layer is sanded by the two different Young's modulus layers, the fracture always propagate more to the softer layer at first.

However, after reaching the layer interface with the low Young's modulus layer, the fracture propagation behavior changes with mechanical properties of each layer.

Which parameter governs the preferential fracture propagation direction?

Model Description

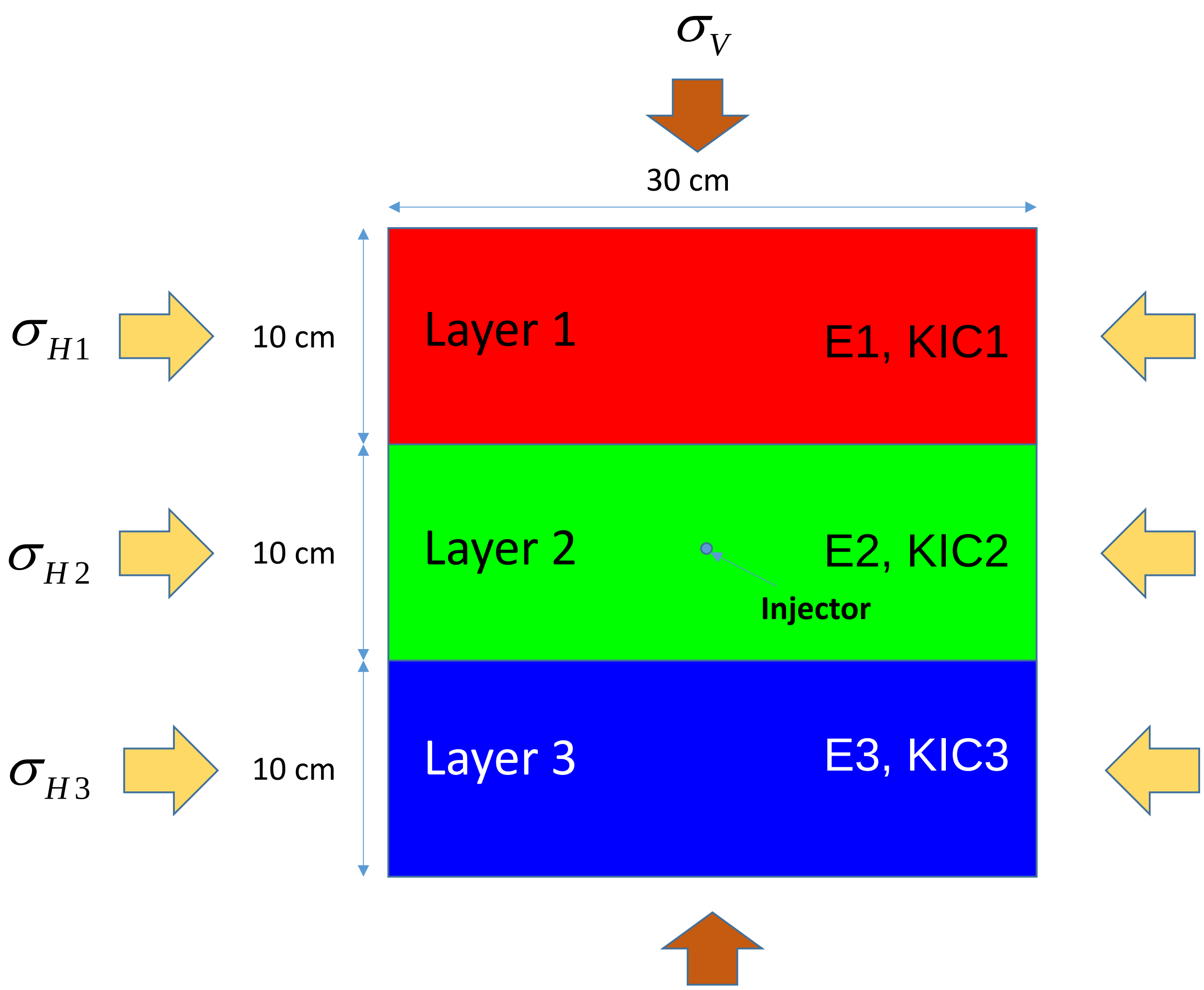

Results

Which parameter controls the preferential propagation direction?

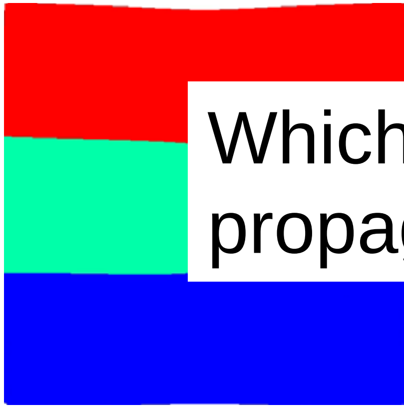

E 40/20/10 GPa,
KIC 0.707/0.5/0.354 MPa m0.5
Sxx 40/40/40 MPa
(Gc 11.7/11.7/11.7 J/m^2)

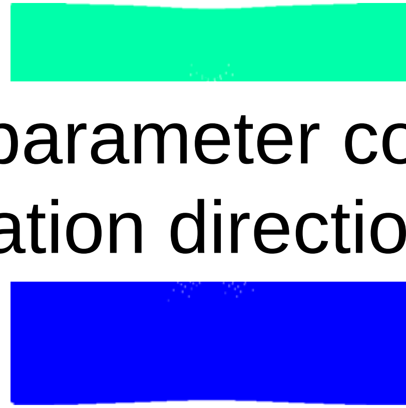

E 20/40/10 GPa,
KIC 0.5/0.707/0.354 MPa m$^{0.5}$
Sxx 40/40/40 MPa
(Gc 11.7/11.7/11.7 J/m^2)

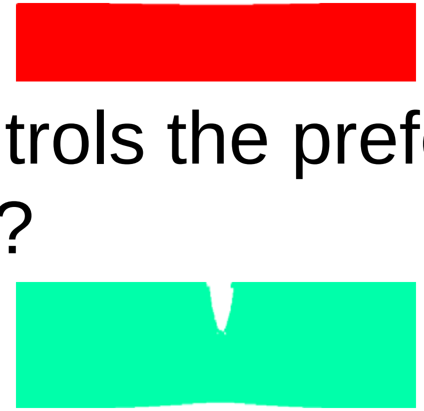

E 40/10/20 GPa,
KIC 0.707/0.354/0.5 MPa m$^{0.5}$
Sxx 40/40/40 MPa
(Gc 11.7/11.7/11.7 J/m^2)

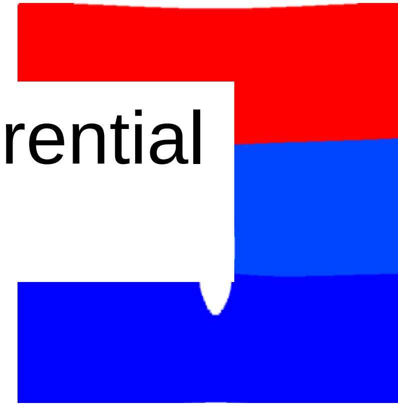

E 40/12/10 GPa,
KIC 0.707/0.5/0.354 MPa m$^{0.5}$
Sxx 40/40/40 MPa
(Gc 11.7/19.5/11.7 J/m^2)

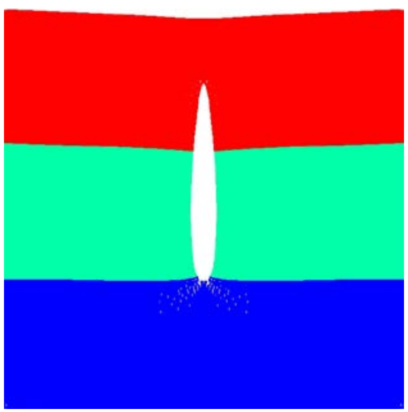

E 40/20/10 GPa,
KIC 1.2/0.5/0.354 MPa m$^{0.5}$
Sxx 40/40/40 MPa
(Gc 23.4/11.7/11.7)

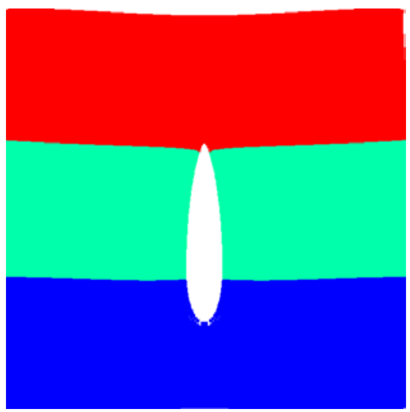

E 40/20/10 GPa,
KIC 1.6/0.5/0.354 MPa m0.5
Sxx 40/40/40 MPa
(Gc 33.8/11.7/11.7)

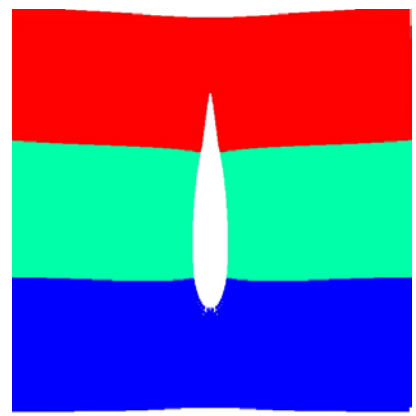

E 40/20/10 GPa,
KIC 0.707/0.5/0.354 MPa m0.5
Sxx 45/40/40 MPa
(Gc 11.7/11.7/11.7 J/m^2)

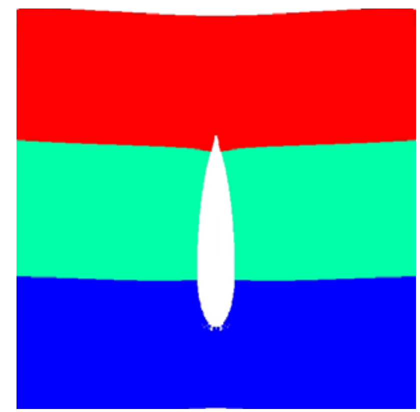

E 40/20/10 GPa,
KIC 0.707/0.5/0.354 MPa m$^{0.5}$
Sxx 50/40/40 MPa
(Gc 11.7/11.7/11.7 J/m^2)

Theoretical Consideration (Critical Displacement)

To break a bond, how much deformation is necessary?

$$\omega_c = \frac{9G_c}{4\delta^3} = \frac{9K_{IC}^2\left(1-\nu^2\right)}{4\delta^3 E} \qquad \omega_\xi = \int_0^{\eta(t_{final})}\left\{\underline{T}^*[\mathbf{x},t]\langle\xi\rangle - \underline{T}^*[\mathbf{x}',t]\langle-\xi\rangle\right\}\cdot d\boldsymbol{\eta}$$

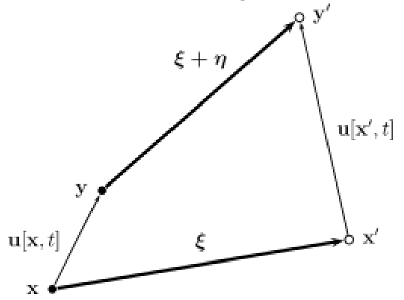

If $\omega_\xi > \omega_c$, bond will break.

background force vector st

$$\underline{T}^*[\mathbf{x},t]\langle\xi\rangle = \underline{t}[\mathbf{x},t]\langle\xi\rangle\frac{\xi+\boldsymbol{\eta}}{\|\xi+\boldsymbol{\eta}\|} + T_0[\mathbf{x}]\langle\xi\rangle$$

For the simplicity, here we neglect back ground vector state term and poroelastic effect.

inserting $\underline{e}^d\langle\xi\rangle = \underline{e}\langle\xi\rangle - \frac{\theta}{3}\underline{x}\langle\xi\rangle$

$$\underline{T}^*[\mathbf{x},t]\langle\xi\rangle = \left[\frac{2\left(\left(K-\frac{G}{3}\right)\theta\right)}{m}\underline{\omega x}\langle\xi\rangle + \frac{8G}{m}\underline{\omega e}^d\langle\xi\rangle\right]\frac{\xi+\boldsymbol{\eta}}{\|\xi+\boldsymbol{\eta}\|}$$

$$= \left[\frac{2\left(\left(K-\frac{G}{3}\right)\theta\right)}{m}\underline{\omega x}\langle\xi\rangle + \frac{8G}{m}\underline{\omega e}^d\langle\xi\rangle\right]\frac{\xi+\boldsymbol{\eta}}{\|\xi+\boldsymbol{\eta}\|}$$

$\underline{e}\langle\xi\rangle = \|\xi+\boldsymbol{\eta}\| - \|\xi\|$

$$= \left[\frac{\underline{\omega}}{m}\left\{\frac{2}{3}(3K-5G)\theta + 8G\underline{e}\right\}\right]\frac{\xi+\boldsymbol{\eta}}{\|\xi+\boldsymbol{\eta}\|} \qquad m = \int_0^\delta\int_0^{2\pi}\underline{\omega}r^2 r\,d\varphi\,dr = \frac{\pi\delta^4}{2}$$

If we assume Poisson's ratio = 0.25 and $\underline{\omega}=1.0$ for the simplicity, the equation above becomes the function of E and delta.

$$= 8\left[\frac{G}{m}\left(\|\xi+\boldsymbol{\eta}\|-\|\xi\|\right)\right]\frac{\xi+\boldsymbol{\eta}}{\|\xi+\boldsymbol{\eta}\|} = \frac{16\left(\frac{3}{5}E\right)}{\pi\delta^4}\left(\|\xi+\boldsymbol{\eta}\|-\|\xi\|\right)\frac{\xi+\boldsymbol{\eta}}{\|\xi+\boldsymbol{\eta}\|} = \frac{48E}{5\pi\delta^4}\left(\|\xi+\boldsymbol{\eta}\|-\|\xi\|\right)\frac{\xi+\boldsymbol{\eta}}{\|\xi+\boldsymbol{\eta}\|}$$

Theoretical Consideration

$$\omega_{\xi} = \int_0^{\boldsymbol{\eta}(t_{final})} \left\{ \underline{T}^* [\mathbf{x}, t] \langle \xi \rangle - \underline{T}^* [\mathbf{x}', t] \langle -\xi \rangle \right\} \cdot d\boldsymbol{\eta}$$

$$= \int_0^{\boldsymbol{\eta}(t_{final})} \frac{96E}{5\pi\delta^4} \left(\|\xi + \boldsymbol{\eta}\| - \|\xi\| \right) \frac{\xi + \boldsymbol{\eta}}{\|\xi + \boldsymbol{\eta}\|} \cdot d\boldsymbol{\eta}$$

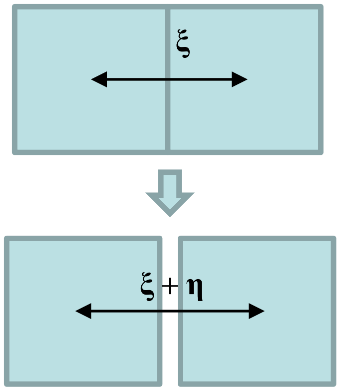

If we consider the element separation in the same direction as ξ ,

$$\omega_{\xi} = \int_0^{\boldsymbol{\eta}(t_{final})} \left\{ \underline{T}^* [\mathbf{x}, t] \langle \xi \rangle - \underline{T}^* [\mathbf{x}', t] \langle -\xi \rangle \right\} \cdot d\boldsymbol{\eta}$$

$$= \int_0^{\boldsymbol{\eta}(t_{final})} \frac{96E}{5\pi\delta^4} \left(\|\xi + \boldsymbol{\eta}\| - \|\xi\| \right) \frac{\xi + \boldsymbol{\eta}}{\|\xi + \boldsymbol{\eta}\|} \cdot d\boldsymbol{\eta}$$

$$\approx \frac{48E}{5\pi\delta^4} \|\boldsymbol{\eta}\|^2$$

$$\omega_{\xi} > \omega_c$$

$$\Leftrightarrow \frac{48E}{5\pi\delta^4} \|\boldsymbol{\eta}\|^2 > \frac{9K_{IC}{}^2 \left(1 - \nu^2\right)}{4\delta^3 E}$$

$$\Leftrightarrow \|\boldsymbol{\eta}\| > \sqrt{\frac{15K_{IC}{}^2 \left(1 - \nu^2\right)\delta}{64E^2}}$$

$$\Leftrightarrow \|\boldsymbol{\eta}\| > \frac{K_{IC}}{E} \sqrt{\frac{45\delta}{256}}$$

The critical displacement for breaking a bond is proportional to

$$\frac{K_{IC}}{E}$$

K/E and horizontal stress control the preferential stress direction.

E 40/20/10 GPa,
KIC 0.707/0.5/0.354 MPa m0.5
Sxx 40/40/40 MPa
(KIC/E 0.018/0.025/0.035)

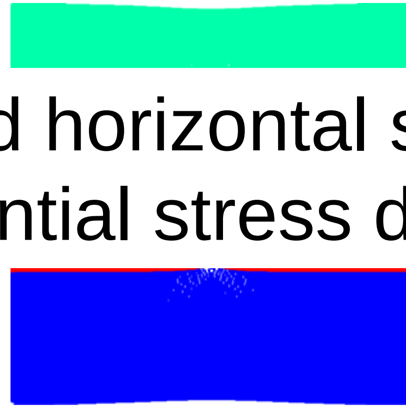

E 20/40/10 GPa,
KIC 0.5/0.707/0.354 MPa $m^{0.5}$
Sxx 40/40/40 MPa
(KIC/E 0.025/0.018/0.035)

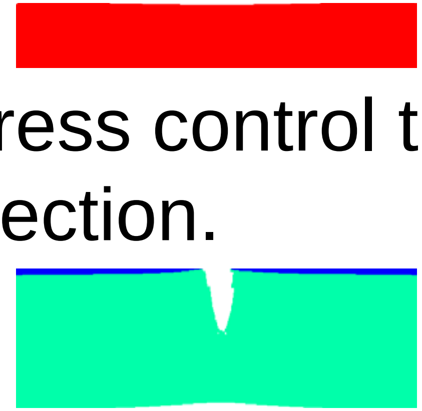

E 40/10/20 GPa,
KIC 0.707/0.354/0.5 MPa $m^{0.5}$
Sxx 40/40/40 MPa
(KIC/E 0.018/0.035/0.025)

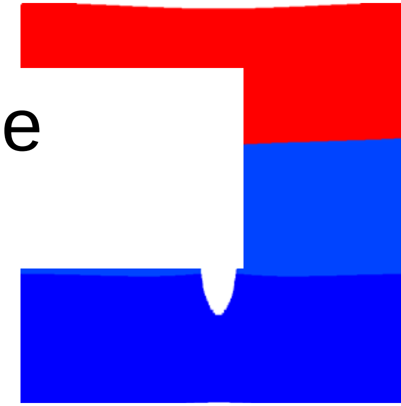

E 40/12/10 GPa,
KIC 0.707/0.5/0.354 MPa $m^{0.5}$
Sxx 40/40/40 MPa
(KIC/E 0.018/0.042/0.035)

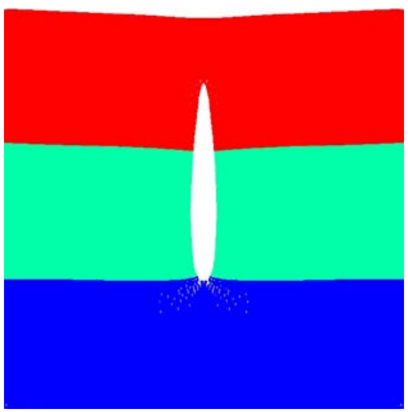

E 40/20/10 GPa,
KIC 1.2/0.5/0.354 MPa $m^{0.5}$
Sxx 40/40/40 MPa
(KIC/E 0.03/0.025/0.035)

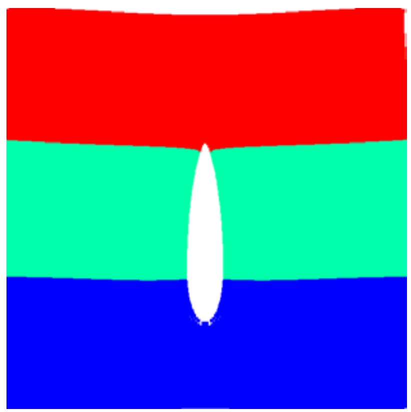

E 40/20/10 GPa,
KIC 1.6/0.5/0.354 MPa m0.5
Sxx 40/40/40 MPa
(KIC/E 0.04/0.025/0.035)

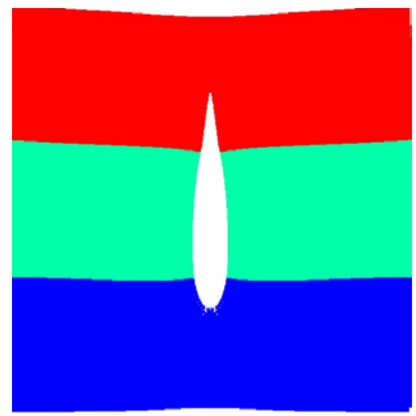

E 40/20/10 GPa,
KIC 0.707/0.5/0.354 MPa m0.5
Sxx 45/40/40 MPa
(KIC/E 0.018/0.025/0.035)

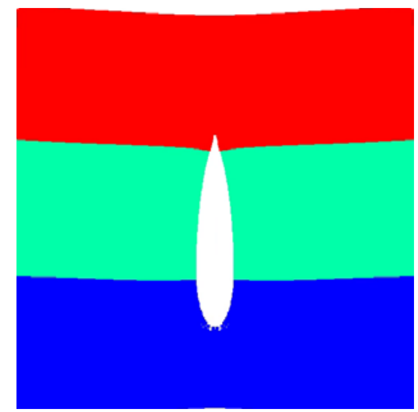

E 40/20/10 GPa,
KIC 0.707/0.5/0.354 MPa $m^{0.5}$
Sxx 50/40/40 MPa
(KIC/E 0.018/0.025/0.035)